UC San Diego

UC San Diego Electronic Theses and Dissertations

Title

Investigation of asymmetric vortex pair interactions

Permalink

https://escholarship.org/uc/item/7d12k3k9

Author

Folz, Patrick John Ryan

Publication Date

2023

Peer reviewed|Thesis/dissertation

eScholarship.org Powered by the California Digital Library
University of California

UNIVERSITY OF CALIFORNIA SAN DIEGO

Investigation of asymmetric vortex pair interactions

A dissertation submitted in partial satisfaction of the
requirements for the degree Doctor of Philosophy

in

Engineering Sciences (Aerospace Engineering)

by

Patrick John Ryan Folz

Committee in charge:

Professor Keiko Nomura, Chair
Professor Juan Carlos del Alamo
Professor Xuanting Hao
Professor Sutanu Sarkar
Professor William Young

2023

Copyright

Patrick John Ryan Folz, 2023

All rights reserved.

The Dissertation of Patrick John Ryan Folz is approved, and it is acceptable in quality and form for publication on microfilm and electronically.

University of California San Diego

2023

DEDICATION

To my grandmother, Ann Folz, who made this possible.
May she rest in peace.

EPIGRAPH

Doubtless we cannot see that other higher Spaceland now, because we have no eye in our stomachs.

Edwin A. Abbott

TABLE OF CONTENTS

LIST OF FIGURES

LIST OF TABLES

ACKNOWLEDGEMENTS

Thank you to my family for supporting me, in every way, through this ordeal. Thank you especially to Ann Folz, my late grandmother, who very generously supported my time at UCSD in life and beyond.

Chapter 3 is a reprint of an article published in the journal Fluid Dynamics Research, Patrick J. R. Folz and Keiko K. Nomura. “Interaction of two equal co-rotating viscous vortices in the presence of background shear”, Fluid Dyn. Res., 46 (3), 031423, 2014. The dissertation author was the primary researcher and the research supervisor was the co-author of the paper.

Chapter 4 is a reprint of an article published in the Journal of Fluid Mechanics, Folz, Patrick J. R.; Nomura, Keiko K., “A quantitative assessment of viscous asymmetric vortex pairs”, Cambridge University Press, 2017. The dissertation author was the primary researcher and author, and the research supervisor was the co-author of the paper.

Chapter 5 is a reprint of an article published in the Journal of Fluid Mechanics, Folz, Patrick J. R.; Nomura, Keiko K., “On asymmetric vortex pair interactions in shear”, Cambridge University Press, 2023. This includes a separate supplement published online but not in the main article. The dissertation author was the primary researcher and author, and the research supervisor was the co-author of the paper and the supplement.

Appendix A is a reprint of a supplement to the article in the Journal of Fluid Mechanics, Folz, Patrick J. R.; Nomura, Keiko K., “On asymmetric vortex pair interactions in shear”, Cambridge University Press, 2023 (i.e., the article contained in Chapter 5), published online at https://www.cambridge.org/core/journals/journal-of-fluid-mechanics/article/on-asymmetric-vortex-pair-interactions-in-shear/2016B7F6F4A9D9028A5E507C95FFA7BB#supplementary-materials. The dissertation author was the primary researcher and author, and the research supervisor was the co-author of the supplement.

VITA

2008 B. S. in Aerospace Engineering *cum laude*, Illinois Institute of Technology, Chicago, IL.

2011 M. S. in Engineering Sciences (Aerospace Engineering), University of California San Diego, La Jolla, CA.

2023 Ph. D. in Engineering Sciences (Aerospace Engineering), University of California San Diego, La Jolla, CA.

PUBLICATIONS

P. J. R. Folz and K. K. Nomura. "On asymmetric vortex pair interactions in shear", *J. Fluid Mech.*, 2023.

P. J. R. Folz and K. K. Nomura. "Quantitative assessment of asymmetric vortex interactions", *J. Fluid Mech.*, 2017.

P. J. R. Folz and K. K. Nomura. "Interaction of two equal co-rotating viscous vortices in the presence of background shear", *Fluid Dyn. Res.*, 46, 031423, 2014.

ABSTRACT OF THE DISSERTATION

Investigation of asymmetric vortex pair interactions

by

Patrick John Ryan Folz

Doctor of Philosophy in Engineering Sciences (Aerospace Engineering)

University of California San Diego, 2023

Professor Keiko Nomura, Chair

Two-dimensional vortex interactions and merging in fluid flows have long been a subject of significant research interest, with particular focus on clarifying their role in the inverse energy cascade of two-dimensional turbulence. Previous research has generally taken one of two forms: detailed study of the interaction of two vortices in isolation, or macroscopic study of a field of many vortices. Bridging the gap between these has been difficult, due to the complexity of the two-vortex, i.e., vortex pair, interaction and its varied outcomes when the vortices are unequal. In order to rectify this, this research considers in detail the interaction of two unequal co-rotating vortices in viscous fluid, and develops a method to quantitatively assess their outcomes. This enables a simple characterization of interaction outcomes in terms of certain key parameters. Using this, the case of a vortex pair interacting in linear shear which serves as a simple model

of the background flow generated by a field of many vortices, is then studied. Collectively, this work establishes a method for studying the influence of background flow on interacting vortices.

For the present research, numerical simulations are performed of vortex pairs having a range of vortex strength ratios in background flow having a linear shear velocity profile having a range of strengths, for finite Reynolds number. A method is introduced to monitor the flow development continuously, enabling the quantitative assessment of interaction outcomes in terms of an enhancement factor, ε, and a merging efficiency. η, which compare the circulations at the start and end of the convective interaction. The variation of these outcomes is found to be well-characterized by a mutuality parameter, a quantity directly related to the vortices' enstrophy ratio. The presence of shear is then found to produce two distinct flow regimes: separation, in which the vortices move apart continuously, and hendition, in which they interact to form a single vortex similar to, and similarly characterized as in, the isolated-pair case. However, the presence of shear is observed to alter the timing of key physical interaction processes, which may in some cases significantly alter the ultimate outcome. Taken together, these findings imply a general framework for two-dimensional co-rotating vortex interactions that can be incorporated into turbulence models.

Chapter 1

Introduction

It is a truth universally acknowledged in fluid dynamics, that the interactions of same-signed vortices must play a role in the inverse energy cascade of two-dimensional turbulence (Austen orig 1813, paraphrased). Yet the precise nature of this role remains unclear. Some of these interactions produce a larger vortex, which concentrates energy in larger-scale motion (e.g., Nielsen *et al.*, 1996; Huang, 2005), while others do not (e.g., Huang, 2006). Likewise, the manner and degree to which vortices and their interactions contribute to the energetics of turbulent flows via "vortex thinning" remains very unclear, appearing to contribute to the inverse cascade in some cases and the direct cascade (i.e., the transfer of energy to smaller scales) in others (vortex thinning is a mechanism by which larger-scale motion affects energy transfers at smaller scales, specifically, inter-scale energy flux resulting from the work done by large-scale strain rates on smaller-scale vorticity, which has been seen to be significant in forced two-dimensional turbulence; Xiao *et al.* 2009). Models and scaling laws considering the field of vortices in aggregate reflect the significance of vortex interactions in the time development of the turbulence (e.g., Carnevale *et al.*, 1991; Riccardi *et al.*, 1995), in particular interactions between vortices of different strength (e.g., Burgess & Scott, 2017), but these do not give much insight into the physical mechanisms by which this occurs. In order to understand the physics of these phenomena, the interaction between two vortices, and the influence on it due to the surrounding vortices, must be studied directly and in detail.

To date, a general understanding of the interaction of two like-signed two-dimensional vortices has not been developed. Most studies of vortex pairs have focused on the seemingly-simplest case of identical vortices, i.e., symmetric pairs, which are well-known to merge into a single stronger vortex from the combined fluid of the original two when a critical merging criterion is achieved (e.g., Melander *et al.*, 1988; Cerretelli & Williamson, 2003; Meunier *et al.*, 2005; Brandt & Nomura, 2007). Yet, in general, the vortices in two-dimensional turbulence may vary in size and intensity. Those studies that have considered unequal co-rotating vortices, i.e., asymmetric pairs, have shown that their interactions lead to varied outcomes (e.g., Melander *et al.*, 1987*b*), including mergers that produce stronger vortices as well as strainings out that do not (e.g., Dritschel & Waugh, 1992; Yasuda & Flierl, 1997; Trieling *et al.*, 2005; Brandt & Nomura, 2010) depending on their relative parameters; an interaction between two like-signed vortices that produces a single vortex is not necessarily a "merger" despite frequently being termed as such in the literature (e.g., Tabeling, 2002; Jing *et al.*, 2012). In inviscid flow, these varied outcomes are categorized in terms of the strength of the resulting vortex or vortices relative to the starting pair, with these results typically presented on complicated "regime maps" that offer neither practical utility nor deep physical explanation for the observed variation. These problems are compounded in viscous flow because of the difficulty of defining "starting" and "resulting" vortices in the continuously-developing flow, with outcomes being assessed only qualitatively by the researchers (prior to the publication of that portion of the present study).

As to the issue of the influence of the surrounding vorties, the few studies that have directly considered this at all have only considered the symmetric pair (e.g., Carton *et al.* 2002; Perrot & Carton 2010; Marques Rosas Fernandes *et al.* 2016), typically modeling the external influence as simple linear background shear. These have found that strong adverse shear (i.e., shear whose rotational sense opposes that of the pair) causes the vortices to separate, precluding merger, while less strongly adverse or favorable shear (i.e., shear whose rotational sense matches that of the pair) causes the distance between the vortices to vary, potentially engendering merger when the distance is sufficiently reduced; it must be noted, though, that, due to the inviscid nature

of the flow, these observed mergers only occur because the shear is so strong as to be inextricable from the merging process. This makes its influence difficult to discern from the vortices' in these cases. No dedicated study of an asymmetric pair in shear had been published prior to that portion of the present study, to the author's knowledge. The lack of studies of the asymmetric case in shear is directly attributable to the relative paucity of asymmetric-pair studies for the more-basic no-shear case.

Nevertheless, these studies collectively suggest that a more generalized understanding of vortex interactions based on underlying physics may be attainable. The occurrence of merger, in or out of background flow, has been seen to derive from the relative distance between the pair in the symmetric case (i.e., the pair's aspect ratio, often phrased as the equivalent "normalized separation distance"), while the regime maps in the asymmetric case suggest dependence on both distance and the vortices' relative strength (in terms of their relative circulation generally, but with particular dependence on sub-variations thereof). A more detailed summary of the relevant body of research is given in each chapter included in the body of this dissertation. Taken together, it is here observed that both relative distance and relative strength ultimately govern the degree of influence each vortex exerts on the other, both in absolute terms and relative to each other. This is the key principle that enables from which a generalized understanding of vortex interactions may be developed.

As a significant step towards developing this general model of vortex interaction, this study investigates the interaction of two unequal co-rotating vortices in viscous flow under the influence of background shear, and from that develops a more general characterization of vortex interactions that is applicable in general, complex two-dimensional flow such as two-dimensional turbulence. This encompasses three principal accomplishments:

- examination of the flow development of a symmetric pair in shear when viscosity is present, which demonstrates the effectiveness in this context of key results previously found for inviscid, isolated symmetric pairs;

- development of a method for the quantitative assessment of two-dimensional asymmetric vortex interactions in viscous flow without background shear that is based upon key underlying physical mechanisms, namely core detrainment and entrainment, enabling a consistent and objective characterization of all interaction outcomes; and

- analysis of the effect of shear on the interaction of two unequal co-rotating vortices, including identification of the interaction regimes and quantitative assessment of the outcomes of henditions (i.e., interactions from which a single vortex results), which establishes that vortex-dominated interaction outcomes are well-characterized by a single parameter (the pair's core enstrophy ratio, discussed later) regardless of the relative strength of the shear or asymmetry of the pair, and that the influence of the shear typically makes merger somewhat more likely and effective.

This study primarily utilizes computational methods, supplemented by analysis and available experimental data.

This dissertation is organized as follows: in Chapter 2, the numerical procedure utilized in the computational sections is described; in Chapter 3, the effects of viscosity and shear on symmetric pair interactions are considered; in Chapter 4, the physics of vortex merger are reviewed and utilized to develop a quantitative assessment of asymmetric pair interactions when viscosity is present without shear, and the trends identified are explained in terms of underlying physics; in Chapter 5, this assessment and physical insight is utilized to examine the effect of shear on asymmetric pair interactions, including the derivation of a result based on a point-vortex model that is utilized to predict the occurrence of vortex separation, and a small study of the evolution of a single vortex in shear; and in Chapter 6 the findings are summarized and future work is discussed. Chapter 3 is a reproduction of an article published in Fluid Dynamics Research, and Chapters 4 and Chapter 5 are reproductions of articles published in Journal of Fluid Mechanics.

Chapter 2

Scaling and operation of the numerical scheme

Here the numerical methods used to perform the simulations are briefly reviewed. The simulations were performed using DISTUF (Gerz *et al.*, 1989).

In all cases, the flow is incompressible, with an initial condition similar to that shown in figure 1 of Chapter 4; for symmetric cases, $\Lambda_0 = \omega_{1,0}/\omega_{2,0} = a_{1,0}/a_{2,0}$ is set equal to 1, and for no-shear cases (primarily Chapter 4), ζ_0 is set to 0. Each vortex $i = 1,2$ initially has a Gaussian vorticity distribution of the form

$$\omega_i(x,z,t) = \omega_{i,0} \exp\left(\frac{-((x_i - x_{i,0})^2 + (z_i - z_{i,0})^2)}{a_{i,0}^2}\right), \tag{2.1}$$

where $\omega_{i,0}$ is the initial vorticity, $x_{i,0}$ and $z_{i,0} = 0$ are the initial coordinates of the vortex center, and $a_{i,0}$ is the initial characteristic vortex radius (giving a circulation of $\Gamma = \pi a_0^2 \omega_0$). The vorticies are initially separated by a distance $b_0 \equiv |x_{2,0} - x_{1,0}|$.

In all cases, the vortices are kept small relative to the domain size L, with $b_0/L = 1/24$ found to keep the pair sufficiently isolated throughout the main interaction, in order to minimize the effect of boundary conditions (a maximum difference of 2.1% was found between simulations done at $b_0/L = 1/12$ and $b_0/L = 1/24$). In all cases, a staggered two-dimensional 2048^2 square grid is utilized, which corresponds to about 27 grid points across the larger core (as defined by initial radius a).

2.1 DISTUF scaling and operation

The DISTUF code was initially developed by Gerz, Schumann and Elghobashi for the simulation of three-dimensional turbulence with optional linear shear and/or stratification; see Gerz *et al.* (1989) and references therein for a thorough description of the code and its capabilities. It is here utilized for the simulation of two-dimensional vortex pairs because of its capability of simulating shear with periodic boundary conditions (shear-periodic boundary condition in the shear direction, when shear is present). This requires a careful consideration of the scaling of the code relative to that of the intended vortex-pair problem. Here, the scalings necessary for the correct initialization of the DISTUF code are first described, and then the general operation of DISTUF is briefly reviewed.

2.1.1 Vortex flow scaling

The appropriate scalings for the vortex flow are:

$$x \sim b_0 \tag{2.2}$$

$$u \sim W_0 \tag{2.3}$$

$$t \sim t_{ref} = t_c, \tag{2.4}$$

where b_0 is the initial peak-peak distance, W_0 is the vortex translation velocity, and t_c is the convection time. The translation velocity W_0 is related to these quantities and the circulation Γ_0 of a vortex by $W_0 = \frac{\Gamma_0}{2\pi b_0}$. The convection time t_c is based on the estimated period of revolution of the pair, neglecting any viscous or deformation effects. It is the distance traveled by one vortex,

i.e. the circumference of the circular trajectory, divided by the initial translational velocity:

$$t_c \equiv \frac{\pi b_0}{W_0} = \frac{\pi b_0}{\frac{\Gamma_0}{2\pi b_0}} = \frac{2\pi^2 b_0^2}{\Gamma_0}. \tag{2.5}$$

The flow is then characterized by the following nondimensional parameters:

- Reynolds number: $Re \equiv \frac{\Gamma_0}{\nu} = \frac{\pi a_0^2 \omega_0}{\nu}$
- Aspect ratio: $\frac{a_0}{b_0}$,

where Γ_0 is the initial vortex circulation, a_0 is the initial vortex characteristic radius, and ω_0 is the initial vortex peak vorticity (in this study, these values are taken from the stronger initial vortex); ν is the kinematic viscosity of the fluid. These reference values are then used to define nondimensional variables for the vortex problem, denoted with $[]^v$:

$$x^v \equiv \frac{x}{b_0} \tag{2.6}$$

$$u^v \equiv \frac{u}{W_0} \tag{2.7}$$

$$w^v \equiv \frac{w}{W_0} \tag{2.8}$$

$$t^v \equiv \frac{t}{t_c} = \frac{t}{\frac{\pi b_0}{W_0}} = t\frac{W_0}{\pi b_0}. \tag{2.9}$$

These can be used to scale the initial condition in both the unsheared and sheared cases.

2.1.2 DISTUF Scaling

The DISTUF code is scaled based on the basic problem of some mean flow, U_{ref}, in a box of size L_{box} (not necessarily square, but in this case it is). By dimensional reasoning, these can be used to construct a time scale $\frac{L_{box}}{U_{ref}}$.

Thus, for this problem we have the reference values:

$$x \sim L_{box} \tag{2.10}$$

$$u \sim U_{ref} \tag{2.11}$$

$$t \sim t_{ref} = \frac{L_{box}}{U_{ref}}. \tag{2.12}$$

These can be used to define nondimensional variables for DISTUF:

$$x^* \equiv \frac{x}{L_{box}} \tag{2.13}$$

and

$$z^* \equiv \frac{z}{L_{box}}, \tag{2.14}$$

$$u^* \equiv \frac{u}{U_{ref}} \tag{2.15}$$

and

$$w^* \equiv \frac{w}{U_{ref}}, \tag{2.16}$$

and

$$t^* \equiv \frac{t}{\frac{L_{box}}{U_{ref}}} = t\frac{U_{ref}}{L_{box}}. \tag{2.17}$$

The reference length scales for the vortex flow and DISTUF are related by

$$L_{box} = \frac{L_{box}}{b_0} b_0 = \Phi b_0, \tag{2.18}$$

where the length scales for the vortex flow problem and the DISTUF code are related by the ratio:

$$\Phi = \frac{L}{b_0}. \tag{2.19}$$

Thus the nondimensional coordinates are related by:

$$x^* \equiv \frac{x}{L_{box}} = \frac{x}{\Phi b_0} = \frac{x^v}{\Phi} \tag{2.20}$$

$$z^* = \frac{z}{\Phi b_0}. \tag{2.21}$$

There is also a Reynolds number for DISTUF based on the mean flow and box size,

$$Re_{box} = Re_{code} = \frac{U_{ref} L_{box}}{\nu}. \tag{2.22}$$

2.1.3 No-shear case scaling

The vortex initial condition is specified in DISTUF in terms of velocities, not vorticity (Garten *et al.*, 1998). The velocity distribution is given by:

$$u = \frac{-a_0^2 \omega_0 (z - z_1)}{2((x-x_1)^2 + (z-z_1)^2)} \left(1 - exp\left(\frac{-((x-x_1)^2 + (z-z_1)^2)}{a_0^2}\right)\right) - \frac{a_0^2 \omega_0 (z - z_2)}{2((x-x_2)^2 + (z-z_2)^2)} \left(1 - exp\left(\frac{-((x-x_2)^2 + (z-z_2)^2)}{a_0^2}\right)\right)$$

$$w = \frac{a_0^2 \omega_0 (x-x_1)}{2((x-x_1)^2+(z-z_1)^2)} \left(1 - exp\left(\frac{-((x-x_1)^2+(z-z_1)^2)}{a_0^2}\right)\right) + \frac{a_0^2 \omega_0 (x-x_2)}{2((x-x_2)^2+(z-z_2)^2)} \left(1 - exp\left(\frac{-((x-x_2)^2+(z-z_2)^2)}{a_0^2}\right)\right).$$

The nondimensionalization procedure is similar for both u and w, and for each term in their respective functions. Therefore, the rest of the analysis will concentrate on the first term of the u function.

First, the length coordinates in the coefficient of the exponential function can be recast in terms of nondimensional variables x^* and z^*:

$$u = \frac{-1}{2} \frac{a_0^2 \omega_0 \Phi b_0}{\Phi^2 b_0^2} \frac{(z^*-z_1^*)}{((x^*-x_1^*)^2+(z^*-z_1^*)^2)} \left(1 - exp\left(\frac{-((x-x_1)^2+(z-z_1)^2)}{a_0^2}\right)\right) - \ldots \tag{2.23}$$

$$u = \frac{-1}{2} \left(\frac{a_0}{b_0}\right)^2 \frac{\omega_0 b_0}{\Phi} \frac{(z^*-z_1^*)}{((x^*-x_1^*)^2+(z^*-z_1^*)^2)} \left(1 - exp\left(\frac{-((x-x_1)^2+(z-z_1)^2)}{a_0^2}\right)\right) - \ldots \tag{2.24}$$

In the no-shear case, since there is no mean background flow, it can be taken that $U_{ref} = W_0$. Since $W_0 = \frac{\Gamma}{2\pi b_0}$,

$$u = \frac{-W_0}{\Phi} \frac{(z^*-z_1^*)}{((x^*-x_1^*)^2+(z^*-z_1^*)^2)} \left(1 - exp\left(\frac{-((x-x_1)^2+(z-z_1)^2)}{a_0^2}\right)\right) - \ldots \tag{2.25}$$

The nondimensional velocity in DISTUF is therefore given by:

$$\frac{u}{W_0} = u^* = \frac{-1}{\Phi} \frac{(z^* - z_1^*)}{((x^* - x_1^*)^2 + (z^* - z_1^*)^2)} \left(1 - exp\left(\frac{-((x-x_1)^2 + (z-z_1)^2)}{a_0^2}\right)\right) - \ldots \quad (2.26)$$

Note that $\frac{u}{W_0} = u^* = u^v$.

The timescales are related by:

$$t^* = t\frac{U_{ref}}{L_{box}} = t\frac{W_0}{L_{box}} = t\frac{W_0}{\Phi b_0} = \frac{t}{t_c}\frac{\pi}{\Phi} = t^v\frac{\pi}{\Phi}. \quad (2.27)$$

We therefore have a set of conversion factors relating the DISTUF variables to those for the vortex flow:

$$x^* = \frac{x^v}{\Phi} \quad (2.28)$$

$$u^* = u^v \quad (2.29)$$

$$t^* = t^v\frac{\pi}{\Phi}. \quad (2.30)$$

The Reynolds numbers for DISTUF and the vortex flow are also related, by:

$$Re_{code} = \frac{U_{ref}L_{box}}{\nu} = \frac{W_0\Phi b_0}{\nu} = \frac{\Gamma}{2\pi b_0}\frac{\Phi b_0}{\nu} = \frac{\Phi}{2\pi}\frac{\Gamma}{\nu} = \frac{\Phi}{2\pi}\frac{\Gamma}{\nu} = \frac{\Phi}{2\pi}Re_\Gamma. \quad (2.31)$$

2.1.4 Shear case scaling

DISTUF can also simulate the case of flow with linear background shear. The shear of the mean flow is given by

$$\frac{dU}{dz}\frac{\Delta U}{L_{box}}, \tag{2.32}$$

where ΔU is the characteristic velocity differential of the shear.

The reference values for the sheared flow are based on the shear:

$$x_{ref} = L_{box} = \Phi b_0 \tag{2.33}$$

$$U_{ref} = \Delta U = \frac{\Delta U}{L_{box}} = \frac{dU}{dz} L_{box} \tag{2.34}$$

$$t_{ref} = \frac{L_{box}}{\Delta U} = \frac{1}{\frac{dU}{dz}}. \tag{2.35}$$

In this case, the initial condition velocity distribution is given by

$$u = \frac{-1}{2}\left(\frac{a_0}{b_0}\right)^2 \frac{\omega_0 b_0}{\Phi} \frac{(z^* - z_1^*)}{((x^* - x_1^*)^2 + (z^* - z_1^*)^2)} \left(1 - exp\left(\frac{-((x-x_1)^2 + (z-z_1)^2)}{a_0^2}\right)\right) - \ldots \tag{2.36}$$

$$\frac{u}{\Delta U} = \frac{1}{\Delta U}\frac{-1}{2}\left(\frac{a_0}{b_0}\right)^2 \frac{\omega_0 b_0}{\Phi} \frac{(z^* - z_1^*)}{((x^* - x_1^*)^2 + (z^* - z_1^*)^2)} \times \left(1 - exp\left(\frac{-((x-x_1)^2 + (z-z_1)^2)}{a_0^2}\right)\right) - \ldots \tag{2.37}$$

$$\frac{u}{\Delta U} = \frac{-1}{2}\left(\frac{a_0}{b_0}\right)^2 \frac{\omega_0 b_0}{\Phi \Delta U} \frac{(z^* - z_1^*)}{((x^* - x_1^*)^2 + (z^* - z_1^*)^2)} \left(1 - exp\left(\frac{-((x-x_1)^2 + (z-z_1)^2)}{a_0^2}\right)\right) - \dots \tag{2.38}$$

$$\frac{u}{\Delta U} = \frac{-1}{2}\left(\frac{a_0}{b_0}\right)^2 \frac{\omega_0 b_0}{\Phi(\Phi \frac{dU}{dz})} \frac{(z^* - z_1^*)}{((x^* - x_1^*)^2 + (z^* - z_1^*)^2)} \times \left(1 - exp\left(\frac{-((x-x_1)^2 + (z-z_1)^2)}{a_0^2}\right)\right) - \dots \tag{2.39}$$

$$\frac{u}{\Delta U} = \frac{-1}{2}\left(\frac{a_0}{b_0}\right)^2 \frac{1}{\Phi^2} \frac{\omega_0}{\frac{dU}{dz}} \frac{(z^* - z_1^*)}{((x^* - x_1^*)^2 + (z^* - z_1^*)^2)} \times \left(1 - exp\left(\frac{-((x-x_1)^2 + (z-z_1)^2)}{a_0^2}\right)\right) - \dots \tag{2.40}$$

We can define a shear parameter to characterize the relative strengths of the vortices' vorticity and the background shear as

$$Sh \equiv \frac{\omega_0}{\frac{dU}{dz}}. \tag{2.41}$$

The time is scaled by t_{ref}:

$$t^* \equiv \frac{t}{t_{ref}} = \frac{t}{\frac{1}{\frac{dU}{dz}}} = t\frac{dU}{dz} = t\frac{\omega_0}{Sh} \tag{2.42}$$

$$t^* = \frac{\Gamma}{\pi a_0^2} \frac{1}{Sh} t \frac{2\pi b_0^2}{2\pi b_0^2} \tag{2.43}$$

$$t^* = \frac{\Gamma}{2\pi^2 b_0^2}\frac{2\pi b_0^2}{a_0^2}\frac{1}{Sh}t = \frac{1}{t_c}2\pi\frac{b_0^2}{a_0^2}\frac{1}{Sh}t \tag{2.44}$$

$$t^* = \frac{t}{t_c}\frac{2\pi}{Sh}\frac{b_0^2}{a_0^2} = t^{\nu}\frac{2\pi}{Sh}\frac{b_0^2}{a_0^2}. \tag{2.45}$$

Thus, the timescales for the flow problem and the sheared DISTUF simulation are related.

DISTUF numerical scheme

DISTUF integrates the continuity equation, the Navier-Stokes equation, and the heat balance equation in time in three dimensions, for fluid with constant diffusivities of momentum and heat, utilizing the Boussinesq approximation. For the present study, the flow is restricted to two-dimensions (by setting the velocity in the third direction to 0 in the initial condition and at every timestep, i.e., enforcing $u_2 = 0$), and the flow is isothermal and incompressible.

With these assumptions, the equations of motion (normalized in terms of L_{box}, U_{ref}, and t_{ref}) are

$$\frac{\partial u_j^*}{\partial x_j^*} = 0 \tag{2.46}$$

and

$$\frac{\partial u_j^*}{\partial t^*} + \frac{\partial}{\partial x_j^*}(u_j^* u_i^*) + Sx_3^*\frac{\partial u_i^*}{\partial x_1^*} + Su_3^*\delta_{i1} = \frac{1}{Re}\frac{\partial^2 u_i^*}{\partial (x^*)_j^2} - \frac{\partial p^*}{\partial x_i^*}, \tag{2.47}$$

where $S = (L_{box}/\Delta U)(dU/dz) = 0,\ 1$ for the no-shear and shear cases, respectively, and $Re = (U_{ref}L_{box})/\nu$ is the box Reynolds number (and terms directly dependent on temperature, including the entire heat balance equation, have been omitted).

These equations are discretized using a a second-order finite-difference scheme on a staggered uniform grid with periodic boundary conditions, except for the mean advection (i.e., the linear background shear) for which pseudospectral methods are used. Boundary conditions

are periodic except in the shear case, in which the boundary condition in the shear direction is shear-periodic, i.e., $f(t^*, x_1^* + m_1, x_3^* + m_3) = f(t^*, x_1^* - Sm_3 t^*, x_3^*)$, where m_n are arbitrary integers. These equations are integrated in time using a second order Adams-Bashforth method, with pressure handled implicitly. For further details, see Gerz *et al.* (1989) and references therein.

Chapter 3

Interaction of two equal co-rotating viscous vortices in the presence of background shear

Interaction of two equal co-rotating viscous vortices in the presence of background shear

Patrick J R Folz and Keiko K Nomura

Department of Mechanical and Aerospace Engineering, University of California, San Diego, 9500 Gilman Drive, La Jolla, CA, 92092-0411, USA

E-mail: pfolz@ucsd.edu and knomura@ucsd.edu

Received 19 July 2013, revised 28 April 2014
Accepted for publication 28 April 2014
Published 28 May 2014

Communicated by S Le Dizès

Abstract

The interactions of two equal co-rotating vortices under the influence of both viscosity and uniform background shear are investigated using two-dimensional numerical simulations. A range of values of the shear strength parameter, $\zeta_0 = -S/\omega_0$, and initial aspect ratio, a_0/b_0, are considered for two values of circulation Reynolds number $\mathrm{Re}_\Gamma = |\Gamma_0|/\nu$. The primary effect of viscosity is to increase the core size $a(t)$ in time while the primary effect of shear is to vary the separation distance $b(t)$ in time. For sufficiently separated vortices, the motion of the vortices is well-described by a point vortex model with linear shear. The present simulations show that for a viscous symmetric vortex pair there are two distinct flow regimes, merger and separation, with the boundaries separating these regimes well-predicted by the point vortex model and largely independent of Re_Γ over the range tested. Results also indicate that the onset of merging occurs when $a(t)/b(t)$ attains the critical value $(a/b)_{cr}$ found for vortex pairs without shear.

(Some figures may appear in colour only in the online journal)

1. Introduction

Vortex pair interactions are fundamental processes in many complex flows of practical and scientific interest, such as aircraft wakes and two-dimensional turbulence. Understanding these interactions is therefore essential to understanding the more complicated flows. For example, it is known that two co-rotating vortices will merge to form a larger compound vortex if the aspect ratio (core size/separation distance), a/b, exceeds a critical value, $(a/b)_{cr}$.

Thus, vortex merging has been considered to be a key process in the inverse energy cascade of two-dimensional turbulence (Benzi *et al* 1987). However, a turbulent flow consists of a field of vortices and other structures, differing in size and strength, and the influence of these factors on the vortex merging process and turbulence dynamics is not well understood.

A great deal of research has been devoted to the study of the simplest vortex pair configuration: two equal co-rotating vortices, i.e., a symmetric vortex pair. Much of this research has focused on inviscid flow (e.g., Dritschel and Waugh 1992, Overman and Zabusky 1982, Saffman and Szeto 1980), while other studies have considered flows with viscosity (e.g., Brandt and Nomura 2007, Cerretelli and Williamson 2003, Melander *et al* 1988, Meunier *et al* 2002). If the vortices are sufficiently separated, their basic behavior is similar to that of two point vortices which rotate about each other. However, for finite-area vortices, the induced strain field will deform and tilt the vortices. The critical aspect ratio can be related to the relative strength of the induced strain rate to the vortex strength; a key factor for the physical mechanism of the onset of merger (Brandt and Nomura 2010). The presence of viscosity ensures that a given pair will achieve the critical aspect ratio given sufficient time to diffusively spread, producing merger in initially well-separated vortices. Increasing the effect of viscosity causes this process to occur more rapidly on a convective timescale, but the merging criterion remains relatively unchanged (Le Dizès and Verga 2002).

The majority of previous studies have considered a single vortex pair, with no external influences. In order to consider vortex merging in a turbulent flow, the influence of neighboring and remote vortices must be considered. A few studies have been carried out which approximate this influence as a simple background shear in which the pair interacts (Maze *et al* 2004, Perrot and Carton 2010, Trieling *et al* 2010). To date these studies have all considered inviscid vortex pairs.

The work of Trieling *et al* (2010) is of particular relevance as they studied the case of two equal finite-area Gaussian vortices in linear shear. Using contour dynamics simulations, they identified four possible interaction regimes: merger, periodic motion, separation without elongation, and separation with elongation; depending on the sign and strength of the background shear relative to the vorticity of the vortices. The basic motion of the vortices, and in particular, the delineation between separative and periodic regimes was found to be well-described by the point vortex model of Kimura and Hasimoto (1985). Conditions for the merging regime were determined by considering the shear-induced variations of the separation distance, b, and using known $(a/b)_{cr}$ values for no-shear flow (see section 2). Though some ambiguities remained, the value of $(a/b)_{cr}$ for the no-shear case was found to provide a reasonably effective criterion for vortices in shear as well.

The previous research has considered separately the effects of viscosity and linear shear on symmetric vortex interactions, but to date their combined effect has not been considered. The current research investigates vortex pair interactions with both effects present by investigating the possible regimes of interaction through a series of numerical simulations for a range of initial parameters.

In section 2, the modified point vortex analysis of Kimura and Hasimoto (1985) and Trieling *et al* (2010) is reviewed. In section 3, the setup and numerical method of the simulations are described. In section 4 results of the simulations are presented. These results are analyzed and the relevance of point vortex results to the viscous flow is demonstrated. Finally, section 5 summarizes the findings and conclusions.

2. Modified point vortex model

The motion of two point vortices in linear shear is described by the following equations (Kimura and Hasimoto 1985):

$$\frac{\mathrm{d}t_1}{\mathrm{d}t} = -\frac{\Gamma_2}{2\pi}\frac{y_1 - y_2}{b^2} + Sy_1 \tag{1}$$

$$\frac{\mathrm{d}y_1}{\mathrm{d}t} = \frac{\Gamma_2}{2\pi}\frac{x_1 - x_2}{b^2} \tag{2}$$

$$\frac{\mathrm{d}t_2}{\mathrm{d}t} = -\frac{\Gamma_1}{2\pi}\frac{y_2 - y_1}{b^2} + Sy_2 \tag{3}$$

$$\frac{\mathrm{d}y_2}{\mathrm{d}t} = \frac{\Gamma_1}{2\pi}\frac{x_2 - x_1}{b^2}, \tag{4}$$

where (x_i, y_i) are the coordinates of the ith vortex, Γ_i is the circulation of the ith vortex, $b^2 = (x_1 - x_2)^2 + (y_1 - y_2)^2$ is the squared separation distance between the vortices, and $S = \mathrm{d}U/\mathrm{d}y$ is the uniform background shear. Considering symmetric vortices ($\Gamma_1 = \Gamma_2 = \Gamma$) and following the methods of Kimura and Hasimoto (1985), these equations can be integrated to find trajectories that are either closed or open, depending on the relative sign and strength of the shear and vortices. A nondimensional shear strength parameter, $\mu = S\, b_0^2/\Gamma$, can be considered (Trieling *et al* 2010) with a critical value determined from results of Kimura and Hasimoto (1985) to be,

$$\mu_{cr} = \left(\frac{S\, b_0^2}{\Gamma}\right)_{cr} = \frac{1}{\pi e}, \tag{5}$$

where e is the base of the natural logarithm and $b_0 = (x_2 - x_1)$ when $y_2 - y_1 = 0$.

Trajectories for initially horizontally-aligned vortices with various μ values are shown in figure 1. In the case of no shear ($\mu = 0$), the trajectory is a circle corresponding to periodic motion. When the shear is favorable ($\mu < 0$), the motion is always periodic since $\mu < 0 < \mu_{cr}$. The corresponding trajectories in figure 1 indicate that the vortex separation, initially b_0 when horizontally-aligned, reduces to a minimum as they revolve to become vertically aligned. When the shear is adverse ($\mu > 0$), the motion may be either separative or periodic. For weakly adverse shear ($0 < \mu < \mu_{cr}$), the motion is periodic but vortex separation instead increases to a maximum when they become vertically aligned. The case of $\mu = \mu_{cr}$ gives the critical separatrix for stationary flow; the vortices revolve to be vertically aligned and then remain in that position indefinitely. For strongly adverse shear ($\mu > \mu_{cr}$), the vortices instead follow open trajectories and their separation increases indefinitely.

The point vortex model has been found to effectively describe the motion of sufficiently separated finite-area vortices in the inviscid limit (Benzi *et al* 1987). Modifications to explicitly incorporate finite-area vortex parameters were made by Trieling *et al* (2010). By substituting $\Gamma = \pi a_0^2 \omega_0$ (where a_0 is the vortex radius and ω_0 is the peak vorticity) for circulation in the point vortex solution, the critical value of the ratio of shear to peak vorticity is found in terms of the initial aspect ratio a_0/b_0:

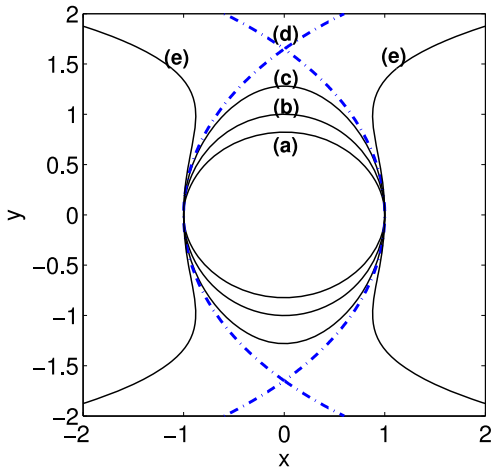

Figure 1. Point vortex trajectories of initially horizontally-aligned vortices ($y_1 = y_2 = 0$) for various initial shear strengths, computed by integrating equations (1)–(4) after substituting $\xi = x_2 - x_1$ and $\eta = y_2 - y_1$. The contours correspond to: (a) favorable shear ($\mu < 0$), (b) no shear ($\mu = 0$), (c) weakly adverse shear ($0 < \mu < \mu_{cr}$), (d) critical separatrix ($\mu = \mu_{cr}$), (e) strongly adverse shear ($\mu > \mu_{cr}$).

$$\left(\frac{S}{\omega_0}\right)_{cr} = \pi\mu_{cr}\left(\frac{a_0}{b_0}\right)^2 = \frac{1}{e}\left(\frac{a_0}{b_0}\right)^2. \tag{6}$$

Thus, the value of $\left(S/\omega_0\right)_{cr}$ depends solely on the initial aspect ratio (a_0/b_0). For a given a_0/b_0, separative motion will occur if S/ω_0 exceeds the corresponding value of $(S/\omega_0)_{cr}$. Results in Trieling *et al* (2010) from contour dynamics calculations demonstrate that (6) effectively distinguishes the separative and periodic regimes for finite-area vortices.

In flows without background shear, finite-area vortices will merge if their separation distance is less than the critical value, i.e., $b/a_0 < (b/a)_{cr}$. In flows with shear, and when the motion is not separative, this may be expected to hold true. As indicated by the point vortex model, the primary effect of shear is to vary $b(t)$ along the trajectory in the periodic regime. By considering $(b/a)_{cr}$ for the no-shear case, a simple merging criterion was formulated by Trieling *et al* (2010): merger will occur if the vortex separation distance is always less than the critical separation distance. This is a stricter condition than observed for the case of favorable shear, in which merger was found to occur if the minimum separation distance is less than the critical separation.

The point vortex model and finite-area results will be considered in our analysis of the case of viscous flow. The numerical simulations of these flows are described in the next section.

3. Setup and numerical simulations

Figure 2 shows the vortex pair initial condition: two like-signed Gaussian vortices of peak vorticity ω_0 and radius a_0 with an initial separation b_0 in a background shear flow of strength S. These are used to define several parameters which characterize the flow. The initial aspect

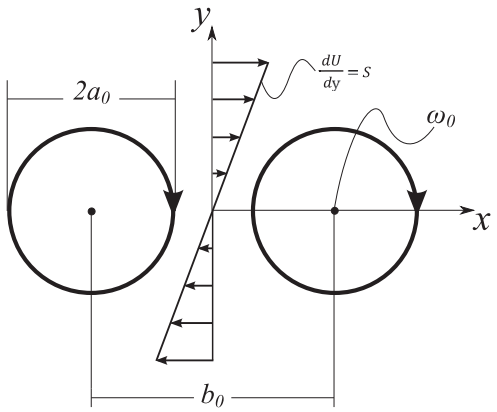

Figure 2. Flow initial condition, including Gaussian vortices of peak vorticity ω_0 and radius a_0 with initial separation b_0 in a uniform background shear of $S = \mathrm{d}U/\mathrm{d}y$. The case shown corresponds to $\zeta_0 = \omega_S/\omega_v = -S/\omega_0 > 0$, i.e. favorable shear.

ratio is a_0/b_0, where a is defined based on the second moment of vorticity (Meunier *et al* 2002). The circulation Reynolds number is $\mathrm{Re}_\Gamma = |\Gamma_0|/\nu$, where $\Gamma_0 = \pi a_0^2 \omega_0$. Here, the shear strength parameter, ζ_0, is defined as the ratio of the vorticity of the background shear to the characteristic vorticity of the vortices,

$$\zeta_0 = \frac{\omega_S}{\omega_v} = \frac{-S}{\omega_0}\,. \tag{7}$$

Thus, shear is considered to be favorable when $\zeta_0 > 0$ and adverse when $\zeta_0 < 0$.

Two-dimensional numerical simulations of the viscous vortex pair are performed using a combination of finite difference and pseudospectral approximations on a uniform staggered grid. The computational domain is periodic except in the shear direction where shear-periodic boundary conditions are employed. Details of the boundary conditions and numerical solution procedure are given in Gerz *et al* (1989).

Resolution tests found that using 1024^2 grid points, giving about 13 points across a vortex core ($2a_0$), was sufficient to capture the characteristic behavior of the vortex pair in the range of Reynolds numbers considered. In order to avoid unrealistic effects of neighboring vortices due to the periodic boundary condition, the size of the vortex pair is kept small relative to the domain size. An initial separation distance relative to the domain size $b_0/L = 1/24$ was found to be sufficient to minimize boundary effects. For further details of the numerical aspects, see Brandt and Nomura (2007).

4. Results and analysis

Figure 3 shows the time development of representative vortex pairs ($a_0/b_0 = 0.157$, $\mathrm{Re}_\Gamma = 5000$) for a range of $\zeta_0 = -S/\omega_0$ values. Results are given in terms of a convective timescale (based on period of revolution for two point vortices with no shear), $t^* = t/\left(2\pi b_0^2/|\Gamma_0|\right)$.

Early in time ($t^* \lesssim 1$) and when the vortices do not significantly interact, their motion can be described qualitatively by the point vortex model. The vortices rotate about each other in

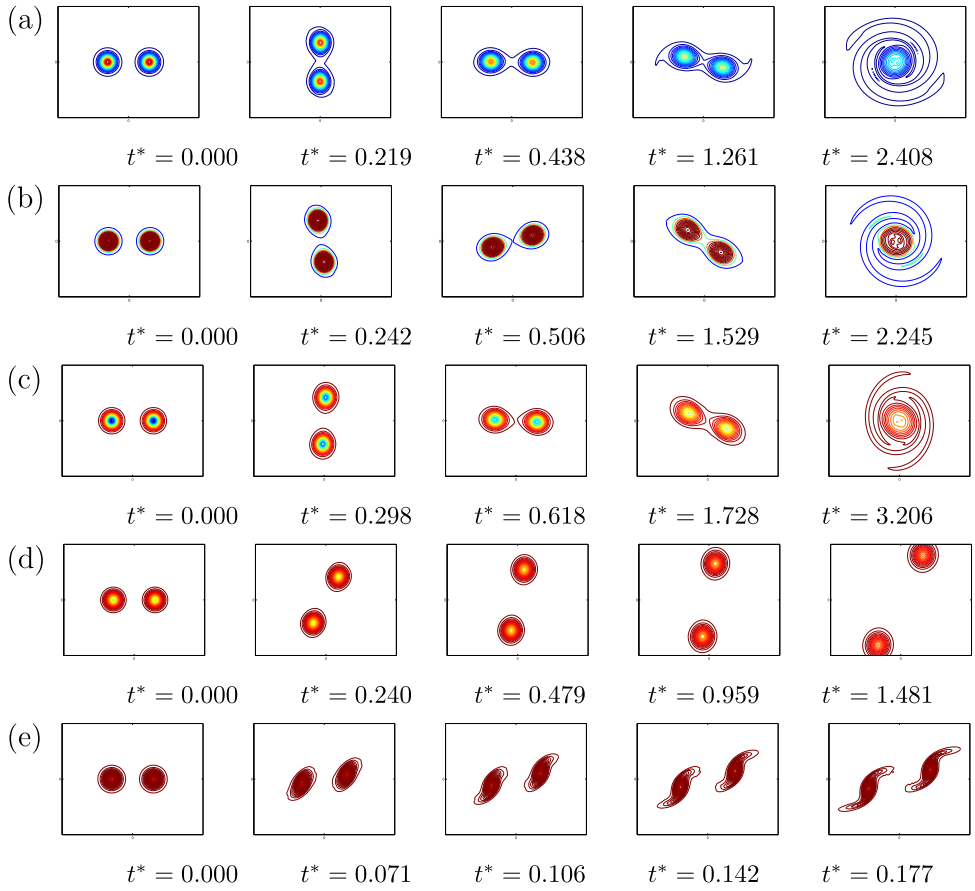

Figure 3. Vorticity contour plots showing time evolution of flows ($a_0/b_0 = 0.157$, $\mathrm{Re}_\Gamma = 5000$) for different $\zeta_0 = -S/\omega_0$: (a) $\zeta_0 = 0.0045$, (b) $\zeta_0 = 0$, (c) $\zeta_0 = -0.0045$, (d) $\zeta_0 = -0.0093$, (e) $\zeta_0 = -0.10$. For (a) and (b), the color red corresponds to the peak (negative) vorticity of the $\zeta_0 = 0.0045$ case and blue indicates lower-level (i.e. less negative) vorticity. For (c), (d) and (e), the color blue corresponds to the peak (positive) vorticity of the $\zeta_0 = -0.0045$ case and red indicates lower-level (positive) vorticity.

closed trajectories for favorable and weakly adverse shear (figures 3(a)–(c)) and separate for strong adverse shear (figures 3(d), (e)). Later in time, the vortices moving in closed trajectories eventually merge into a single vortex (figures 3(a)–(c)). For stronger adverse shear (figure 3(d), $\zeta_0 = -0.0093$), the vortices continue to move apart but are observed to retain their coherence (at least for the duration of these simulations), i.e., there is separation without elongation. For very strong adverse shear (figure 3(e), $\zeta_0 = -0.10$), the vortices are stretched out into filaments by the shear, i.e., there is separation with elongation. The observed interaction regimes are summarized in table 1.

Figure 4 shows the corresponding time development of the vortex separation, $b(t)$. Initially, the behavior of $b(t)$ is consistent with the point vortex trajectories (figure 1) and decreases/increases periodically for favorable/weakly adverse shear ($\zeta_0 = \pm 0.0045$). For strong adverse shear ($\zeta_0 = -0.0093$), the vortices exhibit separative trajectories and $b(t)$ increases monotonically and indefinitely. Later in time, the periodic motion breaks down and

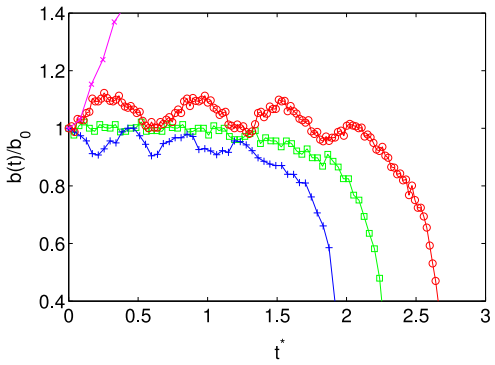

Figure 4. Normalized $b(t)$ for $\mathrm{Re}_\Gamma = 5000$, $a_0/b_0 = 0.157$. +: $\zeta_0 = 0.0045$, □: $\zeta_0 = 0$, ◯: $\zeta_0 = -0.0045$, ×: $\zeta_0 = -0.0093$.

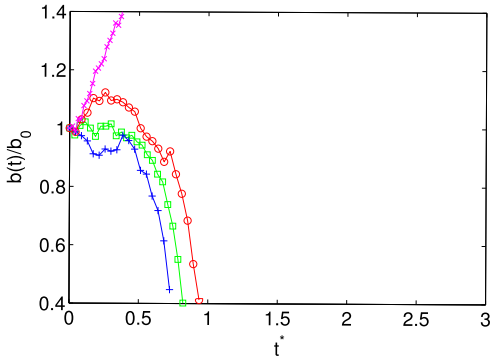

Figure 5. Normalized $b(t)$ for $\mathrm{Re}_\Gamma = 1000$, $a_0/b_0 = 0.157$. +: $\zeta_0 = 0.0045$, □: $\zeta_0 = 0$, ◯: $\zeta_0 = -0.0045$, ×: $\zeta_0 = -0.0093$.

Table 1. Outcome of interaction for vortex pairs of various initial $\zeta_0 = -S/\omega_0$ and $a_0/b_0 = 0.157$ for $\mathrm{Re}_\Gamma = 5000$ and $\mathrm{Re}_\Gamma = 1000$

ζ_0	Outcome, $\mathrm{Re}_\Gamma = 5000$	Outcome, $\mathrm{Re}_\Gamma = 1000$
0.0045	Merger	Merger
0	Merger	Merger
–0.0045	Merger	Merger
–0.0092	Merger	Merger
–0.0093	Separation without elongation	Separation without elongation
–0.10	Separation with elongation	Separation with elongation

we observe a rapid decrease in $b(t)$ corresponding to merger. The onset of merger is seen to occur earlier/later in favorable/weakly adverse shear with respect to the corresponding flow with no shear.

The effect of viscosity on flow development is investigated by performing simulations at $\mathrm{Re}_\Gamma = 1000$ ($a_0/b_0 = 0.157$). The results are included in table 1. The same interaction regimes occur: merging for favorable and weakly adverse shear, and separative for strongly adverse

Table 2. Critical $\zeta_0 = -S/\omega_0$ delineating separation and merger regimes for various a_0/b_0, from point vortex model predictions and empirical results.

		Empirical $\zeta_{0,cr}$	
a_0/b_0	Predicted $\zeta_{0,cr}$	$\mathrm{Re}_\Gamma = 5000$	$\mathrm{Re}_\Gamma = 1000$
0.105	−0.0041	−0.0040 ± 0.0001	−0.0040 ± 0.0001
0.157	−0.0091	−0.0092 ± 0.00004	−0.00926 ± 0.00009
0.235	−0.020	−0.020 ± 0.002	−0.020 ± 0.002

shear. The corresponding $b(t)$ behavior is shown in figure 5 where it is apparent that the lower Reynolds number accelerates establishment of the merging process.

The modified point vortex model in section 2 indicates that for finite-area inviscid vortices with a specified a_0/b_0, sufficiently strong adverse shear, i.e., $\zeta_0 < \zeta_{0,cr} < 0$, will result in separative motion. To test this criterion for viscous vortices, additional simulations are performed with different initial aspect ratios a_0/b_0. Equation (6) was used to predict the value of $\zeta_{0,cr}$ for a given a_0/b_0. For each a_0/b_0 considered, a series of simulations varying ζ_0 was performed until a pair was found to bracket the boundary between merging and separation regimes. An empirical estimate for $\zeta_{0,cr}$ was then obtained using the midpoint of the two bracketing ζ_0 values. The results are presented in table 2. The findings affirm the expectation: the value of $\zeta_{0,cr}$ between separation and merging varies with a_0/b_0, and in fact these values correspond quite well with the predictions based on the point vortex model.

The above results indicate that in viscous flow, for the range of Re_Γ considered and for the duration of the simulations, there are two distinct flow regimes: merger and separation (without or with elongation), and the boundary of the regimes is described well by the modified point vortex model in (6). This may be expected if we consider that, in the case of inviscid flow, the vortex pair evolves with constant $\mu = \mu_0$ (constant Γ) and therefore $\mu_0 > \mu_{cr}$ in (5) still distinguishes the separation regime for finite-area vortices. In the case of viscous flow, this criterion (and therefore, $\zeta_0 < \zeta_{0,cr} < 0$) may also remain valid for indicating separative motion, since Γ (and therefore μ) remains nearly constant until any significant interaction occurs (maximum computed deviation of Γ_0 before the onset of merger was 5.25%).

In inviscid flow, if $\mu < \mu_{cr}$, periodic motion will prevail if the aspect ratio a/b remains below the critical value for merger. In viscous flow, for $\mu < \mu_{cr}$ ($\zeta_0 > \zeta_{0,cr}$), then if $a/b < (a/b)_{cr}$ the vortices follow trajectories similar to the point vortex periodic regime for some duration of time. However, a primary effect of viscosity is that the cores will diffuse and grow in time. If the vortices are sufficiently separated, the viscous growth of the cores may be described by

$$a^2(t) = a_0^2 + 4\nu t. \tag{8}$$

Eventually this growth causes $a(t)/b(t) > (a/b)_{cr}$, resulting in merger. Stationary or continued periodic flow regimes are therefore not expected for finite Re_Γ. However, the early phase of development may be considered a quasi-periodic phase whose duration depends on Re_Γ (as indicated in figures 4 and 5). This is consistent with the initial quasi-steady phase of development in the no-shear flow, during which $b(t)$ remains nearly constant while $a(t)$ grows by diffusion (Brandt and Nomura 2007).

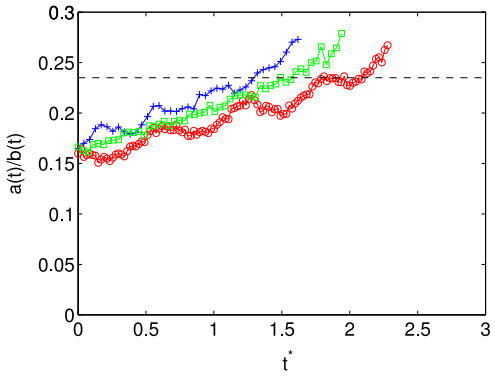

Figure 6. Aspect ratio $a(t)/b(t)$ as a function of convective time t^* for $\mathrm{Re}_\Gamma = 5000$. +: $\zeta_0 = 0.0045$, □: $\zeta_0 = 0$, ◯: $\zeta_0 = -0.0045$. Dashed line corresponds to $(a/b)_{cr} = 0.235$. Note that $a(t)$ is computed from simulation results using the azimuthal average of the radial location of maximum azimuthal velocity, then dividing by 1.12 to obtain an estimate for the second moment of vorticity (Brandt and Nomura 2007).

The onset of merger is identified as the time at which the vortices begin to significantly interact (transition from a diffusive-dominated to convective-dominated process), and this is effectively indicated by the deviation of $a^2(t)$ from its linear viscous growth (equation (8)) (see e.g. Brandt and Nomura 2007). This time is denoted here as $t^* = t^*_{cr}$ and values determined from the simulations (from computed $a^2(t)$) are shown in table 3. The results indicate that in favorable shear ($\zeta > 0$), $t^*_{cr} < t^*_{cr,\zeta=0}$, and in adverse shear ($\zeta < 0$), $t^*_{cr} > t^*_{cr,\zeta=0}$, indicating merger onset occurring earlier and later, respectively, than the time of merger onset observed in the no-shear case ($t^*_{cr,\zeta=0}$). At $\mathrm{Re}_\Gamma = 1000$, the vortices spread more rapidly relative to their advection and therefore the onset of merging occurs more quickly on the advective timescale than for $\mathrm{Re}_\Gamma = 5000$, otherwise the results are similar (table 3). We note that for these lower Reynolds number simulations, the vortices begin to interact very quickly on the t^* scale and so determination of the value of t^*_{cr} becomes difficult.

The time development of the vortex pair aspect ratio, $a(t)/b(t)$, is shown in figure 4 for $\mathrm{Re}_\Gamma = 5000$. For a pair of initially Gaussian vortices in viscous fluid with no shear, the onset of merger is found to occur at $(a/b)_{cr} = 0.235 \pm 0.006$ (Brandt and Nomura 2007), which is indicated by the dashed line in figure 6. Evaluating $a(t)/b(t)$ for $t^* = t^*_{cr}$ from table 3 gives $(a/b)_{cr}$ values of 0.230, 0.231, and 0.235 for $\zeta_0 = 0.0045$, 0, and −0.0045 respectively, for $\mathrm{Re}_\Gamma = 5000$. These results are in agreement with the reported $(a/b)_{cr}$ range.

Since favorable shear acts to periodically reduce $b(t)$, this will increase a/b values thereby promoting merger. Even in the inviscid case, Trieling *et al* (2010) found that favorable shear could induce merger even when $a_0/b_0 < (a/b)_{cr}$. In contrast, weakly adverse shear ($\zeta_{0,cr} < \zeta_0 < 0$) acts to periodically increase $b(t)$ which will tend to reduce a/b values and thereby impede merger. When viscosity is present, $a(t)$ grows in time, so when both shear and viscous effects are present $a(t)/b(t)$ increases but does not necessarily do so monotonically. The oscillatory behavior of $a(t)/b(t)$ may mean that the time of attaining $(a/b)_{cr}$ does not necessarily correspond to the start of merging, though no case was observed of $a(t)/b(t) = (a/b)_{cr}$ being attained and then the vortices failing to merge.

Table 3. Time to start of merging process t^*_{cr} for vortex pairs in the merging ζ_0 regime for $\mathrm{Re}_\Gamma = 5000$ and $\mathrm{Re}_\Gamma = 1000$ and $a_0/b_0 = 0.157$.

	$\mathrm{Re}_\Gamma = 5000$	$\mathrm{Re}_\Gamma = 1000$
ζ_0	t^*_{cr}	t^*_{cr}
0.0045	1.26	0.336
0	1.53	0.373
–0.0045	1.73	0.417

For the $\mathrm{Re}_\Gamma = 1000$ results, evaluating $a(t)/b(t)$ at the t^*_{cr} values from table 3 gives $(a/b)_{cr}$= 0.238, 0.233, and 0.229 for $\zeta_0 = 0.0045$, 0, and –0.0045 respectively. These values are also in agreement with the merging criterion found for vortex pairs without shear.

5. Conclusion

The interactions of two equal co-rotating vortices under the influence of both viscosity and uniform background shear have been investigated using numerical simulations. It is found that the observed interactions can be classified into two distinct regimes, merger and separation, depending on the relative significance of the background shear (as characterized by ζ_0) for a given vortex pair (as characterized by ζ_0 and a_0/b_0).

Early in the flow development when the vortices are sufficiently separated and Γ is constant, their motion is altered by the shear, as described by the point vortex model, while their cores grow by viscous diffusion. During this time, the primary effect of shear is to vary $b(t)$ in time, while the primary effect of viscosity is to increase $a(t)$ in time. If the shear is both adverse and sufficiently strong, i.e., $\zeta_0 < \zeta_{0,cr} < 0$, $b(t)$ will increase indefinitely: this is the separation regime. In this case, if the shear, and thus the corresponding strain rate, is very strong, the vortices will also begin to elongate. If the shear is only weakly adverse or favorable, i.e. $\zeta_0 > \zeta_{0,cr}$, the vortices will revolve along elliptical trajectories with $b(t)$ periodically increasing or decreasing, respectively, as $a(t)$ grows in time until $a(t)/b(t)$ reaches $(a/b)_{cr}$ and the vortices begin to merge into a single compound vortex: this is the merger regime. The value of $(a/b)_{cr}$ determined from the simulations is found to be within the range previously reported for the no-shear case, $(a/b)_{cr} = 0.235 \pm 0.006$, over the range of parameters tested. The boundary separating the merger and separation regimes, $\zeta_{0,cr}$, is accurately predicted by the point vortex model and varies with a_0/b_0. Both of these critical values were found to be largely independent of Re_Γ over the range considered. Therefore, for the purpose of determining whether a co-rotating viscous vortex pair in the presence of background shear will merge, $\zeta_0 > \zeta_{0,cr}\,(a_0/b_0)$ constitutes a sufficient criterion.

Although a study of the long time evolution of the vortex pair is beyond the scope of this paper, some remarks can be made based on the results presented here. As the vortices diffuse and spread, their peak vorticity will decrease. In the separation regime, since $|\zeta(t)| = |S/\omega(t)|$ increases in time, it is expected that vortices initially exhibiting separation without elongation would eventually exhibit elongation if simulations were to run long enough and boundary effects were to remain inconsequential. Likewise, in the merger regime, the compound vortex formed by merger would ultimately diffuse until it too would become weak enough to be deformed by the background strain and elongate.

Thus, in contrast with the case of inviscid flow where periodic motion, merger, and separation with and without elongation constitute distinct regimes determined by initial conditions (Trieling *et al* 2010), viscous vortices may evolve in time through these flow conditions. If sufficiently strong adverse shear is present, the vortices will separate and thereby limit any mutual interaction. Otherwise, the vortices will develop in a manner similar to the no-shear flow. Initially, a quasi-steady diffusive phase will occur in which the vortices revolve in an orbit; the effect of shear is to vary $b(t)$ along the orbit. This is followed by a convective/merging phase; where favorable/adverse shear promotes/hinders mutual interaction and merger. Finally, another diffusive phase is expected to occur in which the single vortex may ultimately be deformed and elongated by the background shear.

It is possible that the efficacy of the inviscid/point vortex predictions when viscous effects are present breaks down at very low Reynolds numbers, when the spreading is so rapid as to violate the 'sufficiently separated' requirement very shortly after the start of the simulation. In such cases merger may result even when their ζ_0 and a_0/b_0 might correspond to the separation regime as indicated by the point vortex criterion. Furthermore, it is known that interactions of unequal vortices in the absence of shear produce a richer variety of outcome regimes than do symmetric pairs (e.g. Brandt and Nomura 2010), so the regimes of interaction of such pairs when shear is present are undoubtedly more complex and nuanced than those presented here. These topics remain to be addressed in future work.

References

Benzi R, Patarnello S and Santangelo P 1987 On the statistical properties of two-dimensional decaying turbulence *Europhys. Lett.* **3** 811–8

Brandt L K and Nomura K K 2007 The physics of vortex merger and the effects of ambient stable stratification *J. Fluid Mech.* **592** 413–46

Brandt L K and Nomura K K 2010 Characterization of the interactions of two unequal co-rotating vortices *J. Fluid Mech.* **646** 233–53

Cerretelli C and Williamson C H K 2003 The physical mechanism for vortex merging *J. Fluid Mech.* **475** 41–77

Dritschel D G and Waugh D W 1992 Quantification of the inelastic interaction of unequal vortices in two-dimensional vortex dynamics *Phys. Fluids* A **4** 1737–44

Gerz T, Schumann U and Elghobashi S E 1989 Direct numerical simulation of stratified homogeneous turbulent shear flows *J. Fluid Mech.* **200** 563–94

Kimura Y and Hasimoto H 1985 Motion of two identical point vortices in a simple shear flow *J. Phys. Soc. Japan* **54** 4096–8

Le Dizès S and Verga A 2002 Viscous interactions of two co-rotating vortices before merging *J. Fluid Mech.* **467** 389–410

Maze G, Carton X and Lapeyre G 2004 Dynamics of a 2D vortex doublet under external deformation *Regul. Chaotic Dyn.* **9** 477–94

Melander M V, Zabusky N J and McWilliams J C 1988 Symmetric vortex merger in two dimensions: causes and conditions *J. Fluid Mech.* **195** 303–40

Meunier P, Ehrenstein U, Leweke T and Rossi M 2002 A merging criterion for two-dimensional co-rotating vortices *Phys. Fluids* **24** 2757–66

Overman E A and Zabusky N J 1982 Evolution and merger of isolated vortex structures *Phys. Fluids* **25** 1297–305

Perrot X and Carton X 2010 2D vortex interaction in a non-uniform flow *Theor. Comput. Fluid Dyn.* **24** 95–100

Saffman P G and Szeto R 1980 Equilibrium shapes of a pair of equal uniform vortices *Phys. Fluids* **23** 2339–42

Trieling R R, Dam C E C and van Heijst G J F 2010 Dynamics of two identical vortices in linear shear *Phys. Fluids* **22** 117104

The contents of this chapter are published in Fluid Dynamics Research. Keiko K. Nomura. "Interaction of two equal co-rotating viscous vortices in the presence of background shear", Fluid Dyn. Res., 46 (3), 031423, 2014. The dissertation author was the primary researcher and the research supervisor was the co-author of the paper.

Chapter 4

A quantitative assessment of viscous asymmetric vortex pairs

A quantitative assessment of viscous asymmetric vortex pair interactions

Patrick J. R. Folz[1] **and Keiko K. Nomura**[1,†]

[1]Department of Mechanical and Aerospace Engineering, University of California, San Diego, 9500 Gilman Drive, La Jolla, CA 92093-0411, USA

(Received 4 December 2016; revised 21 July 2017; accepted 27 July 2017)

The interactions of two like-signed vortices in viscous fluid are investigated using two-dimensional numerical simulations performed across a range of vortex strength ratios, $\Lambda = \Gamma_1/\Gamma_2 \leqslant 1$, corresponding to vortices of circulation, Γ_i, with differing initial size and/or peak vorticity. In all cases, the vortices evolve by viscous diffusion before undergoing a primary convective interaction, which ultimately results in a single vortex. The post-interaction vortex is quantitatively evaluated in terms of an enhancement factor, $\varepsilon = \Gamma_{end}/\Gamma_{2,start}$, which compares its circulation, Γ_{end}, to that of the stronger starting vortex, $\Gamma_{2,start}$. Results are effectively characterized by a mutuality parameter, $MP \equiv (S/\omega)_1/(S/\omega)_2$, where the ratio of induced strain rate, S, to peak vorticity, ω, for each vortex, $(S/\omega)_i$, is found to have a critical value, $(S/\omega)_{cr} \approx 0.135$, above which core detrainment occurs. If MP is sufficiently close to unity, both vortices detrain and a two-way mutual entrainment process leads to $\varepsilon > 1$, i.e. merger. In asymmetric interactions and mergers, generally one vortex dominates; the weak/no/strong vortex winner regimes correspond to $MP <, =, >1$, respectively. As MP deviates from unity, ε decreases until a critical value, MP_{cr} is reached, beyond which there is only a one-way interaction; one vortex detrains and is destroyed by the other, which dominates and survives. There is no entrainment and $\varepsilon \sim 1$, i.e. only a straining out occurs. Although $(S/\omega)_{cr}$ appears to be independent of Reynolds number, MP_{cr} shows a dependence. Comparisons are made with available experimental data from Meunier (2001, PhD thesis, Université de Provence-Aix-Marseille I).

Key words: vortex dynamics, vortex flows, vortex interactions

1. Introduction

Vortex interactions are an important and often dominant aspect of many fundamental and practical flows. In the case of decaying two-dimensional turbulence, the interaction of two like-signed vortices is considered to be a driving mechanism for the inverse energy cascade, producing larger scales through the merging of two vortices, and breaking down smaller, weaker vortices (McWilliams 1990; Tabeling 2002). This has led to the development of models and scaling laws for two-dimensional turbulence that employ simplified descriptions of vortex merger, typically based on the highly idealized case of inviscid symmetric merger (Carnevale *et al.* 1991; Riccardi, Piva

† Email address for correspondence: knomura@ucsd.edu

& Benzi 1995; Sire, Chavanis & Sopik 2011). In order to improve such models, and more generally to better understand two-dimensional vortex interactions, more accurate characterizations of these vortex interactions and their outcomes are needed.

Most fundamental studies of interacting co-rotating vortices (see, e.g. Brandt & Nomura (2010) for a review) consider inviscid flow and symmetric vortex pairs, wherein the two vortices are equal in size and strength. These studies indicate that two equal vortices will merge when they are separated within a critical distance, i.e. if $b/a \leqslant (b/a)_{cr}$, where b is the linear distance between vorticity peaks and a is the vortex radius (e.g. Saffman & Szeto 1980; Overman II & Zabusky 1982). Vortices separated beyond this critical value revolve about each other and the two vortices persist in time: at intermediate distances, the vortices deform each other and exchange vorticity while at large distances they do not interact significantly. These three regimes (merger, exchange, no significant interaction) are well characterized by the initial b/a and $(b/a)_{cr}$ (Waugh 1992). For the case of Rankine (uniform vorticity) vortices, a merging efficiency,

$$H = \Gamma_{tot,f}/\Gamma_{tot,0}, \tag{1.1}$$

which compares the total circulation of the final vortex, $\Gamma_{tot,f}$, to the combined total circulation of the original two vortices, $\Gamma_{tot,0}$, was evaluated by Waugh (1992). Results indicate that the resulting compound vortex may have less circulation than the total of the original vortices due to the ejection of vorticity from the cores in the form of filaments during the merging process.

Inviscid interactions between two unequal vortices, i.e. an asymmetric pair, are found to produce more varied outcomes (e.g. Dritschel & Waugh 1992; Yasuda & Flierl 1997; Trieling, Velasco Fuentes & van Heijst 2005). Dritschel & Waugh (1992) considered a pair of Rankine vortices with equal vorticity and unequal areas. They found that within some separation distance, which varied with the asymmetry of the pair, one vortex ejects a filament of vorticity which then may or may not be incorporated into the other. Interactions could then be divided into five regimes based on the values of the enhancement factor for each vortex $i = 1, 2$,

$$\epsilon_i = \Gamma_{i,f}/\Gamma_{i,0}, \tag{1.2}$$

which compares the final circulation of each vortex to its circulation at the start of interaction. Outcomes with the initially larger vortex unchanged $\epsilon_1 = 1$ and the smaller vortex reduced $\epsilon_2 < 1$ correspond to partial or complete straining-out regimes, the latter with $\epsilon_2 = 0$ (i.e. only one vortex survives). Outcomes with the initially larger vortex enhanced, i.e. $\epsilon_1 > 1$, and the smaller vortex reduced $\epsilon_2 < 1$ correspond to partial or complete merger regimes, the latter having $\epsilon_2 = 0$ (i.e. only one vortex survives). An elastic interaction regime is then associated with the limiting case in which $\epsilon_1 = 1$ and $\epsilon_2 = 1$. Results from contour surgery simulations were presented on a regime diagram as a function of the ratio of initial vortex radii a_2/a_1 and non-dimensional separation distance b/a_1 and showed complicated dependencies on these parameters. Although this study suggests that only the initially stronger vortex can be enhanced, in general the weaker vortex could instead be the enhanced final vortex, i.e. be the 'winner' of the interaction (Melander, Zabusky & McWilliams 1987*b*). The exact conditions for this to occur are not yet entirely clear. Trieling *et al.* (2005) consider various vorticity distributions, including a Gaussian profile, and asymmetric vortex pairs with equal-vorticity/unequal-area and equal-area/unequal-vorticity combinations. Regime maps comparable to those of Dritschel and Waugh (indicating the five regimes)

were presented and again complex dependencies on the parameters considered (radii ratio, peak vorticity ratio and initial separation distance) were exhibited, and were found to also depend on the vorticity distribution. Although enhancement factors were evaluated, the flow regimes in this study were ultimately identified by visual inspection due to ambiguities in these quantities when the two vortices exchange fluid to negligible net effect.

In viscous flow, diffusion causes the vortices to grow in time, so b/a will thereby inevitably be reduced below $(b/a)_{cr}$. The interaction of two equal vortices thus always results in merger (Melander, Zabusky & McWilliams 1988). Distinct flow regimes occur in the time development of the vortex pair (Melander *et al.* 1988; Le Dizès & Verga 2002; Meunier *et al.* 2002; Cerretelli & Williamson 2003; Brandt & Nomura 2007). In the first (diffusive) phase of development, when b/a is sufficiently large, the flow is dominated by the viscous growth of the vortices. During this time, each vortex responds to the strain field induced by the other, which elliptically deforms the vortices. In the second (convective) phase of development, the induced strain and deformation leads to the detrainment of core vorticity. The detrained fluid is circulated (exchanged) between vortices and the weakened cores eventually undergo mutual entrainment. These processes result in the primary motion of the vortices towards each other (Huang 2005; Brandt & Nomura 2007). The onset of merger ($(b/a)_{cr}$) is considered to correspond to the start of the convective phase (Meunier *et al.* 2002). A third (second diffusive) phase consists of the eventual elimination of the two vorticity peaks of the merged structure, which occurs on a diffusive time scale (Meunier *et al.* 2002; Cerretelli & Williamson 2003), followed by axisymmetrization of the final structure (Melander, McWilliams & Zabusky 1987*a*).

Viscous interactions between two unequal vortices also ultimately result in a single vortex, although the vortex may not be enhanced, as in the inviscid flow straining-out regimes. A detailed study of the associated physics was carried out by Brandt & Nomura (2010) using numerical simulations. Three interactions were considered to occur: complete merger, partial merger and straining out. Here, although the inviscid flow regime terminology is used, the definitions of each are given in terms of the relative timing of core detrainment and core destruction. A critical strain rate parameter, corresponding to the establishment of core detrainment, was defined and determined for each vortex. The onset of merger was then considered to be the achievement of the critical strain rate parameter by both vortices. In the case of symmetric merger, the critical strain rate parameter was shown to be related to $(b/a)_{cr}$. Although the developed merging criterion and flow classification provide physical insight and allow for a more generalized characterization of the vortex interactions, it is not clear how it can be used in a practical manner. In particular, the classifications depend on the relative timing of the vortex detrainment and destruction processes, and the strain rate parameter is defined in the co-rotating frame. It is also noted that in this study, verification of merger and the extent of entrainment were determined by visual inspection rather than a more objective and quantitative means. Jing, Kanso & Newton (2012) also examined the viscous interaction of an asymmetric pair (along with a symmetric pair) using a low-dimensional core growth model and identified a sequence of topological bifurcations in the instantaneous streamline patterns as the flow evolves into a single Gaussian vortex, although notably their model did not include an entrainment process. To the authors' knowledge, no quantitative assessment of the interactions have been performed for either symmetric or asymmetric pairs in viscous flows, likely due to difficulties associated with the continuous development, both in space and time, inherent to these flows.

The present study seeks to extend the ϵ-type framework of Dritschel & Waugh (1992) to viscous flow, and to use these metrics to quantitatively assess for the first time co-rotating viscous vortex pair interactions. Two-dimensional numerical simulations are performed for a wide range of initial asymmetries including both unequal size and unequal peak vorticity, allowing for more possible outcomes and enabling a more general characterization of these flows. A procedure is developed which allows the vortex cores and associated properties to be monitored in time, thereby enabling the identification of the times of start (t^*_{start}) and end (t^*_{end}) of the primary (convective) interaction. Values of an appropriately defined enhancement factor, ε, and merging efficiency, η, are then evaluated and used to objectively assess each interaction. Since these viscous interactions all result in a single vortex, there are two general outcomes: enhancement (merger) and no enhancement (straining out). A new parameter, which measures the degree of mutuality of the interaction, is defined based on the relative straining of each vortex. It is found to effectively characterize ε and η of the post-interaction vortex for the range of parameters considered and observed interaction regimes. Results are compared with available experimental data of Meunier (2001).

The flow parameters and numerical simulations are described in § 2. The basic time development of the flows and the associated physical processes are first reviewed in § 3. The procedure for the quantitative assessment is then developed in § 4. Results are presented in § 5. The new parametrization is described in § 6. This is followed by comparisons with the lower Reynolds number simulations and experimental results in § 7. Summary and conclusions are given in § 8 along with some implications for two-dimensional turbulence.

2. Flow set-up and parameters

The two-dimensional flow initially consists of two Gaussian vortices $i = 1, 2$, separated by a distance b_0 (figure 1). Each vortex has an initial circulation $\Gamma_{i,0} = \pi a^2_{i,0}\omega_{i,0}$, where $a_{i,0}$ is the initial vortex radius and $\omega_{i,0}$ is the initial peak vorticity, giving an initial aspect ratio $a_{2,0}/b_0$ and circulation ratio $\Lambda_0 = \Gamma_{1,0}/\Gamma_{2,0} \leqslant 1$. The simulations cover three subcategories of asymmetric pairs: those having unequal vorticity peaks but equal areas (UPEA: $\Lambda_0 = \omega_{1,0}/\omega_{2,0} < 1$), those having equal peaks but unequal areas (EPUA: $\Lambda_0 = a^2_{1,0}/a^2_{2,0} < 1$) and those having both unequal peaks and unequal areas (UPUA: $\Lambda_0 = a^2_{1,0}\omega_{1,0}/a^2_{2,0}\omega_{2,0} < 1$), as well as the limiting case of a symmetric pair ($\Lambda_0 = a^2_{1,0}/a^2_{2,0} = \omega_{1,0}/\omega_{2,0} = 1.0$). The circulation Reynolds number, $Re_\Gamma = \Gamma_{2,0}/\nu = 5000$, is based on the stronger vortex. Additional UPEA simulations are performed with $Re_\Gamma = 1000$ in order to compare with the experimental data. All simulations are performed with $a_{2,0}/b_0 = 0.157$. This value satisfies computational requirements (see Brandt & Nomura 2007) and is comparable to those in the experiments. The simulations performed are summarized in tables 1 and 2. All times are given in terms of a convective time scale based on the period of revolution of two point vortices $T = 2\pi^2 b_0^2/(0.5\Gamma_{2,0}(1 + \Lambda_0))$, $t^* = t/T$.

The flow is incompressible and is integrated in time using finite-difference schemes on a uniform grid with periodic boundary conditions (see Gerz, Schumann & Elghobashi 1989; Orlandi 2000). The domain consists of 2048^2 points with side lengths of $L_x = L_z = 24b_0$, giving approximately 27 points across the larger core. Resolution and domain size testing on both local and integrated quantities showed these values to be sufficient; for further discussion see Brandt & Nomura (2007).

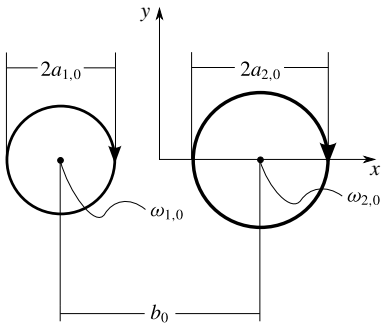

FIGURE 1. The initial condition consisting of two Gaussian vortices $i = 1, 2$ each having initial radius $a_{i,0}$, peak vorticity $\omega_{i,0}$, separated by peak–peak distance b_0. Initial aspect ratio $a_{2,0}/b_0 = 0.157$ and circulation ratio $\Lambda_0 = \Gamma_{1,0}/\Gamma_{2,0} \leqslant 1$.

3. Basic flow behaviour

The flow development of three illustrative cases, a symmetric and two UPEA asymmetric pairs ($\Lambda_0 = 1.0, 0.90, 0.70$), is presented in figure 2, with vorticity contour plots given in each of the upper rows of figure 2(*a–c*). Although only UPEA asymmetric pairs are shown, these cases depict the key processes involved in all interactions, which were investigated in detail by Brandt & Nomura (2007, 2010). Here, we review these processes and consider further details in order to facilitate the current analysis.

The mutually induced flow of the two vortices initially causes the vortices to revolve about each other with a nearly constant rotation rate ($\approx 2\pi/T$) and separation. These features are indicated in figure 3, which shows the translational speed of the vorticity peak of each vortex, and figure 4, which shows the trajectories of the vorticity peaks, for each of the cases shown in figure 2. The flow begins in a diffusive phase in which the flow evolves from the initial condition (column 1 of figure 2) primarily by viscous spreading of each vortex, which increases core size. The vortices also deform elliptically in response to the induced strain field of the other vortex. In the co-rotating frame, in the vicinity of the hyperbolic points where the vorticity magnitude is low, a tilt in the vorticity contours with respect to the streamlines develops (Brandt & Nomura 2006). This results in filamentation at the outer ends of the vortex pair. At the central (hyperbolic) point, the tilt results in detrainment of core vorticity which is circulated and exchanged between the vortices. It is the establishment of this core detrainment process that is the predominant cause of the change from diffusion-dominated to convective-dominated behaviour, and is considered to be the beginning of the primary convective interaction.

In the symmetric pair (figure 2*a*), the detrainment process is reciprocal and both vortices are detrained at the same rate (figure 2*a*, columns 2–3). This weakens the vortex cores and at some point, they become mutually entrained (figure 2*a*, columns 3–4) which corresponds to a rapid movement of the cores towards each other (figure 3*a*). The original vortices are destroyed as they intertwine (figure 4*a*) and the flow is transformed into a single compound structure (figure 2*a*, column 4), which continues to axisymmetrize (figure 2*a*, column 5).

In the asymmetric pairs (figure 2*b*,*c*), the greater induced strain rate at the weaker vortex results in earlier deformation and detrainment (figure 2*b*,*c*, columns 2–3). As the disparity of the vortices increases, more significant detrainment and even

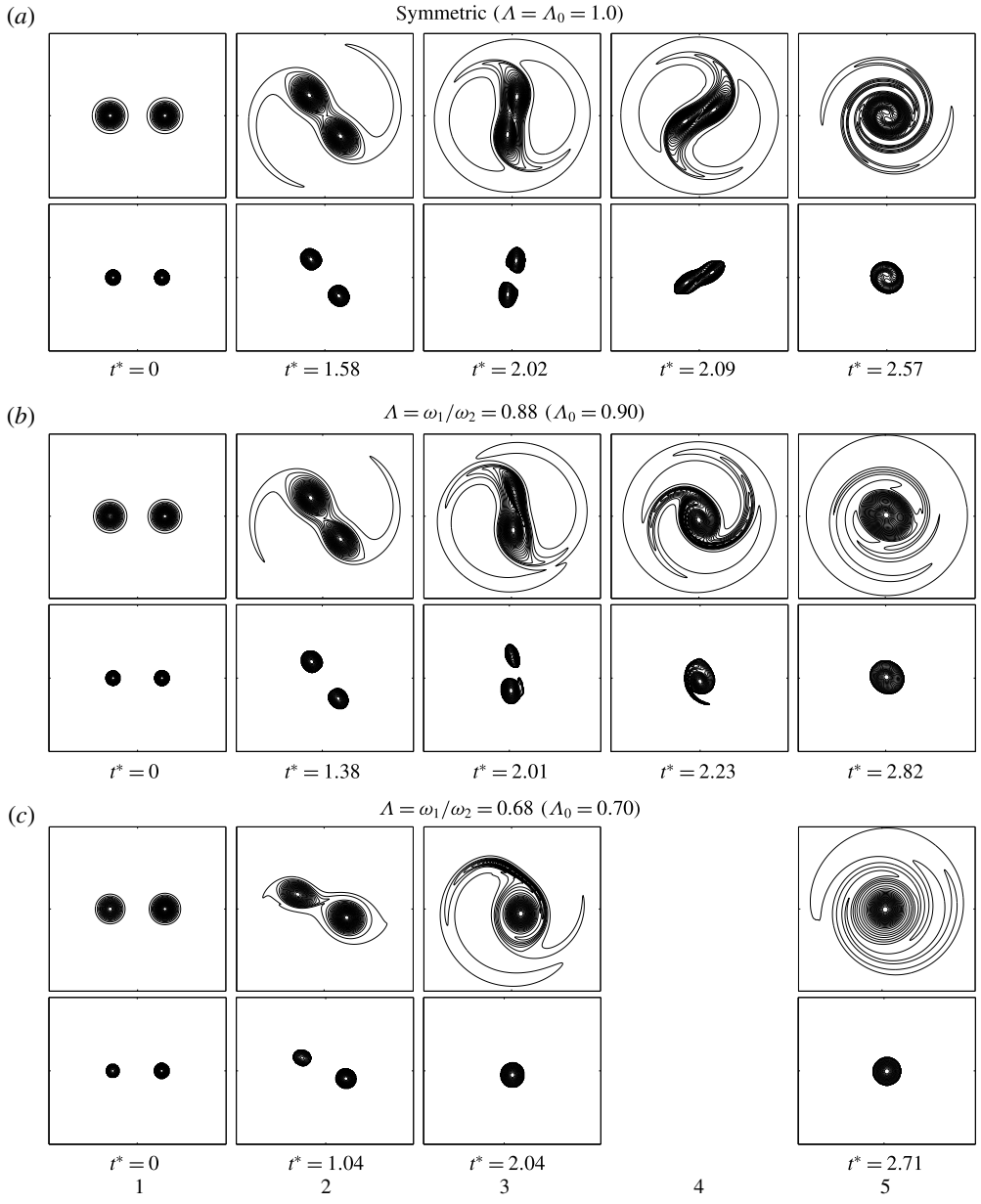

FIGURE 2. Vorticity contours at the initial condition and key times during the interaction for (*a*) symmetric ($\Lambda = \Lambda_0 = 1.0$) and UPEA (*b*) $\Lambda = 0.88$ ($\Lambda_0 = 0.90$) and (*c*) $\Lambda = 0.68$ ($\Lambda_0 = 0.70$) cases at $Re_\Gamma = 5000$. For each case, the upper row depicts the vorticity contours of the total flow and the lower row depicts the vorticity contours within the region considered 'core' using $II > II_t$. Column 1: initial condition; column 2: $t^* = t^*_{start}$; column 3: $t^* = t^*_{det}$; column 4: $t^* = t^*_{ent}$ (omitted for $\Lambda = 0.68$ since no entrainment process occurs); column 5: axisymmetrization. See § 4 for details and definitions of t^*_{start}, t^*_{det} and t^*_{ent}.

	Starting (t^*_{start})		Initial ($t^* = 0$)		Ending (t^*_{end})		Weak
	Λ	ω_1/ω_2	Λ_0	$\omega_{1,0}/\omega_{2,0}$	ε	η	winner
Symmetric	1.00	1.00	1.00	1.00	2.10	1.05	
	0.93	0.95	0.95	0.95	1.93	1.00	
	0.88	0.90	0.90	0.90	1.83	0.98	
	0.82	0.85	0.85	0.85	1.74	0.95	
	0.80	0.82	0.825	0.825	1.58	0.88	
	0.79	0.81	0.8125	0.8125	1.49	0.84	
UPEA	0.78	0.80	0.80	0.80	1.33	0.75	
	0.77	0.78	0.785	0.785	1.08	0.61*	
	0.76	0.77	0.775	0.775	1.07	0.61*	
	0.72	0.75	0.75	0.75	1.04	0.60*	
	0.68	0.70	0.70	0.70	1.02	0.61*	
	0.63	0.65	0.65	0.65	1.02	0.63*	
	0.58	0.60	0.60	0.60	1.01	0.64*	
	0.90	0.95	0.90	1.00	1.82	0.96	
EPUA	0.79	0.91	0.80	1.00	1.69	0.95	
	0.70	0.90	0.70	1.00	1.04	0.62*	
	0.55	0.80	0.60	1.00	1.01	0.65*	
	0.92	1.18	0.90	1.82	1.84	0.96	X
	0.91	1.16	0.90	1.67	1.87	0.98	X
	0.91	1.11	0.90	1.54	1.93	1.01	X
	0.91	1.09	0.90	1.43	1.95	1.02	X
	0.90	1.04	0.90	1.25	2.00	1.05	
	0.89	0.99	0.90	1.11	1.91	1.01	
	0.86	1.11	0.85	1.82	1.91	1.03	X
	0.85	1.10	0.85	1.67	1.91	1.03	
UPUA	0.84	0.96	0.85	1.11	1.77	0.97	
	0.80	1.08	0.80	2.00	1.88	1.04	
	0.80	1.03	0.80	1.67	1.81	1.01	
	0.78	0.92	0.80	1.11	1.74	0.98	
	0.68	0.95	0.70	1.67	1.60	0.95	
	0.68	0.92	0.70	1.43	1.46	0.87	
	0.69	0.91	0.70	1.25	1.32	0.78	
	0.67	0.85	0.70	1.11	1.08	0.65*	
	0.58	0.85	0.60	1.67	1.03	0.6*	
	0.57	0.77	0.60	1.11	1.02	0.65*	

TABLE 1. Summary of simulation parameters and results for $Re_\Gamma = 5000$. Values for ε and η are evaluated at t^*_{end}. Starting $\Lambda = \Gamma_1/\Gamma_2$ is evaluated at t^*_{start}. See § 4 for details and definitions of t^*_{start} and t^*_{end}. $*$ indicates that the straining-out regime has been reached and η is therefore not a meaningful physical quantity. 'Weak winner' indicates that the peak of the weaker initial vortex becomes the peak of the resulting post-interaction vortex (see § 5).

destruction of the weaker vortex may occur before detrainment can be established at the stronger vortex. The implication is that either a mutual but unequal entrainment process occurs ($\Lambda_0 = 0.90$, figure 2*b*, columns 3–4) or no entrainment occurs ($\Lambda_0 = 0.70$, figure 2*c*, column 3). In the former case, there is some intertwinement (figure 4*b*) with only the weaker vortex destroyed. The stronger vortex entrains

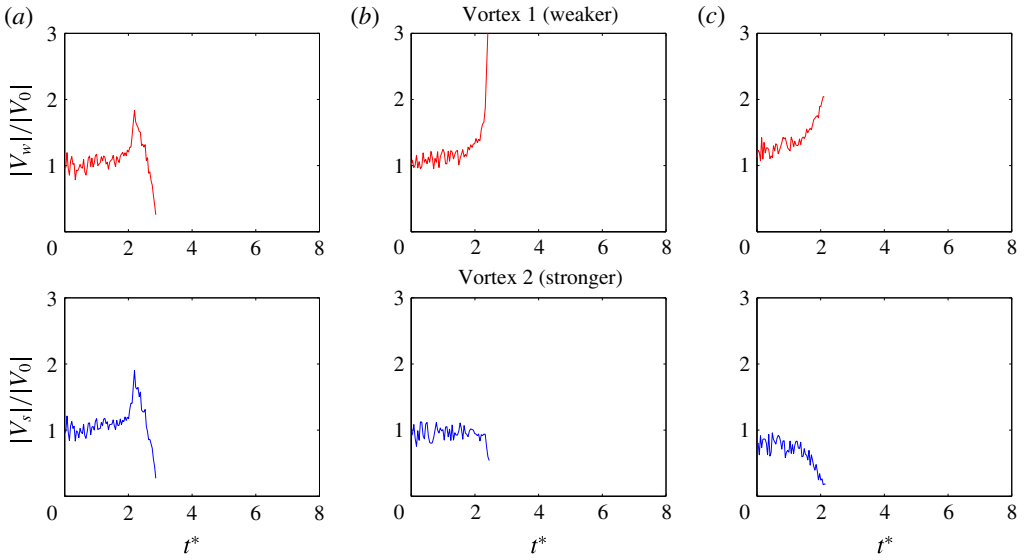

FIGURE 3. (Colour online) Time development of the normalized translational speed $|V|/|V_0|$ of each of the vorticity peaks, based on the initial translational speed of each vortex V_0, for the cases depicted in figure 2. (*a*) $\Lambda = \Lambda_0 = 1.0$, (*b*) $\Lambda = 0.88$ ($\Lambda_0 = 0.90$), (*c*) $\Lambda = 0.68$ ($\Lambda_0 = 0.70$).

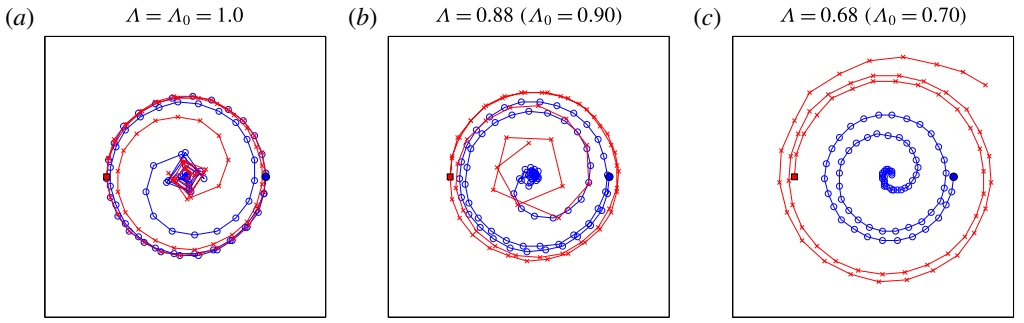

FIGURE 4. (Colour online) Trajectories of vortex peaks for the cases depicted in figure 2. Red $\times$: vortex 1 (weaker), blue $\bigcirc$: vortex 2 (stronger). Initial positions indicated by filled square and circle respectively. Plotted data points correspond to intervals of approximately 200 time steps.

vorticity from the weaker vortex thereby yielding a compound vortex. In the latter case, there is no apparent interpenetration of vorticity from the original vortices (figure 4*c*); the weaker vortex is destroyed while the stronger vortex remains, surrounded by vorticity from the weaker vortex.

The entrainment mechanism can be understood by considering the influence that each vortex exerts on the other. Huang (2005) elucidated this in a Lagrangian study of symmetric merger which showed that the vorticity that is detrained from one core and advected around the companion core, induces motion of the companion core towards it. In the symmetric case, since the cores are equal, the process is reciprocal and results in the rapid motion of the vorticity peaks towards each other as they are

mutually entrained, as observed in figures 3(*a*) and 4(*a*) ($\Lambda_0 = 1.0$). In the asymmetric case, as discussed in Brandt & Nomura (2010), the outcome depends on the relative time scales of each core's detrainment and destruction. Consider two vortices 1 and 2 with $\Gamma_1/\Gamma_2 < 1$. If vortex 1 is moderately weaker than vortex 2, although vortex 2 will detrain vortex 1 more quickly, vortex 1 will still detrain vortex 2, and the associated detrained vorticity will advect it inwards towards vortex 2. Since both vortices detrain, subsequently a mutual but non-reciprocal entrainment process will occur. This is observed in figures 3(*b*) and 4(*b*) ($\Lambda_0 = 0.9$) which show vortex 1 accelerating with its trajectory moving inward while vortex 2 maintains its induced motion. Since vortex 1 is eventually eroded, its advection inward is limited, and only fluid from vortex 2 will become the centre of the resulting flow (figure 4*b*). If vortex 1 is significantly weaker than vortex 2, it will be unable to detrain vortex 2 before it is eroded away by vortex 2 and thus will not be advected inwards. Hence, in this case, entrainment will not occur. This is seen in figures 3(*c*) and 4(*c*) ($\Lambda_0 = 0.7$), wherein the peak of vortex 1 accelerates somewhat as it weakens but undergoes no inward motion, while vortex 2 decelerates as it establishes itself as the sole vortex in the flow. This is consistent with the results presented in a Lagrangian study of a highly asymmetric pair with $\Lambda_0 = \omega_1/\omega_2 = 0.5$ by Huang (2006).

In all cases, whether or not entrainment occurs, by the end of the primary convective phase there exists only a single vortex structure, comprised of fluid from one or both starting cores, shown in column 4 of figure 2 for $\Lambda_0 = 1.0$, 0.9 cases and in column 3 for $\Lambda_0 = 0.7$ case (since no entrainment occurs). Beyond the convective phase, the resulting structure undergoes a final phase (column 5 of figure 2) during which it axisymmetrizes into a circular Gaussian vortex which continues to evolve by viscous diffusion.

4. Assessing the product of asymmetric interactions

In order to quantitatively assess the interaction, an ϵ-type enhancement factor is evaluated,

$$\varepsilon \equiv \frac{\Gamma_{end}}{\Gamma_{2,start}}, \tag{4.1}$$

and, since ε (Γ_{end}) depends directly on the total available circulation of the starting pair, a corresponding merging efficiency,

$$\eta \equiv \frac{\Gamma_{end}}{\Gamma_{tot,start}}, \tag{4.2}$$

is also considered. Both quantities are based on the circulation of the vortex, Γ_{end}, at the end time of the interaction (t^*_{end}) relative to the circulation of the stronger vortex, $\Gamma_{2,start}$, and of the total circulation of both vortices combined, $\Gamma_{tot,start}$, respectively, at the starting time of the interaction (t^*_{start}). Since the key processes that lead to a single vortex occur in the primary convective phase, the vortex pair interaction is considered to be the primary convective interaction only (see appendix A), and the start and end times are considered to be those of this phase.

In order to evaluate (4.1) and (4.2) for viscous flow, the vortex cores must be identified in a consistent manner throughout the entire flow development including the transition from two vortices into one. To do this, a criterion is used based on the second invariant of the velocity gradient tensor: $II = 1/2(\omega^2/2 - S^2) > II_t$, where II_t is an arbitrary threshold level (Hunt, Wray & Moin 1988). For the present study, the

threshold level is set by $II_t^* \equiv II_t(t)/II_{peak}(t) = 0.10$, where $II_{peak}(t)$ is the instantaneous value of II at the location of the higher of the values of II_i evaluated at the location of each vorticity peak $i = 1, 2$ (or at the location of the only peak, if only one exists) unless otherwise noted. The value $II_t^* = 0.10$ corresponds to the characteristic radius of a single isolated Gaussian vortex based upon the second moment of vorticity, $r = a_\omega$, and is therefore used to identify the cores throughout the present study (Saffman 2001; Meunier *et al.* 2002). For more discussion of the choice of II_t, see appendix A. Each lower row of figure 2 depicts the portion of the flow considered to be core by $II > II_t$. It is seen that low-level peripheral and filamentary vorticity is excluded and the transformation of the flow from two distinct structures into one is captured.

Since the interaction between two isolated co-rotating vortices in viscous fluid always ultimately results in a single vortex, aggregate area and circulation of the vortex core(s) are evaluated by

$$A_{II}(t) = \int_{II>II_t} \mathrm{d}A \tag{4.3}$$

and

$$\Gamma_{II}(t) = \int_{II>II_t} \omega \, \mathrm{d}A, \tag{4.4}$$

where $\mathrm{d}A$ refers to an area element of fluid (properties of each individual vortex $i = 1, 2$ are computed similarly using a separate $II_{t,i}$ for each, not shown). While this means that the definition of the weaker vortex core is somewhat inconsistent across Λ, by monitoring the properties continuously, the times of start (t^*_{start}) and end (t^*_{end}) of the interaction can be identified without presupposing when the vortices are destroyed or when a new one is formed. Illustrative plots of $A_{II}(t)$ and $\Gamma_{II}(t)$ are presented in figure 5 which correspond to the cases depicted in figure 2. The aggregate properties are normalized by their values at the initial condition. Equivalent plots for a single Gaussian vortex having the same Re_Γ as one member of the symmetric pair ($Re_\Gamma = 5000$) are also included in figure 5(*d*) for reference. In this case, $A_{II}(t)$ increases linearly in time while $\Gamma_{II}(t)$ remains very nearly constant, as expected, which verifies the evaluation of (4.3) and (4.4). Prior to t^*_{start}, each individual vortex's $\Gamma_{II,i}$ and $A_{II,i}$ evolve similarly to those of the single vortex (not shown).

In each of the pair interactions in figure 5(*a–c*), at first $A_{II}(t)$ grows linearly by viscous diffusion (i.e. during the first diffusive phase), while $\Gamma_{II}(t)$ decreases slightly due to the intensifying induced strain. There is then a deviation from linear growth of $A_{II}(t)$ due to filamentation and core detrainment. Since the start of detrainment is considered to be the start of the main convective interaction, t^*_{start} is chosen to be the earlier time at which the evolution of either of the individual $A_{II,i}(t)$ begins a continual deviation from linear growth, reaching and thereafter maintaining at least a 0.5 % deviation from the $A_{II,i}$ value predicted by continual linear growth (note that computed ε and η are relatively insensitive to choice of t^*_{start} since Γ_{II} remains approximately constant prior to detrainment, see appendix A for details). This essentially corresponds to the departure from linear growth of aggregate $A_{II}(t)$ but is somewhat easier to detect in UPUA cases. Note that for the remainder of this study, unless otherwise noted, vortex parameters such as $\Gamma_{II,1}$, $\Gamma_{II,2}$, and Λ refer to quantities evaluated at t^*_{start}, and that cases are identified by these properties (e.g. $\Lambda = 0.88$ rather than $\Lambda_0 = 0.90$).

Subsequent to t^*_{start} in figure 5(*a–c*), $\Gamma_{II}(t)$ rapidly decreases to a local minimum, at time t^*_{det}, as vorticity detrains from the cores (column 3 of figure 2 corresponds to this

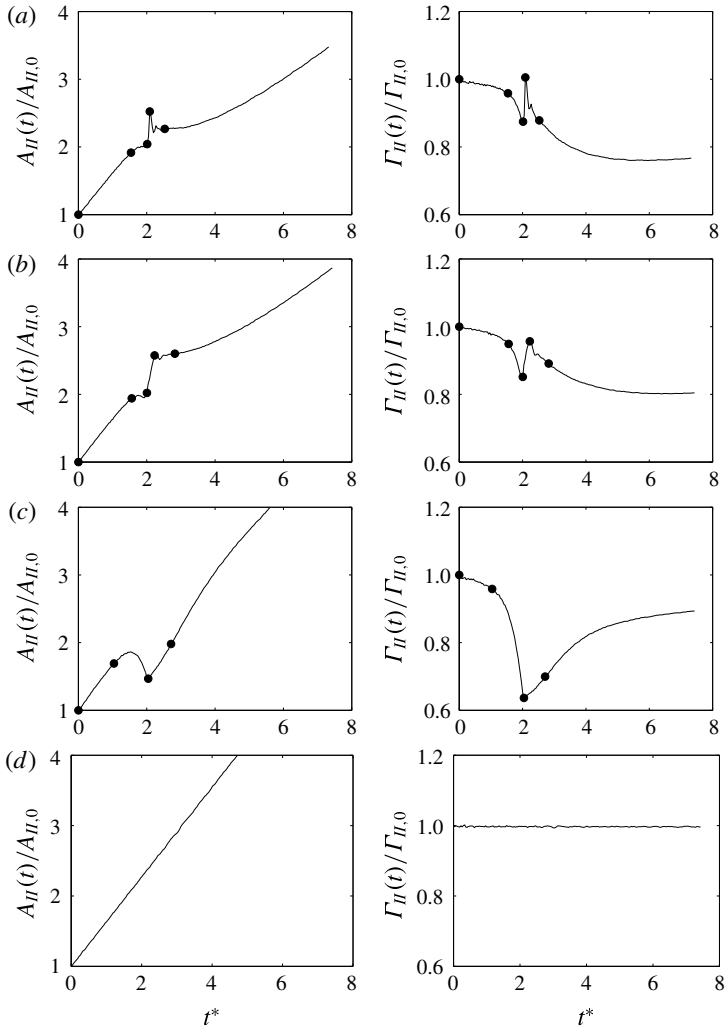

FIGURE 5. Time development of normalized aggregate core area $A_{II}(t)/A_{II,0}$ and circulation $\Gamma_{II}(t)/\Gamma_{II,0}$ (see (4.3) and (4.4)) for (*a–c*) the cases depicted in figure 2 and (*d*) a single vortex with same Re_Γ. The dots in (*a–c*) correspond to the times of the columns in figure 2. (*a*) Symmetric ($\Lambda = \Lambda_0 = 1.0$), (*b*) $\Lambda = \omega_1/\omega_2 = 0.88$ ($\Lambda_0 = 0.90$), (*c*) $\Lambda = \omega_1/\omega_2 = 0.68$ ($\Lambda_0 = 0.70$), (*d*) single vortex.

minimum). For vortices similar in strength (figure 5*a*,*b*), immediately after the time the $\Gamma_{II}(t)$ local minimum is reached, both $A_{II}(t)$ and $\Gamma_{II}(t)$ grow rapidly, with $\Gamma_{II}(t)$ quickly reaching a sharp peak, at time t^*_{ent}, before diminishing again (column 4 of figure 2 corresponds to this maximum). For vortices having more disparate strengths (figure 5*c*), after $A_{II}(t)$ and $\Gamma_{II}(t)$ reach their (simultaneous) local minima they both experience smooth, nonlinear behaviour without any spike, and ultimately return to single Gaussian vortex behaviour which is maintained until the end of the simulation. Note that there is not a sharp or sudden change in qualitative behaviour: intermediate cases contain qualitative elements of both (not pictured; these cases are treated as spike-occurring cases in all subsequent analysis).

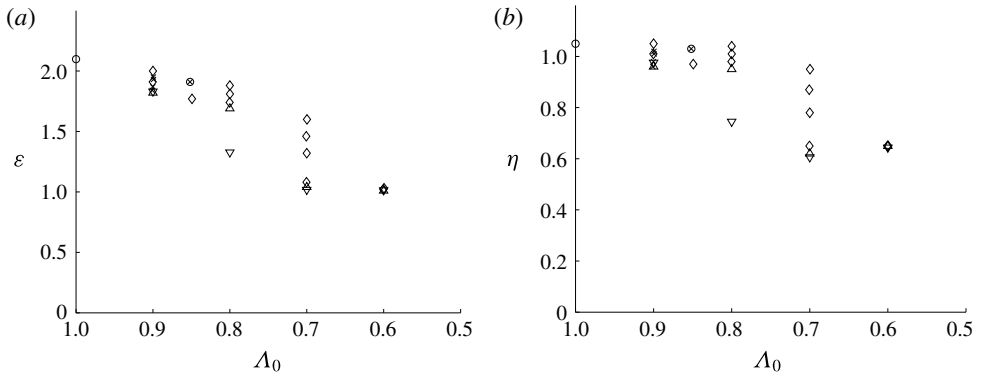

FIGURE 6. Results for ε and η versus initial circulation ratio, Λ_0: (*a*) ε versus Λ_0 and (*b*) η versus Λ_0, for $Re_\Gamma = 5000$ cases. $\triangledown$: UPEA; $\triangle$: EPUA; $\diamondsuit$: UPUA, stronger wins; $\times$: UPUA, weaker wins; $\bigcirc$: no winner (includes symmetric).

Comparing figures 5(*a*,*b*) and 3(*a*,*b*), it is seen that the spikes in the symmetric and $\Lambda_0 = 0.90$ cases coincide with the speed increase that is associated with mutual entrainment as described in § 3. It is also seen that there is no spike or rapid acceleration in the UPEA $\Lambda_0 = 0.70$ case for which no entrainment occurs. The spike in the $\Gamma_{II}(t)$ plot is therefore associated with entrainment, in these cases t^*_{end} is chosen to be t^*_{ent} since at this time there exists only one continuous $II > II_t$ region, i.e. effectively one vortical structure (see lower rows of figure 2*a*,*b*). Then for cases having no spike, t^*_{end} is chosen to be t^*_{det} since at that point there is already only one continuous region because no entrainment occurs (see lower row of figure 2*c*). If multiple local minima or maxima exist, t^*_{det} and t^*_{ent} are taken at the extremum with the smallest or largest Γ_{II}, as appropriate.

With t^*_{start} and t^*_{end} determined, ε and η can be computed and results are discussed in the following sections. Alternative choices of t^*_{start} and t^*_{end} were considered and found to yield similar results in terms of both values and trends of ε (and η) (see appendix A for details). It is noted that $A_{II}(t)$ and $\Gamma_{II}(t)$ continue to evolve subsequent to t^*_{end}, and careful observation shows that this corresponds to the axisymmetrization of the combined (i.e. final) structure and the diffusion of this structure into the non-quiescent post-interaction surrounding fluid (see appendix A). Since this predominantly viscous process occurs after the conclusion of the convective phase, it is not considered to be a part of the main interaction of the two vortices (i.e. not a part of the convective merging) and is therefore not considered in the evaluation of the interaction.

5. Results

Numerical values for ε and η are tabulated in table 1 along with the initial condition and start of interaction pair properties for each case. Note that although the theoretical maximum value is $\varepsilon_{max} = \Gamma_{end,max}/\Gamma_{2,start} = (\Gamma_{1,start} + \Gamma_{2,start})/\Gamma_{2,start} = \Lambda + 1$, this limit could be exceeded due to the use of II_t. These values of ε and η are plotted against initial Λ_0 in figure 6 and starting Λ in figure 7 on a reversed horizontal axis, and the similarity of the plots suggests that the observed variance is not a consequence of the choice of the evaluation time of the parameter.

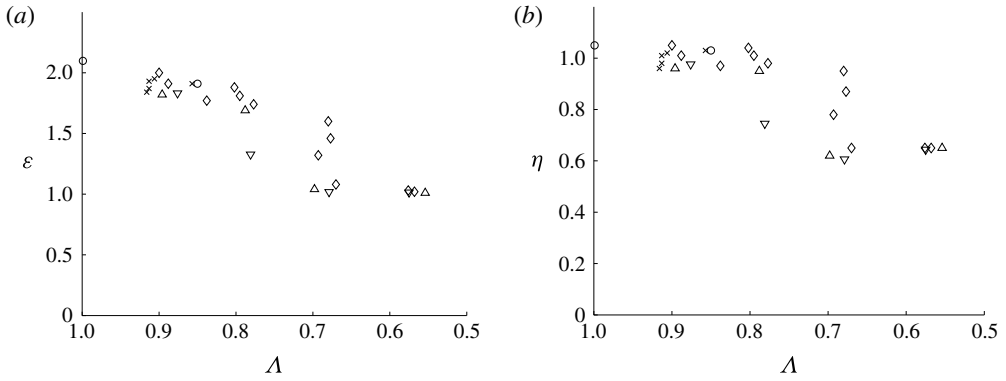

FIGURE 7. Results for ε and η versus starting circulation ratio, Λ: (*a*) ε versus Λ and (*b*) η versus Λ, for $Re_\Gamma = 5000$ cases. $\triangledown$: UPEA; $\triangle$: EPUA; $\diamondsuit$: UPUA, stronger wins; $\times$: UPUA, weaker wins; $\bigcirc$: no winner (includes symmetric).

5.1. *Symmetric merger*

The symmetric interaction ($\Lambda = \Lambda_0 = 1.0$, no winner) produces an enhancement $\varepsilon \approx 2.1$. This value indicates that the core circulation is essentially conserved in the interaction, having $\eta \approx 1.0$, and comparable to the values of $\epsilon \approx 1.6$–1.8 and $\eta \approx 0.8$–0.9 found for inviscid symmetric pair interactions (with Gaussian initial vorticity distribution) by Waugh (1992), Maze, Carton & Lapeyre (2004) and Trieling *et al.* (2005). It is noted that the presence of viscosity does not appear to induce any significant additional losses in the symmetric case in the present study. This is attributed to the fact that losses during merging arise primarily due to the dissipation of the vorticity filaments, which are associated with the low-level vorticity at the periphery of the vortex, which itself does not meet the $II_t^* > 0.10$ threshold even at t^*_{start}. This effect was noted by Trieling *et al.* (2005), whose radius method used to define the 'core' is comparable to using $II_t^* \approx 0.10$. This exclusion of the low-level vorticity accounts for ϵ and η here being higher than has been found in studies of inviscid Rankine vortices (Waugh 1992; Maze *et al.* 2004; Trieling *et al.* 2005). That ε and η found in the present study are somewhat higher than those found by Trieling *et al.* (2005) for Gaussian vortices is attributed primarily to the differing choice of initial aspect ratio, as well as viscous effects.

5.2. *Asymmetric interactions: UPEA and EPUA cases*

For vortices with unequal initial vorticity peaks but equal areas (UPEA), ε is found to decrease monotonically from $\varepsilon \approx 2.0$ in the symmetric case to $\varepsilon \approx 1.0$, reaching this value at $\Lambda = \omega_1/\omega_2 = 0.77$ for $Re_\Gamma = 5000$, and remains at approximately 1 for further decreases in Λ (see figure 7). The value of $\varepsilon \approx 1$ corresponds to a straining-out interaction.

That ε decreases with Λ is to be expected since total initial circulation is proportional to $1 + \Lambda_0$, but η decreases monotonically as well, indicating that a progressively greater percentage of the initial circulation is lost during interaction. These η values are found to be relatively high (greater than 90 %) until decreasing rapidly between $0.80 \geqslant \Lambda \geqslant 0.77$ (corresponding to approximately $0.825 \geqslant \Lambda_0 \geqslant 0.785$ for the UPEA case), a relatively small transition region in the parameter space. Note

that once $\varepsilon = 1$ is reached, $\eta = 1/(1 + \Lambda)$ and ceases to be a meaningful quantity for further changes in Λ.

Cases having equal peak vorticity and unequal areas (EPUA cases), $\omega_1/\omega_2 = 1.0$ and $A_1/A_2 < 1.0$, proceed qualitatively similarly to the UPEA cases, achieving somewhat higher enhancement for $\Lambda \approx 0.8$ but similarly reaching $\varepsilon \approx 1$ for $\Lambda \approx 0.7$ (see figure 7).

The results are in reasonable agreement with the qualitative assessments of other asymmetric flows (Dritschel & Waugh 1992; Brandt & Nomura 2010) if 'straining out' is taken to correspond to $\varepsilon \approx 1$ and 'merging' to ε significantly greater than 1. Trieling *et al.* (2005) found a similar qualitative trend for enhancement produced by the mergers of inviscid initially Gaussian vortices, although they found the $\varepsilon \approx 1.0$ regime occurs at much smaller Λ (strictly, Λ_0) than the present study (approximately 0.36 for unequal area pairs), with similarly high η values (minimal $\eta \approx 0.8$, some nearly 95 %). Since Trieling *et al.* (2005) consider inviscid flows, and other studies of viscous merging at comparable Re_Γ indicate an upper bound for Λ for the straining-out regime to be between 0.6–0.7 (Brandt & Nomura 2010) and between 0.5–1.0 (Huang 2005, 2006), this discrepancy is attributed to Trieling *et al.*'s use of much larger initial aspect ratios $(a/b)_0$ (i.e. smaller initial separations $(b/a)_0$).

5.3. *Asymmetric interactions: UPUA cases*

Though most prior studies have considered asymmetric pair interactions having either unequal peaks or unequal areas, vortex pairs may in general simultaneously have both $\omega_1/\omega_2 \neq 1$ and $A_1/A_2 \neq 1$, including those in which $\Lambda = \Gamma_1/\Gamma_2 < 1.0$ but $\omega_1/\omega_2 > 1.0$. Simulations of pairs having unequal peaks and unequal areas (UPUA) were performed within the range of parameters judged to be computationally feasible.

Unlike the UPEA and EPUA cases, the enhancement produced by these UPUA cases does not follow simple monotonic behaviour with respect to Λ, leading to the scatter seen in figure 7 for $Re_\Gamma = 5000$. The most extreme discrepancy is found to occur around $\Lambda = 0.7$, with interactions capable of producing significant enhancement ($\varepsilon \approx 1.60$) or none at all ($\varepsilon \approx 1.01$) depending on the exact parameters of the pair.

An interesting aspect of these UPUA cases is that in some cases the peak of the initially weaker vortex is found to become that of the resulting final vortex, a result not possible in the UPEA and EPUA cases. An example is presented in figure 8, where for a given $\Lambda \approx 0.9$, vortices of differing ω_1/ω_2 at the start of detrainment are observed to each follow trajectories qualitatively similar to the UPEA $\Lambda_0 = 0.90$ ($\Lambda = 0.88$) asymmetric merger case shown in figure 4(*b*), but in figure 8(*b*) the peak of the initially weaker vortex becomes the peak of the resulting compound structure. Careful consideration of the underlying physics yields a simple explanation that generalizes this finding and the observed ε and η trends, as discussed in § 6.

6. Relative straining and the mutuality parameter

The relationship between the metrics characterizing the interaction outcome (ε and η) and the basic parameters of the starting vortex pair (i.e. Λ, ω_1/ω_2, A_1/A_2) presented in figure 7 and table 1 is unclear. A more effective parametrization may be developed by considering the underlying physics of the interaction. The analysis is given below and results are presented in figures 9–12. These figures include the $Re_\Gamma = 5000$ cases as well as the $Re_\Gamma = 1000$ cases. This section will focus on the $Re_\Gamma = 5000$ results except where indicated; discussion of the $Re_\Gamma = 1000$ results and viscous effects will be given in § 7.

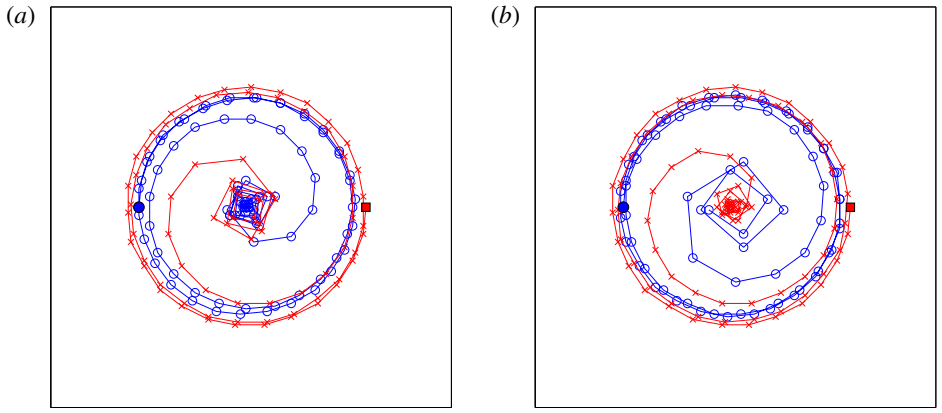

FIGURE 8. (Colour online) Trajectories of vortex peaks of UPUA pairs having $\Lambda \approx 0.9$ with differing peak vorticity ratios. Red $\times$: vortex 1 (weaker), blue $\bigcirc$: vortex 2 (stronger). Initial positions indicated by filled square and circle respectively. (*a*) The stronger vortex's peak becomes the post-interaction vortex centre (i.e. the stronger wins) for $\omega_1/\omega_2 = 1.04$, (*b*) the weaker vortex's peak becomes the post-interaction vortex centre for $\omega_1/\omega_2 = 1.18$ (i.e. the weaker wins).

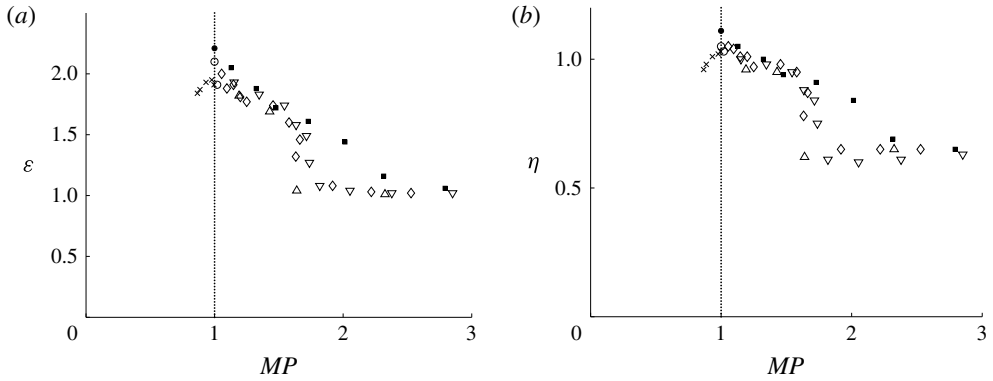

FIGURE 9. Results for ε and η versus mutuality parameter, MP: (*a*) ε versus MP and (*b*) η versus MP, for all cases. For $Re_\Gamma = 5000$ cases, $\triangledown$: UPEA; $\triangle$: EPUA; $\diamondsuit$: UPUA, stronger wins; $\times$: UPUA, weaker wins; $\bigcirc$: no winner. For the $Re_\Gamma = 1000$ cases, $\blacksquare$: UPEA; $\bullet$: no winner.

As discussed in § 3, for vortex merger to occur, i.e. for a compound vortex with $\varepsilon > 1$ to be produced, mutual entrainment must occur to some extent so that there is some interpenetration of vorticity of the two vortices. This requires detrainment to be established in both vortices. If the disparity between the vortices is too great, detrainment will only be initiated in one vortex, which will then erode and be destroyed before it can induce detrainment of the other vortex, leaving it unenhanced, i.e. $\varepsilon \sim 1$. Since detrainment of a vortex is initiated by the induced strain and resulting deformation of vorticity, it may be characterized by a ratio of the strain rate to vorticity, $(S/\omega)_i$, which is here referred to as the relative straining. Here, S_i and ω_i are evaluated at the location of the vorticity peak of vortex i at the start of convective interaction t^*_{start} (note $S = \sqrt{\boldsymbol{S}^2}$ where $\boldsymbol{S}^2 = \mathrm{tr}[S_{mn}S_{mn}]$). A mutuality parameter MP is

then defined as the ratio of the relative straining of each vortex,

$$MP = \frac{(S/\omega)_1}{(S/\omega)_2} \tag{6.1}$$

which indicates the degree of mutuality of the interaction. A value of $MP = 1$ corresponds to a fully two-way interaction. When $MP \sim 1$, the vortices experience comparable relative straining so that both vortices are detrained, resulting in entrainment and $\varepsilon > 1$. As MP deviates from unity, it is expected that the interaction will become increasingly dominated by one vortex and ε will decrease until some critical value is reached, beyond which $\varepsilon \sim 1$, i.e. a one-way interaction.

Figure 9 shows ε and η as functions of MP. Note that figure 9 includes all the cases in figure 7 (i.e. $Re_\Gamma = 5000$) as well as $Re_\Gamma = 1000$ cases. For the $Re_\Gamma = 5000$ results, the previous scatter in both ε and η across all cases (UPEA, EPUA and UPUA) is seen to be significantly reduced, indicating a more effective characterization than Λ. The dependence is peaked at $MP = 1$ and generally monotonic to either side with both ε and η decreasing as MP varies from 1.

The majority of results correspond to $MP > 1$; in this case, since $(S/\omega)_1 > (S/\omega)_2$, the weaker vortex detrains first and the stronger vortex then dominates. The associated values of ε decrease as MP increases from 1, at first relatively gradually and then quite rapidly near a critical value of MP, beyond which they remain constant at $\varepsilon \sim 1$. The critical value, $MP_{cr} \approx 1.78 \pm 0.04$, thus gives a criterion for merger in these cases. These interactions may then be characterized as follows: for $MP = 1$, symmetric merger (and in principle asymmetric merger with $(S/\omega)_1/(S/\omega)_2 = 1$, see figure 10) occurs and ε exhibits peak values; for $1 < MP < MP_{cr}$, $\varepsilon > 1$, asymmetric merger occurs resulting in the stronger vortex being enhanced; and for $MP > MP_{cr}$, $\varepsilon \sim 1$, straining out occurs with the stronger vortex surviving unenhanced. The behaviour of η is similar, although for $MP < MP_{cr}$, the decline is somewhat more muted; asymmetric merger is seen to be relatively high efficiency (most having $\eta > 0.85$) indicating relatively minor losses for mergers in general.

When $MP < 1$, $(S/\omega)_1 < (S/\omega)_2$, and the corresponding cases in figure 9 are asymmetric mergers in which the weaker vortex dominates (as seen in figure 8*b*) and is ultimately enhanced by the interaction, i.e. wins (computed ε is based on the stronger starting vortex regardless of which wins). It is expected that straining out will occur for $MP < MP_{cr} \approx 1/1.78 = 0.56$, however, resolution considerations preclude further investigation of this weak-winner regime. When $MP \approx 1$, neither vortex dominates or clearly wins (identified as 'no winner' in figure 9). Recall that in the symmetric case where $MP = 1$, both vortices are destroyed as they become mutually entrained and the flow transforms into a new vortex. This scenario can also occur in asymmetric (UPUA) cases when the relative straining on each vortex is nearly equal. An example of a no-winner UPUA case is given in figure 10, which shows that neither vortex dominates and the interaction proceeds in a similar manner to the symmetric case (figure 2*a*). The symmetric and no-winner UPUA $MP \approx 1$ cases in the present study are seen to produce similar η, implying comparably effective merging.

It is useful to relate MP to the previously considered vortex parameters. Simple expressions for $(S/\omega)_i$ can be obtained by considering the external strain rate produced by a point vortex, i.e. the strain rate induced by one vortex at the location of the other were the other not present, e.g. $S_1 = \Gamma_2/(2\pi b^2)$ (a similar expression can be obtained

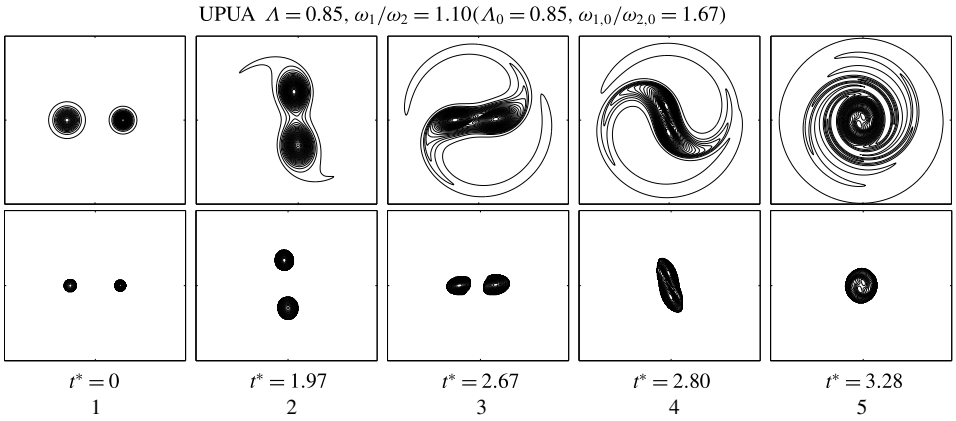

FIGURE 10. Vorticity contours at the initial condition and key times during the interaction for a UPUA case ($\Lambda = 0.85$, $\omega_1/\omega_2 = 1.10$, $Re_\Gamma = 5000$) in which no winner can be determined ($MP = 1.02$). See figure 2 for meanings of the rows and columns.

using the expression for strain rate produced by a Lamb–Oseen vortex Saffman 2001), and using $\Gamma_i = \pi a_i^2 \omega_i$,

$$\left(\frac{S}{\omega}\right)_1 \sim \frac{1}{2\Lambda}\left(\frac{a_1}{b}\right)^2, \tag{6.2}$$

$$\left(\frac{S}{\omega}\right)_2 \sim \frac{\Lambda}{2}\left(\frac{a_2}{b}\right)^2. \tag{6.3}$$

This relates $(S/\omega)_i$ to the vortex aspect ratios. For symmetric and UPEA pairs, equations (6.2)–(6.3) imply $MP = 1/\Lambda^2$, which is observed to hold approximately true across the range of Λ considered in the present study (not shown). The critical $MP_{cr} \approx 1.78$ then implies a critical $\Lambda_{cr} \approx \sqrt{1/1.78} = 0.75$, very close to the observed UPEA $\Lambda_{cr} \approx 0.79$ (figure 7).

A simple relation for MP may then be obtained from (6.2)–(6.3),

$$MP = \frac{(S/\omega)_1}{(S/\omega)_2} \sim \frac{{\omega_2}^2 {a_2}^2}{{\omega_1}^2 {a_1}^2}, \tag{6.4}$$

where $\omega_i^2 a_i^2$ is the enstrophy of a Rankine vortex. This suggests that the enstrophy ratio at the onset of convective interaction may capture the same physical principles and consequent ε and η behaviour as $(S/\omega)_1/(S/\omega)_2$. More generally, the enstrophy ratio can be defined as

$$\frac{Z_2}{Z_1} = \frac{\displaystyle\int_{II>II_{t,2}} \omega_2^2 \, \mathrm{d}A_2}{\displaystyle\int_{II>II_{t,1}} \omega_1^2 \, \mathrm{d}A_1}, \tag{6.5}$$

where the integral is evaluated for each vortex at t^*_{start}. Figure 11 shows ε and η plotted against Z_2/Z_1; the observed dependence is similar to that of MP. It is noted, however, that this parameter is somewhat less successful at indicating the

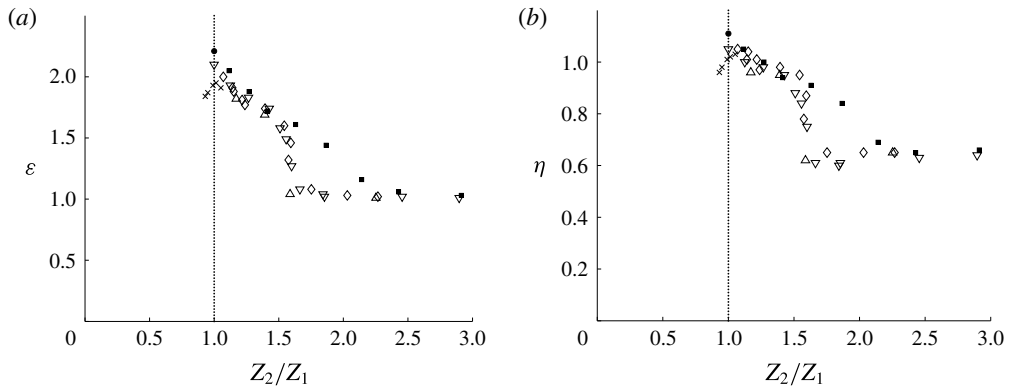

FIGURE 11. Results for ε and η versus enstrophy ratio, Z_2/Z_1: (*a*) ε versus Z_2/Z_1 and (*b*) η versus Z_2/Z_1, for all cases. For the $Re_\Gamma = 5000$ cases, $\triangledown$: UPEA; $\triangle$: EPUA; $\diamond$: UPUA, stronger wins; $\times$: UPUA, weaker wins; $\circ$: no winner. For the $Re_\Gamma = 1000$ cases, $\blacksquare$: UPEA; $\bullet$: no winner.

weak-winner regime boundary (figure 11). The critical enstrophy ratio beyond which no enhancement occurs is found to be $(Z_2/Z_1)_{cr} \approx 1.63 \pm 0.03$ for $Re_\Gamma = 5000$.

To the authors' knowledge, the only other study to consider strong-winner and weak-winner interactions is Melander *et al.* (1987*b*), who found a transition region between these cases in their parameter space, which they approximated by $(\omega_1/\omega_2) = (A_1/A_2)^{-0.36}$. A similar expression can be obtained from (6.4) with $MP = 1$ (the boundary for the weak-winner regime in the present study), $(\omega_1/\omega_2) = (A_1/A_2)^{-0.5}$, which approximately corresponds to the 'lower edge' of the transition region of Melander *et al.* (see their figure 2). Considering the slightly different definitions of 'winner' and the presence of viscosity in the present study, this correspondence is notable.

Examining $(S/\omega)_i$ of each vortex separately, it is observed that the convective interaction begins when the relative straining of the first vortex to detrain reaches some consistent value. Figures 12(*a*) and 12(*b*) show the starting $(S/\omega)_1$ and the maximum value of $(S/\omega)_2$ reached before the end of detrainment, respectively, plotted against the corresponding MP for all numerical cases. For each case the interaction outcome is coded as binary 'merger' or 'straining out' based on whether an entrainment process is evident in the $A_{II}(t)$ and $\Gamma_{II}(t)$ plots (this classification is consistent with a ε-based assessment, but avoids invoking an arbitrary ε cutoff to classify the $\varepsilon \approx 1$ cases). Considering the results at both $Re_\Gamma = 5000$ and $Re_\Gamma = 1000$, it is observed that entrainment only occurs if the stronger vortex achieves a maximum $(S/\omega)_{2,max} \geqslant 0.138$ prior to the end of detrainment and never occurs for $(S/\omega)_{2,max} \leqslant 0.132$, suggesting a critical $(S/\omega)_{cr} \approx 0.135$ (see figure 12*b*), which is comparable to the relatively consistent mean value of starting $(S/\omega)_1 = 0.147$ with an average deviation of 0.016 (figure 12*a*). The scatter in the starting $(S/\omega)_1$ values in the present study is attributed to imprecision in determining the exact starting time (see § 4). Thus, the critical value $(S/\omega)_{cr} \approx 0.135$ generally characterizes the onset of detrainment of Gaussian vortices having Re_Γ in the range considered in this study.

A critical strain rate to vorticity ratio has also been considered in a number of related studies. Le Dizès & Laporte (2002) and Le Dizès & Verga (2002) showed that a similar quantity evaluated in the co-rotating frame is a leading-order approximation

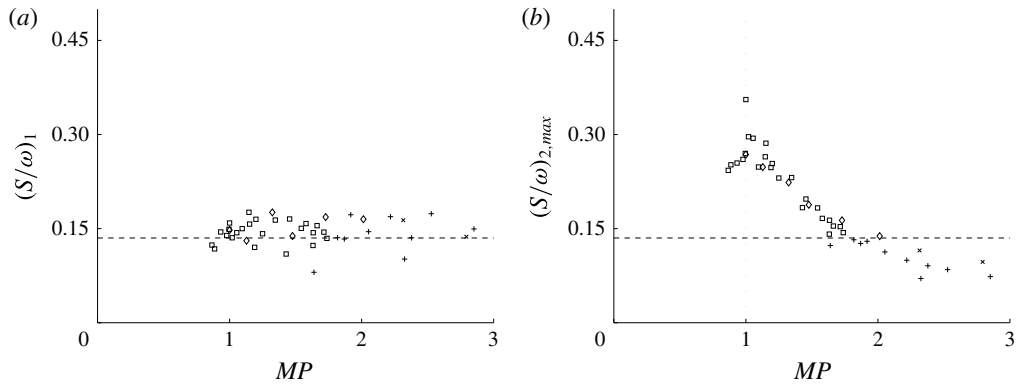

FIGURE 12. Results for the relative straining at each vortex with indication of occurrence of detrainment: (*a*) $(S/\omega)_1$ versus *MP* at t^*_{start}, (*b*) maximum $(S/\omega)_2$ prior to the end of detrainment t^*_{det} versus *MP*. $Re_\Gamma = 5000$: □: merger, +: straining out. $Re_\Gamma = 1000$: ◇: merger, ×: straining out. Dashed line indicates the critical $(S/\omega)_{cr} = 0.135$, obtained from (*b*) (see § 6). Merger and straining out assessed by occurrence of entrainment phase and lack thereof respectively.

of the eccentricity of streamlines near the centre of an elliptical Gaussian vortex, i.e. a local eccentricity. Brandt & Nomura (2010) identified a critical value of their strain rate parameter (the strain rate evaluated at the central hyperbolic point in the co-rotating frame) that characterized the start of detrainment. Their results also show that start of detrainment corresponds to an approximately consistent local eccentricity $\varepsilon_l \approx 0.2$ at the start of interaction (compare their figures 6*a* and 8), equivalent to $(S/\omega) \approx 0.14$ (although here (S/ω) is not evaluated in the co-rotating frame), which is similar to the observed $(S/\omega)_{cr} \approx 0.135$ in the present study. Mariotti, Legras & Dritschel (1994) considered the similar phenomenon of vortex stripping of a single vortex by external adverse shear and likewise found a comparable critical ratio of strain rate to vorticity, equivalent to $S/\omega \approx 0.095$ in the present study, and moreover found this value to be consistent over a range of Re_Γ, i.e. that this 'stripping' (and ultimately vortex breakup) is an inviscid mechanism, even in viscous flow. Trieling *et al.* (2005) utilized a similar critical strain rate to characterize the boundary between complete and partial straining-out regimes in inviscid flow, relating the critical shear required to destroy the weaker vortex to a critical separation distance. This effectively distinguished partial (two vortices survive) and complete (one vortex completely destroyed) straining-out cases in inviscid flow for EPUA and UPEA pairs having small radius ratio R_2/R_1 and small peak vorticity ratio ω_1/ω_2, respectively, for distributed vortices having various vorticity distributions, including a Gaussian profile. Since viscous effects in the present study reduce ω in (S/ω), the critical value $(S/\omega)_{cr}$ (directly related to critical separation distance for symmetric merger; see (6.2)–(6.3)) is always attained by at least one of the vortices which is ultimately destroyed, precluding two-vortex outcomes. Trieling *et al.* (2005) attributed the inefficacy of this criterion for pairs of low asymmetry (i.e. those having higher R_2/R_1 or ω_1/ω_2) to spatial effects and captured circulation by the stronger vortex altering its induced strain. In light of the present analysis, it is suggested that this could be attributed to the mutual detrainment of both vortices activating the convective entrainment mechanism before either is completely destroyed (i.e. before the critical (S/ω) for vortex destruction in inviscid flow is reached).

		Starting (t^*_{start})		Initial ($t^* = 0$)		Ending (t^*_{end})		Weak
	Re_Γ	Λ	ω_1/ω_2	Λ_0	$\omega_{1,0}/\omega_{2,0}$	ε	η	winner
	1000	1.00	1.00	1.00	1.00	2.21	1.11	
	1000	0.95	0.95	0.95	0.95	2.05	1.05	
	1000	0.88	0.90	0.90	0.90	1.88	1.00	
	1000	0.83	0.85	0.85	0.85	1.72	0.94	
Num.	1000	0.77	0.79	0.80	0.80	1.61	0.91	
	1000	0.71	0.74	0.75	0.75	1.44	0.84	
	1000	0.67	0.69	0.70	0.70	1.16	0.69*	
	1000	0.63	0.65	0.65	0.65	1.06	0.65*	
	1000	0.57	0.60	0.60	0.60	1.03	0.66*	
	1000	0.47	0.50	0.50	0.50	1.00	0.68*	
	1500	0.97 ± 0.02	0.86 ± 0.06	0.86	0.88	1.89 ± 0.20	0.96 ± 0.09	
	1100	0.92 ± 0.08	1.15 ± 0.13	0.85	1.29	2.11 ± 0.24	1.09 ± 0.09	X
Expt.	1000	0.69 ± 0.06	0.74 ± 0.05	0.76	0.78	1.23 ± 0.19	$0.70^* \pm 0.08$	
	1300	0.58 ± 0.05	0.59 ± 0.02	0.68	0.67	1.21 ± 0.07	$0.73^* \pm 0.04$	
	900	0.42 ± 0.01	0.50 ± 0.02	0.49	0.52	0.96 ± 0.05	$0.68^* \pm 0.04$	

TABLE 2. Summary of parameters and results for $Re_\Gamma = 1000$ computational simulations ('Num.') and laboratory experiments ('Expt.'). Here all numerical cases are UPEA cases. ε and η are evaluated at t^*_{end}. Starting $\Lambda = \Gamma_1/\Gamma_2$ is evaluated at t^*_{start}. Due to the nature of the experiments, only Λ_0 was controlled in the initial condition. $*$ indicates that the 'straining-out' regime has been reached and η is therefore not a meaningful physical quantity. 'Weak winner' indicates that the peak of the weaker initial vortex becomes the peak of the resulting post-interaction vortex (see § 5). Margins of error for the experimental cases correspond to extrema of error bars in figure 16 (for details see § 7).

7. Comparison with experimental results and Re_Γ effects

A series of UPEA numerical simulations at $Re_\Gamma = 1000$ are performed in order to facilitate comparison with available experimental data. The simulation parameters and results are summarized in table 2. Contour plots for illustrative cases (symmetric $\Lambda = 1.0$ and UPEA $\Lambda = 0.88$, 0.67), corresponding to those for $Re_\Gamma = 5000$ in figure 2, are presented in figure 13. It is clear that diffusion and the onset of detrainment occur more rapidly for each case than in the comparable higher-Re_Γ case. These basic effects are also seen in the evolutions of $A_{II}(t)$ and $\Gamma_{II}(t)$ (figure 14*a*,*b*; symmetric case not shown). Otherwise, these results exhibit qualitatively similar features indicating that the flows experience the same underlying processes.

The most significant implication of decreasing Re_Γ is to increase MP_{cr} ($\approx 2.15 \pm 0.16$) and increase $(Z_2/Z_1)_{cr}$ ($\approx 2.00 \pm 0.14$) relative to the $Re_\Gamma = 5000$ case, as indicated in the plots of ε and η versus MP and Z_2/Z_1 for $Re_\Gamma = 1000$ (figures 9 and 11). Careful examination of the $\Gamma_{II}(t)$ and vorticity contour plots for all the simulations verifies that an entrainment process occurs in some low-Re_Γ cases where there is none at the corresponding high Re_Γ case with similar Λ and ω_1/ω_2. As discussed in the previous section, $(S/\omega)_{cr} \approx 0.135$ is consistent for both Re_Γ considered (see figure 12). The increase of MP_{cr} with decreasing Re_Γ is therefore attributed to the more rapid diffusion enabling comparatively stronger vortices to achieve $(S/\omega)_{cr}$ by reducing ω more quickly. This is consistent with the results of Mariotti *et al.* (1994) for a single vortex, which indicate that the critical S/ω for vortex breakup by erosion, found to be independent of Re_Γ, is reached more

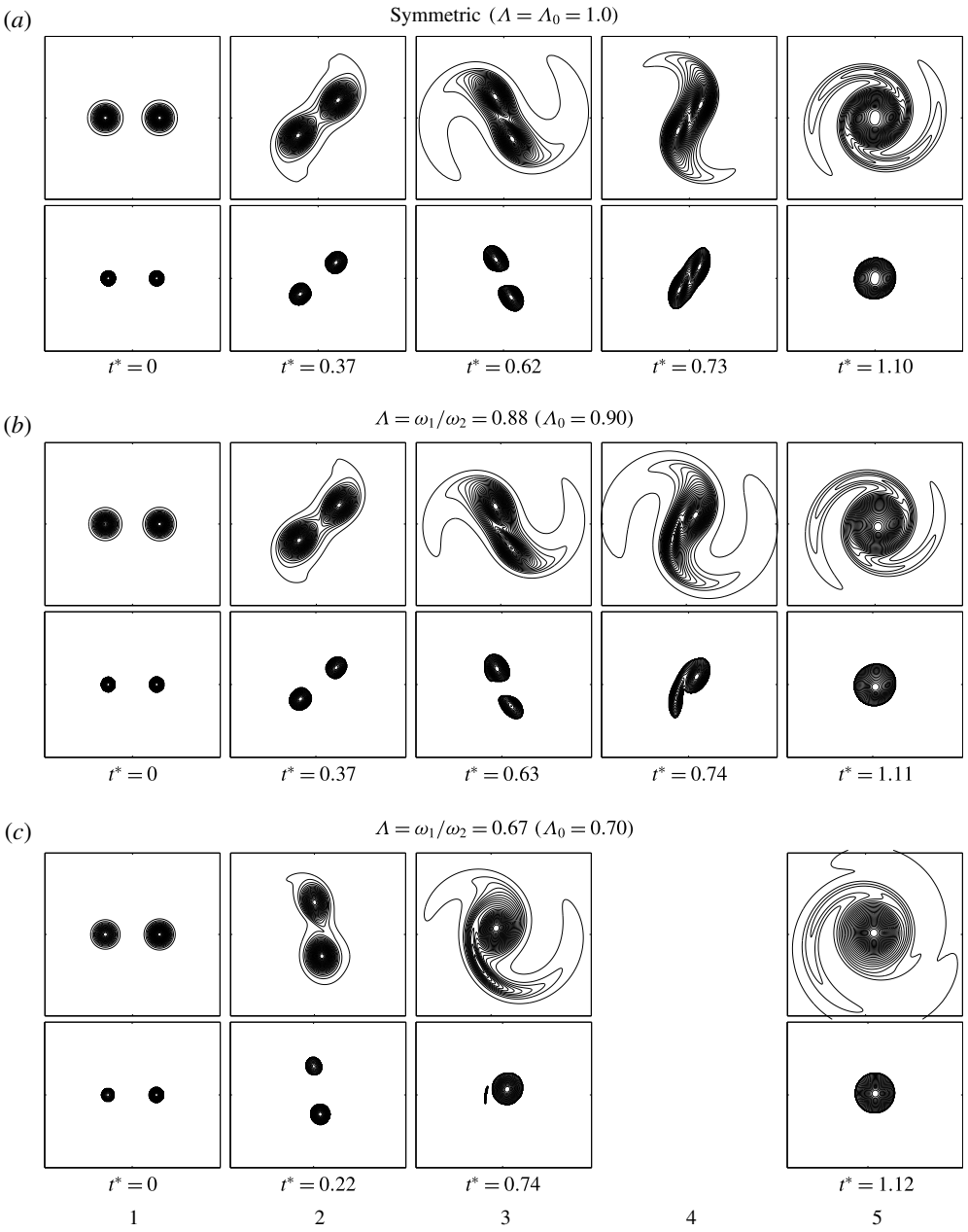

FIGURE 13. Vorticity contours at the initial condition and key times during the interaction for (*a*) Symmetric ($\Lambda_0 = 1.0$) and UPEA (*b*) $\Lambda = 0.88$ ($\Lambda_0 = 0.90$) and (*c*) $\Lambda = 0.67$ ($\Lambda_0 = 0.70$) cases at $Re_\Gamma = 1000$. The first row depicts the vorticity contours of the total flow, and the second row depicts the vorticity contours within the region considered 'core' using $II > II_t$ (see § 4). See figure 2 for meanings of columns.

quickly for lower Re_Γ. Although the case of interacting vortices is more complex, the processes underlying the onset of detrainment are similar (Kimura & Herring 2001; Brandt & Nomura 2006). Additional effects of reducing Re_Γ may include

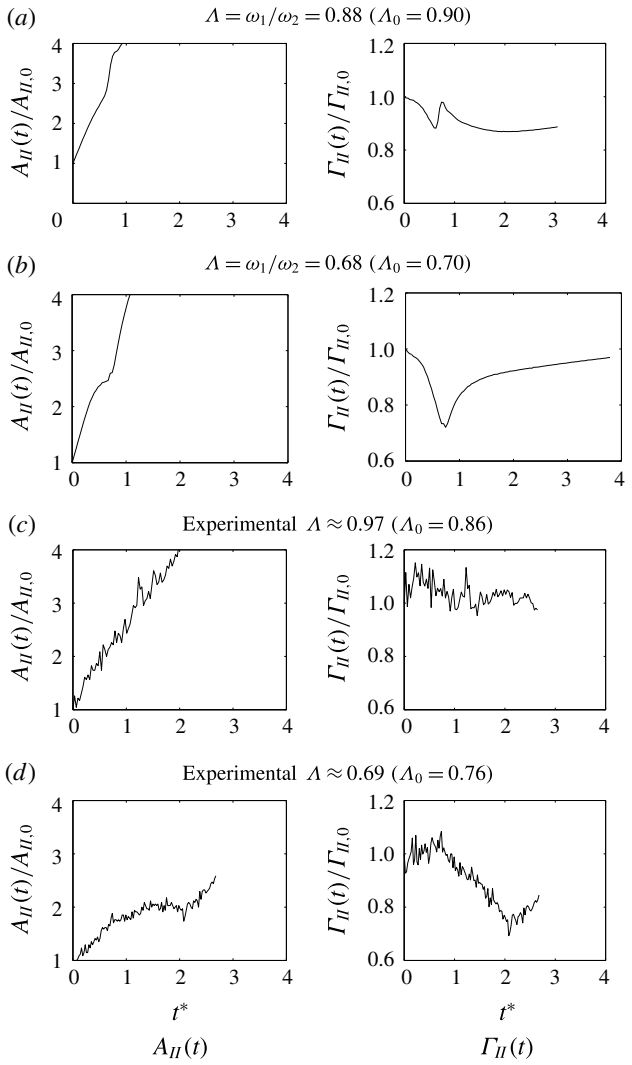

FIGURE 14. Time development of normalized aggregate core area $A_{II}(t)/A_{II,0}$ and circulation $\Gamma_{II}(t)/\Gamma_{II,0}$ ($II > II_t$) for $Re_\Gamma = 1000$ numerical cases (*a*) $\Lambda = 0.88$ and (*b*) $\Lambda = 0.67$, and comparable experimental cases (*c*) $\Lambda \approx 0.97$, $Re_\Gamma \approx 1500$ and (*d*) $\Lambda \approx 0.69$, $Re_\Gamma \approx 1000$. Note that the 'initial' time for (*c*) and (*d*), i.e. time of evaluation of $X_{II,0}$ quantities, corresponds to the time at which vortices are judged to have formed.

an increase in ε values as a result of the earlier onset of detrainment potentially reducing the amount of filamentation that can occur (although such a reduction is difficult to quantify), as well as increased diffusion of vorticity directly from one vortex into the other (although this effect is considered to be minor since the vortices are well-separated prior to convective merging, which then occurs on a much more rapid time scale than diffusion).

The numerical results are compared with digital particle image velocimetry (DPIV) data taken from water tank experiments of co-rotating symmetric and asymmetric vortex pairs (see Meunier 2001; Meunier *et al.* 2002). The vortices are generated

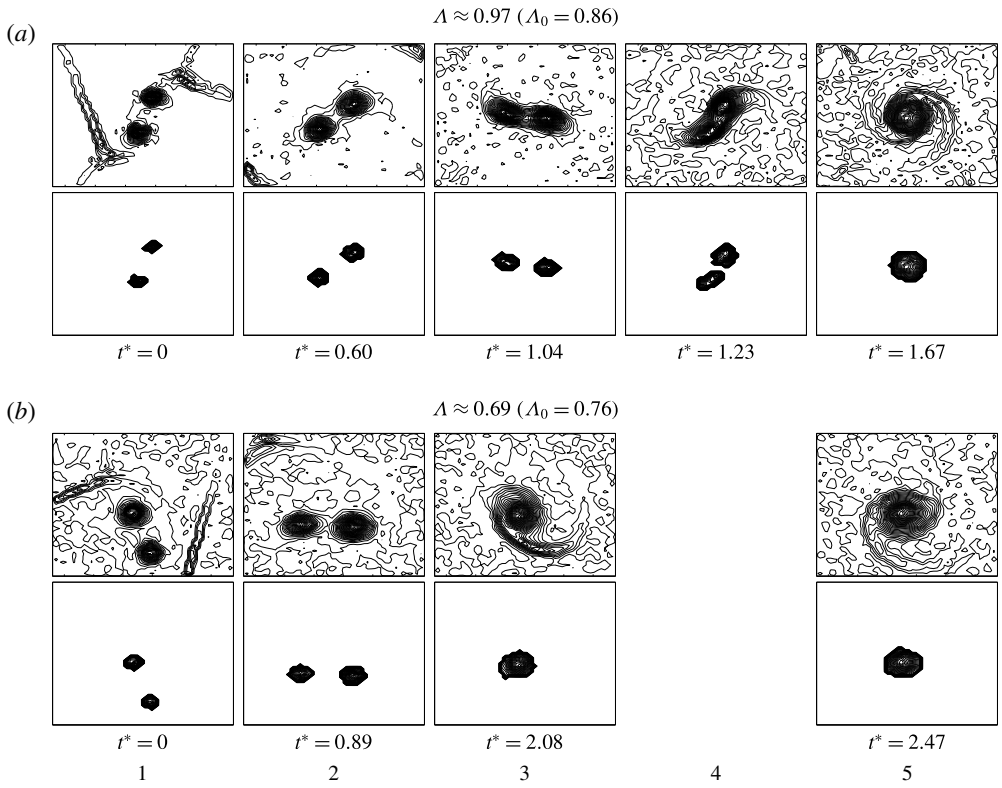

FIGURE 15. PIV results for experimental cases having (*a*) $\Lambda \approx 0.97$, $Re_\Gamma \approx 1500$ and (*b*) $\Lambda \approx 0.69$, $Re_\Gamma \approx 1000$. The first row depicts the vorticity contours of the entire flow and the second row depicts the vorticity contours of the portion considered 'core' using $II > II_t$. See figure 2 for meanings of columns. Note that the 'initial condition' corresponds to the time at which vortices are judged to have formed.

impulsively by the rotation of sharp-edged flat plates about their vertical axes such that they behave as laminar, two-dimensional vortices without axial velocity in the observation volume, with Λ_0 adjusted by varying the relative angular velocity of the plates. The experimental cases are summarized in table 2. The Λ_0 value is evaluated at the time at which the vortices are judged to have become coherent and detached from the flaps by visual examination (which may differ slightly from Meunier *et al.* 2002). The starting Λ value in each case is the average of the highest and lowest of several possible Λ values computed using different plausible choices of starting time in order to minimize the effect of the variability in these values (since with noisy data slight differences in choice of start/end times can have a relatively pronounced effect).

Contours of vorticity comparable to those in figure 13 are presented in figure 15 for the $\Lambda \approx 0.97$, $Re_\Gamma \approx 1500$ and $\Lambda \approx 0.69$, $Re_\Gamma \approx 1000$ experimental cases. The oblong structures visible at the early times are the plates that produce the vortices and should be disregarded. Despite the noise, these appear qualitatively similar to those of the comparable numerical cases.

Plots of $A_{II}(t)$ and $\Gamma_{II}(t)$ for the experimental results are presented in figure 14(*c*,*d*) along with the $Re_\Gamma = 1000$ numerical cases. No smoothing or averaging has been

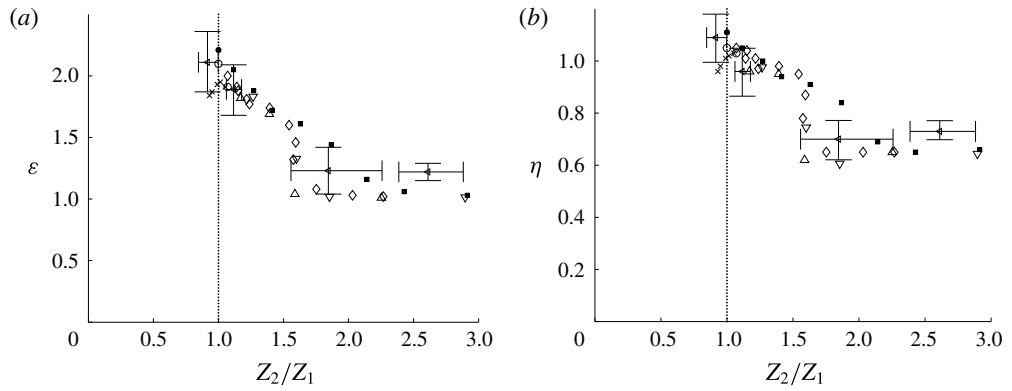

FIGURE 16. Results for ε and η versus enstrophy ratio, Z_2/Z_1: (*a*) ε versus Z_2/Z_1 and (*b*) η versus Z_2/Z_1, for all cases. For the $Re_\Gamma = 5000$ cases, ▽: UPEA; △: EPUA; ◇: UPUA, stronger wins; ×: UPUA, weaker wins; ○: no winner. For the $Re_\Gamma = 1000$ cases, ■: UPEA; ●: no winner. The experimental results are indicated by ◁ with error bars, see § 7 for explanation.

applied to the experimental data, but despite the noise they qualitatively resemble those of the comparable numerical cases: the $A_{II}(t)$ of both experimental cases suggest a linear growth at first, then nonlinear behaviour before returning to linear viscous growth, while $\Gamma_{II}(t)$ of both appears to grow slightly at first (attributed to the method used to create the vortices) followed by a decline to a local minimum, then a spike in the $\Lambda \approx 0.97$ case but not in the $\Lambda \approx 0.69$ case, followed by relatively smooth nonlinear behaviour. These features are interpreted to correspond to the diffusive, convective and final phases of interaction that are observed in the numerical cases. The longer diffusive phase in the experimental $\Lambda \approx 0.69$ case (compared to the numerical $\Lambda = 0.67$, $Re_\Gamma = 1000$ case) is attributed to its having a somewhat lower initial aspect ratio a_0/b_0.

Results for ε and η for the experimental cases are summarized in table 2 and plotted with the low- and high-Re_Γ numerical results in figure 16. As with Λ, for each case several ε and η were computed using a number of plausible choices for ending times due to the noise in the data. The integrated quantity Z_2/Z_1 is used to examine the trends since the local quantities (S/ω) and MP are too uncertain to give meaningful results. The experimental results in figure 16 are shown with horizontal error bars indicating the maximum and minimum plausible Z_2/Z_1 and vertical error bars indicating the maximum and minimum potential ε and η within this range, and ε and η plotted at the midpoint. It is noted that one experimental case ($\Lambda \approx 0.92$ with $\omega_1/\omega_2 > 1$, $Re_\Gamma \approx 1100$) is a UPUA weak-winner case. Despite the limitations of the data, the experimental values are in reasonable accordance with the numerical results.

8. Summary and discussion

The interactions of two unequal co-rotating vortices in viscous fluid have been further investigated and for the first time, their outcomes quantitatively assessed. A new parameterization of the possible interaction outcomes has been developed. Numerical simulations were performed to consider a range of vortex strength ratios, $\Lambda = \Gamma_1/\Gamma_2 \leqslant 1$, corresponding to vortices of differing size and/or peak vorticity, and

with $Re_\Gamma = 5000$. An additional set of simulations at lower Re_Γ was also performed in order to compare with available data from the experiments of Meunier (2001).

The primary convective interaction between the two vortices is initiated by the induced strain of each vortex on the other, and in viscous flow, leads to a single vortex. The post-interaction vortex is quantitatively assessed in terms of an enhancement factor, $\varepsilon = \Gamma_{end}/\Gamma_{2,start}$, and a corresponding merging efficiency, $\eta = \Gamma_{end}/\Gamma_{total,start}$, similar to the analysis of inviscid flow by Dritschel & Waugh (1992), which compare the vortex strengths at the start and end of the convective interaction. An effective parameterization is developed by characterizing the degree of mutuality of the interaction with the mutuality parameter, $MP \equiv (S/\omega)_1/(S/\omega)_2$, where the relative straining $(S/\omega)_i$, evaluated at the start of the interaction, is an indicator for core detrainment of each vortex.

Analysis of the simulation results demonstrates the general description: two vortices will undergo mutual entrainment (merger) if MP is sufficiently close to unity, i.e. within some critical value, MP_{cr}. For the present results, $MP_{cr} \approx 1.8$ for $MP > 1$ (stronger vortex dominates). Asymmetric merger with $MP_{cr} < MP < 1$ may also occur, and in this case the originally weaker vortex dominates and survives enhanced. Symmetric merger ($MP = 1$) is the limiting case of a fully two-way reciprocal interaction with $\varepsilon \sim 2$ and correspondingly, $\eta \sim 1$; the most efficient merger. As MP increasingly deviates from unity, both ε and η diminish until $MP \sim MP_{cr}$, beyond which $\varepsilon \approx 1$ and the interaction is essentially one-way; entrainment does not occur and the dominating vortex erodes the other away (straining out) and survives relatively unaffected. The enstrophy ratio Z_2/Z_1 is found to characterize the behaviour of ε and η similarly to MP overall, although it is somewhat less effective at distinguishing the weak-winner regime. Results also indicate that core detrainment is initiated when $(S/\omega)_i$ reaches a critical value of $(S/\omega)_{cr} \approx 0.135$. A simple analysis shows that $(S/\omega)_i$ can be related to Λ and a_i/b. In the case of symmetric merger, this is consistent with the initiation of detrainment corresponding to the critical aspect ratio, $(a/b)_{cr}$, which is inevitably achieved in viscous flow. This may then also explain, more generally, why the outcome of interactions in viscous flow is always a single vortex: diffusion of core vorticity will weaken the cores so that eventually $(S/\omega)_{cr}$ is attained by at least one of the vortices, which in time becomes completely eroded.

These observations generally hold for the lower Re_Γ simulations and for the available experimental data. Since initiation of detrainment is essentially an inviscid mechanism, we may expect the value of $(S/\omega)_{cr}$ to remain constant with Re_Γ, as the present results support. However, the value of MP_{cr} (and $(Z_2/Z_1)_{cr}$) is found to vary somewhat (favouring merger) as Re_Γ decreases. Since MP may be considered a ratio of time scales, i.e. the disparity in timing for detrainment to be established in each of the vortices, this is influenced by viscous effects. With decreasing Re_Γ, the more rapid diffusion of vorticity will accelerate the achievement of $(S/\omega)_{cr}$ so that more disparate vortices may still both detrain within the interaction time.

The present results have implications for two-dimensional turbulence. The observation that in asymmetric interactions, one of the original vortices essentially survives with its peak becoming that of the post-interaction vortex, may explain the noted persistence of vorticity extrema throughout the evolution of turbulent flow (McWilliams 1990; Carnevale *et al.* 1991, 1992; Dritschel *et al.* 2008). Moreover, the findings of the present study show how the peak of the post-interaction vortex can be related directly to the original pair, which in principle allows for modelling and perhaps analytical consideration of two-dimensional turbulent flows having vortices of varying peak vorticity. Such analysis remains for future work.

The present findings also suggest that the simple transformation rule utilized in a number of point vortex models of two-dimensional turbulence to incorporate vortex merging may not accurately reflect the enhancement produced by interactions of real vortices. This rule is derived from conservation of energy and typically takes the form $\Gamma_A^2 + \Gamma_B^2 = \Gamma_C^2$, where A and B are the interacting vortices and C is the resulting vortex, which 'replaces' A and B to emulate merging (Carnevale *et al.* 1991; Riccardi *et al.* 1995; Sire *et al.* 2011). This expression can be written in terms of enhancement as $1 + \Lambda^2 = \varepsilon_{model}^2$ by dividing by the Γ of the stronger initial vortex, and it can be seen that this generally underestimates the enhancement produced by symmetric or slightly asymmetric mergers (e.g. for symmetric pairs, $\varepsilon_{model} = 1.41$ but observed $\varepsilon \approx 2$), but overestimates the enhancement produced by very asymmetric pairs (e.g. for the $\Lambda = 0.7$ UPEA case, $\varepsilon_{model} = 1.22$ but observed $\varepsilon \approx 1$). It is emphasized that this theory was never intended to be precise at the level of individual interactions, but it is nevertheless at odds with the findings of isolated vortex pair studies. Trieling *et al.* (2005) reported a similar finding and proposed that conservation of circulation may be more accurate, although they found this overestimates the enhancement produced by straining-out interactions, a finding supported by the rapid diminishing of η with increasing MP (and Z_2/Z_1) observed here.

Based on the present findings, it is suggested that a simple binary transformation rule could improve accuracy without adding prohibitive complication: when (S/ω) of a vortex in a two-dimensional turbulent flow exceeds $(S/\omega)_{cr}$ ($\approx$0.135), this value is compared with the (S/ω) of the nearest vortex to determine MP. If $MP < MP_{cr}$, the merger conserves circulation, i.e. the two vortices A and B are replaced with a single vortex C having circulation $\Gamma_C = \Gamma_A + \Gamma_B$. If $MP > MP_{cr}$, the stronger's circulation is preserved, i.e. $\Gamma_C = \Gamma_A$, where $\Gamma_A > \Gamma_B$. Further study is needed to determine MP_{cr} as a function of Re_Γ, but it is expected that for most typical flows values of MP_{cr} in the range presented here will constitute reasonably accurate choices. A more nuanced transformation rule, perhaps incorporating the continuous variation of ε and η with MP and/or incorporating the concept of interaction winners, could also be considered. This remains for future work.

One major aspect of two-dimensional turbulence not considered in this study is the influence of the surrounding vortices in the flow on the interacting pair, which could be simply approximated by an imposed external strain. Although a few studies have considered the effect of a background flow on the interactions of symmetric vortex pairs (see, e.g. Maze *et al.* 2004; Perrot & Carton 2010; Trieling, Dam & van Heijst 2010; Folz & Nomura 2014), none have considered the case of asymmetric pairs. Such a study, using the present analysis framework, is currently in progress by the authors.

Acknowledgements

The authors gratefully acknowledge Dr P. Meunier for providing his experimental data and for his helpful support and feedback. We also acknowledge Dr P. Orlandi for providing the code used for the EPUA simulations, Dr G. Carnevale for providing invaluable discussion and feedback and Mr M. Corson for his preliminary analysis of the experimental data.

Appendix A. Details of the assessment method

A method to quantitatively assess the interaction outcomes was presented in § 4. Here, further details of the method are provided, and the sensitivity of the assessment to key parameter values is examined.

		$II_t^* = II_t/II_{peak}$		
		0.10	0.25	0.50
Λ_0	1	2.10	2.15	2.31
	0.9	1.83	1.76	1.04
	0.6	1.00	0.99	0.97

TABLE 3. Effect of II_t^* on computed ε values for UPEA cases having various values of Λ_0 at $Re_\Gamma = 5000$.

A.1. *Effect of choice of* II_t^*

In general, values of $II_t^* = 0.01$–0.15 are found to approximately correspond to the values of $II|_{r=a}/II_{peak}$ at a_ω and the characteristic radius based on the azimuthal velocity maximum, a_θ, for a vortex in a co-rotating pair and therefore effectively capture what has commonly been considered to be the 'core' in prior vortex merger studies (e.g. Meunier *et al.* 2002; Brandt & Nomura 2007). For all choices of II_t^* within this range, the time development of $A_{II}(t)$ and $\Gamma_{II}(t)$ proceeds similarly and yields quantitatively similar values for ε and η for a given case and choice of (t_{start}, t_{end}).

For this study, the value of $II_t = 0.10$ was chosen due to its correspondence with the characteristic vortex radius based upon second moment of vorticity, a_ω. For a single isolated axisymmetric Gaussian vortex, $II^* = II(r)/II_{peak} = (\omega(r)^2/2 - S_{r\theta}(r)^2)/(\omega_{peak}^2/2)$ because there is zero strain at the location of the peak. Evaluating this using expressions for the vorticity distribution $\omega(r) = \omega_{peak}\exp(-r^2/a_\omega^2)$ and strain distribution $S_{r\theta} = a_\omega^2(\omega_{peak}/2)[-1/r^2 + (1/a_\omega^2 + 1/r^2)\exp(-r^2/a_\omega^2)]$ at $r = a_\omega$ implies a value for $II^* = 0.10$ (Saffman 2001).

For $II_t^* > 0.15$, the behaviour of $A_{II}(t)$ and $\Gamma_{II}(t)$ for asymmetric $\Lambda > \Lambda_{cr}$ cases exhibits significant qualitative change as II_t^* increases, losing the characteristic entrainment spike and resembling the straining-out case, and eventually exhibiting essentially single vortex behaviour when II_t^* is so high that the weaker vortex is not counted at all, even in the initial condition. Note that the portion counted by II_t^* in the initial condition in this manner may belong to the losing vortex, in certain UPUA cases. Choosing $II_t^* > 0.15$ therefore can affect the computed values of ε, and so are not used in this study and not recommended in general. In the other extreme case, approximately $II_t^* < 0.01$, the threshold captures too much of the low-level vorticity surrounding the core, and so this threshold cannot be said to capture what is commonly considered to be the 'vortex core'. Example results for various II_t^* are tabulated in table 3.

A.2. *Effect of choice of* t_{start}^*

The influence of choice of t_{start}^* on the assessment was examined by computing ε and η using several alternative choices of t_{start}^* in the vicinity of the departure from linear $A_{II}(t)$ growth (using $II_t^* = 0.10$ and maintaining the same choice of t_{end}^* for a given case as was used in the main body of this study). Results are presented in figure 17. Even when the most extreme plausible values of t_{start}^* are used (approximately 37 % earlier and 15 % later than the selected t_{start}^*), a maximum ε deviation of only 2.4 % was observed relative to the canonical value of ε (i.e. that used in the main body of the study) for the UPEA cases (EPUA and UPUA cases were not tested). Moreover,

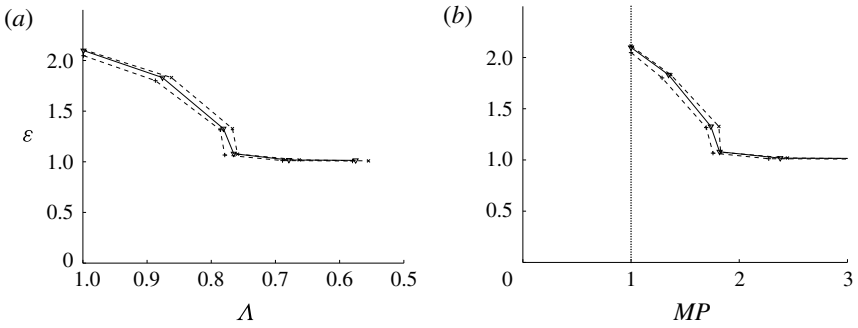

FIGURE 17. Collected results for ε of UPEA as a function of (*a*) Λ and (*b*) MP for various choices of t^*_{start}, $\Pi^*_t = 0.10$, $Re_\Gamma = 5000$. Solid line with $\triangledown$ indicates t^*_{start} as selected in the main body (figures 7 and 9); $+$ indicates earlier choice of t^*_{start}, $\times$ indicates later choice of t^*_{start}.

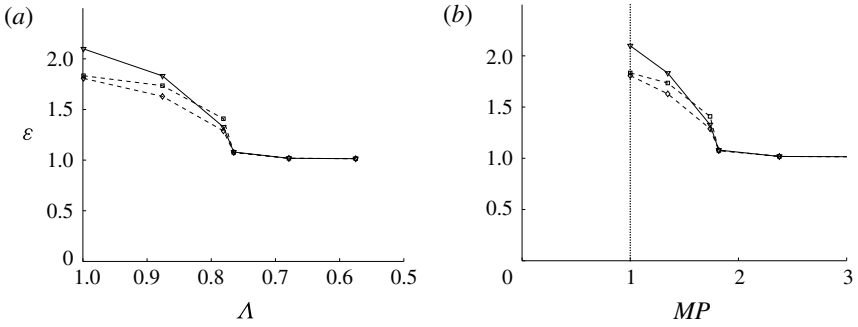

FIGURE 18. Collected results for ε of UPEA cases as a function of (*a*) Λ and (*b*) MP for various choices of t^*_{end}, $\Pi^*_t = 0.10$, $Re_\Gamma = 5000$. $\triangledown$ indicates t^*_{end} as selected in the main body (figures 7 and 9), $\diamond$ indicates t^*_{det} used for all cases, $\square$ indicates t^*_{single} used for all cases. Note that these methods give identical results in the straining-out regime.

a similar general trend was found for ε (and η, not pictured) with respect to Λ and MP for all t^*_{start} considered (see figure 17), indicating that the choice of t^*_{start} has little influence on the findings discussed in the present study.

A.3. *Effect of choice of* t^*_{end}

Likewise, the effect of choice of t^*_{end} was examined by considering two alternative choices: t^*_{det} for every case, since it constitutes a consistent objective time identifiable in every case even though it does not mark the 'end' of the interaction for cases in which entrainment occurs, as well as a time t^*_{single} subsequent to both t^*_{det} and t^*_{ent} at which the final vortex is judged to have formed (using $\Pi^*_t = 0.10$ and maintaining the same choice of t^*_{start} for a given case as was used in the main body of this study). Results are presented in figure 18, where it can be seen that although different choices can give different values of ε and η (with t^*_{ent} giving somewhat higher values for high Λ and MP near 1), all three capture essentially the same trend with respect to Λ and MP, and the critical value MP_{cr} remains unchanged. Note that this is true even using exclusively t^*_{det}, despite this not being the 'end' of interaction for cases in which entrainment occurs.

REFERENCES

BRANDT, L. K. & NOMURA, K. K. 2006 The physics of vortex merger: further insight. *Phys. Fluids* **18** (5), 051701.

BRANDT, L. K. & NOMURA, K. K. 2007 The physics of vortex merger and the effects of ambient stable stratification. *J. Fluid Mech.* **592**, 413–446.

BRANDT, L. K. & NOMURA, K. K. 2010 Characterization of the interactions of two unequal co-rotating vortices. *J. Fluid Mech.* **646**, 233–253.

CARNEVALE, G. F., MCWILLIAMS, J. C., POMEAU, Y., WEISS, J. B. & YOUNG, W. R. 1991 Evolution of vortex statistics in two-dimensional turbulence. *Phys. Rev. Lett.* **66** (21), 2735–2737.

CARNEVALE, G. F., MCWILLIAMS, J. C., POMEAU, Y., WEISS, J. B. & YOUNG, W. R. 1992 Rates, pathways, and end states of nonlinear evolution in decaying two-dimensional turbulence: scaling theory versus selective decay. *Phys. Fluids* A **4** (6), 1314–1316.

CERRETELLI, C. & WILLIAMSON, C. H. K. 2003 The physical mechanism for vortex merging. *J. Fluid Mech.* **475**, 41–77.

DRITSCHEL, D. G., SCOTT, R. K., MACASKILL, C., GOTTWALD, G. A. & TRAN, C. V. 2008 Unifying scaling theory for vortex dynamics in two-dimensional turbulence. *Phys. Rev. Lett.* **101** (9), 094501.

DRITSCHEL, D. G. & WAUGH, D. W. 1992 Quantification of the inelastic interaction of unequal vortices in two-dimensional vortex dynamics. *Phys. Fluids* A **4** (8), 1737–1744.

FOLZ, P. J. R. & NOMURA, K. K. 2014 Interaction of two equal co-rotating viscous vortices in the presence of background shear. *Fluid Dyn. Res.* **46** (3), 031423.

GERZ, T., SCHUMANN, U. & ELGHOBASHI, S. E. 1989 Direct numerical simulation of stratified homogeneous turbulent shear flows. *J. Fluid Mech.* **200**, 563–594.

HUANG, M. J. 2005 The physical mechanism of symmetric vortex merger: a new viewpoint. *Phys. Fluids* **17** (7), 074105.

HUANG, M. J. 2006 A comparison between asymmetric and symmetric vortex mergers. *WSEAS Trans. Fluid Mech.* **1** (5), 488–496.

HUNT, J. C. R., WRAY, A. A. & MOIN, P. 1988 Eddies, streams, and convergence zones in turbulent flows. *Center for Turbulence Research Report* CTR-S88.

JING, F., KANSO, E. & NEWTON, P. K. 2012 Insights into symmetric and asymmetric vortex mergers using the core growth model. *Phys. Fluids* **24** (7), 073101.

KIMURA, Y. & HERRING, J. R. 2001 Gradient enhancement and filament ejection for a non-uniform elliptic vortex in two-dimensional turbulence. *J. Fluid Mech.* **439**, 43–56.

LE DIZÈS, S. & LAPORTE, F. 2002 Theoretical predictions for the elliptical instability in a two-vortex flow. *J. Fluid Mech.* **471**, 169–201.

LE DIZÈS, S. & VERGA, A. 2002 Viscous interactions of two co-rotating vortices before merging. *J. Fluid Mech.* **467**, 389–410.

MARIOTTI, A., LEGRAS, B. & DRITSCHEL, D. G. 1994 Vortex stripping and the erosion of coherent structures in two-dimensional flows. *Phys. Fluids* **6** (12), 3954–3962.

MAZE, G., CARTON, X. & LAPEYRE, G. 2004 Dynamics of a 2D vortex doublet under external deformation. *Regular Chaotic Dyn.* **9** (4), 477–497.

MCWILLIAMS, J. C. 1990 The vortices of two-dimensional turbulence. *J. Fluid Mech.* **219**, 361–385.

MELANDER, M. V., MCWILLIAMS, J. C. & ZABUSKY, N. J. 1987*a* Axisymmetrization and vorticity-gradient intensification of an isolated two-dimensional vortex through filamentation. *J. Fluid Mech.* **178**, 137–159.

MELANDER, M. V., ZABUSKY, N. J. & MCWILLIAMS, J. C. 1987*b* Asymmetric vortex merger in two dimensions: which vortex is victorious? *Phys. Fluids* **30** (9), 2610–2612.

MELANDER, M. V., ZABUSKY, N. J. & MCWILLIAMS, J. C. 1988 Symmetric vortex merger in two dimensions: causes and conditions. *J. Fluid Mech.* **195**, 303–340.

MEUNIER, P. 2001 Etude expérimentale de deux tourbillons corotatifs. PhD thesis, Université de Provence-Aix-Marseille I.

MEUNIER, P., EHRENSTEIN, U., LEWEKE, T. & ROSSI, M. 2002 A merging criterion for two-dimensional co-rotating vortices. *Phys. Fluids* **14** (8), 2757–2766.

ORLANDI, P. 2000 *Fluid Flow Phenomena: A Numerical Toolkit. Fluid Flow Phenomena: A Numerical Toolkit*, vol. 1. Springer.

OVERMAN, E. A. II & ZABUSKY, N. J. 1982 Evolution and merger of isolated vortex structures. *Phys. Fluids* **25** (8), 1297–1305.

PERROT, X. & CARTON, X. 2010 2D vortex interaction in a non-uniform flow. *Theoret. Comput. Fluid Dyn.* **24** (1–4), 95–100.

RICCARDI, G., PIVA, R. & BENZI, R. 1995 A physical model for merging in two-dimensional decaying turbulence. *Phys. Fluids* **7** (12), 3091–3104.

SAFFMAN, P. G. 2001 *Vortex Dynamics*. Cambridge University Press.

SAFFMAN, P. G. & SZETO, R. 1980 Equilibrium shapes of a pair of equal uniform vortices. *Phys. Fluids* **23** (12), 2339–2342.

SIRE, C., CHAVANIS, P. H. & SOPIK, J. 2011 Effective merging dynamics of two and three fluid vortices: application to two-dimensional decaying turbulence. *Phys. Rev.* E **84** (5), 056317.

TABELING, P. 2002 Two-dimensional turbulence: a physicist approach. *Phys. Rep.* **362** (1), 1–62.

TRIELING, R. R., DAM, C. E. C. & VAN HEIJST, G. J. F. 2010 Dynamics of two identical vortices in linear shear. *Phys. Fluids* **22** (11), 117104.

TRIELING, R. R., VELASCO FUENTES, O. U. & VAN HEIJST, G. J. F. 2005 Interaction of two unequal corotating vortices. *Phys. Fluids* **17** (8), 087103.

WAUGH, D. W. 1992 The efficiency of symmetric vortex merger. *Phys. Fluids* A **4** (8), 1745–1758.

YASUDA, I. & FLIERL, G. R. 1997 Two-dimensional asymmetric vortex merger: merger dynamics and critical merger distance. *Dyn. Atmos. Oceans* **26** (3), 159–181.

The contents of this chapter have been published in the Journal of Fluid Mechanics, Folz, Patrick J. R.; Nomura, Keiko K., “A quantitative assessment of viscous asymmetric vortex pairs”, Cambridge University Press, 2017. The dissertation author was the primary researcher and author, and the research supervisor was the co-author of the paper.

Chapter 5

On asymmetric vortex pair interactions in shear

JFM PAPERS

On asymmetric vortex pair interactions in shear

Patrick J.R. Folz[1],† **and Keiko K. Nomura**[1]

[1]Department of Mechanical and Aerospace Engineering, University of California, San Diego, 9500 Gilman Drive, La Jolla, CA 92093-0411, USA

(Received 6 November 2022; revised 10 April 2023; accepted 13 June 2023)

This study examines the two-dimensional interaction of two unequal co-rotating viscous vortices in uniform background shear. Numerical simulations are performed for vortex pairs having various circulation ratios $\Lambda_0 = \Gamma_{1,0}/\Gamma_{2,0} = (\omega_{1,0}/\omega_{2,0})(a_{1,0}^2/a_{2,0}^2) \leqslant 1$, corresponding to different initial characteristic radii $a_{i,0}$ and peak vorticities $\omega_{i,0}$ of each vortex $i = 1, 2$, in shears of various strengths $\zeta_0 = \omega_S/\omega_{2,0}$, where ω_S is the constant vorticity of the shear. Two primary flow regimes are observed: separations ($\zeta_0 < \zeta_{sep} < 0$), in which the vortices move apart continuously, and henditions ($\zeta_0 > \zeta_{sep}$), in which the interaction results in a single vortex (where ζ_{sep} is the adverse shear strength beyond which separation occurs). Vortex motion and values of $\zeta_{sep}(\Lambda_0)$ are well-predicted by a point-vortex model for unequal vortices. In vortex-dominated henditions, shear varies the peak–peak distance b, and vortex deformation. The main convective interaction begins when core detrainment of one vortex is established, and proceeds similarly to the no-shear ($\zeta_0 = 0$) case: merger occurs if the second vortex also detrains, engendering mutual entrainment; otherwise straining out occurs. Detrainment requires persistence of straining of both sufficient magnitude, as indicated by relative straining above a consistent critical value, $(S/\omega)_i > (S/\omega)_{cr}$, where S is the strain rate magnitude at the vorticity peak, and conducive direction. Hendition outcomes are assessed in terms of an enhancement factor $\varepsilon \equiv \Gamma_{end}/\Gamma_{2,start}$. Although ε generally varies with ζ_0, $(a_{1,0}^2/a_{2,0}^2)$ and $(\omega_{1,0}/\omega_{2,0})$ in a complicated manner, this variation is well-characterized by the pair's starting enstrophy ratio, Z_2/Z_1. Within a transition region between merger and straining out (approximately $1.65 < Z_2/Z_1 < 1.9$), shear of either sense may increase ε.

Key words: vortex dynamics, vortex interactions

† Email address for correspondence: pjfolz@ucsd.edu

1. Introduction

Vortices and their interactions play significant roles in myriad flows ranging from the astrophysical (Fu *et al.* 2014) to the quantum mechanical (Baggaley & Barenghi 2018), and as such, have attracted intense research interest for decades. A large portion of this research has focused on the relatively simplified case of two-dimensional vortices, which are generally agreed to play a role in the famous inverse energy cascade in two-dimensional turbulence, although by what means and to what extent remain uncertain (Xiao *et al.* 2009; Burgess, Dritschel & Scott 2017*a*,*b*; Sutyrin 2019). Studies of two-dimensional vortices and their role in inter-scale flow phenomena have generally fallen into one of two categories: macroscopic studies of the vortex population in aggregate, which generally focus on the evolution of the number of vortices in the flow field and the distribution of their properties (Tabeling 2002); and atomic studies that consider in detail a single pair of vortices, whose interaction is often considered a 'building block' of the more complicated flows (Leweke, Le Dizès & Williamson 2016). The vast majority of these atomic studies have considered a symmetric pair – two identical vortices – interacting in isolation; a handful have considered unequal vortices interacting in isolation; a small number have considered a symmetric pair in a background flow such as linear shear; and to date none have considered the most general case of two unequal vortices interacting in background flow. This is despite that last-mentioned case being, self-evidently, the most common in turbulent flows; to study it necessitates a robust, general understanding of the isolated two-vortex interaction, which until recently has remained elusive. However, recent developments have elucidated a general underlying physical model for vortex interactions, enabling the more general case to now be considered.

An isolated symmetric pair of two-dimensional co-rotating vortices undergoes merger, combining the fluid of each into a single compound vortex, when its aspect ratio surpasses a critical value, $a/b > (a/b)_{cr}$, where a is the characteristic vortex radius, and b is the peak–peak distance; prior to the onset of the merging process, $a = a(t)$ grows (in viscous flow) and $b = b_0$ remains constant (see e.g. Melander, Zabusky & McWilliams 1988; Cerretelli & Williamson 2003; Meunier, Le Dizès & Leweke 2005). This critical distance corresponds to the point at which their mutual strain causes the vortices to become sufficiently deformed that fluid detrains from the vortex cores, in the vicinity of a central hyperbolic point in the instantaneous streamline pattern (e.g. Velasco Fuentes 2005; Brandt & Nomura 2006). This engenders a mutual entrainment process whereby the vortex cores move together rapidly, producing the compound vortical structure (Huang 2005; Brandt & Nomura 2007). When viscosity is present, the continuous growth of a ensures that $(a/b)_{cr}$ is always eventually met (Melander *et al.* 1988).

An isolated asymmetric pair – two unequal co-rotating vortices – on the other hand, may interact in one of several different ways, depending on a number of factors (e.g. Melander, Zabusky & McWilliams 1987; Dritschel & Waugh 1992; Yasuda & Flierl 1997; Trieling, Velasco Fuentes & van Heijst 2005). There is therefore no simple critical merging distance or similar criterion for interaction (Dritschel & Waugh 1992). When viscosity is present, the interaction always produces a single vortex, but the interaction may be either a merger similar to the symmetric case, or a straining out in which only one vortex is induced to detrain and is ultimately broken up and destroyed, while the survivor remains essentially unaffected (Huang 2006). Thus the outcome of interaction depends upon the relative timing of detrainment and destruction (Brandt & Nomura 2010): once the first vortex is induced to detrain, if it can induce the second to also detrain before the first breaks up, then mutual entrainment ensues (i.e. merger occurs); otherwise, the first-detraining vortex is simply destroyed (i.e. straining out occurs).

In other words, the outcome of an asymmetric pair interaction derives from the degree of mutuality of the interaction. Folz & Nomura (2017) assessed these outcomes quantitatively in terms of an enhancement factor $\varepsilon \equiv \Gamma_{end}/\Gamma_{2,start}$ and a merging efficiency $\eta \equiv \Gamma_{end}/\Gamma_{tot,start}$, and found that all interaction outcomes across a wide range of pair parameters (including initial peak vorticity ratio $\omega_{1,0}/\omega_{2,0}$ and initial radius ratio $a_{1,0}/a_{2,0}$) were well-characterized by a mutuality parameter

$$MP = \frac{(S/\omega)_1}{(S/\omega)_2}, \tag{1.1}$$

which compares the relative straining $(S/\omega)_i$ of each vortex $i = 1, 2$, where S is the strain rate magnitude (note that $S = \sqrt{\boldsymbol{S^2}}$, where $\boldsymbol{S^2} = \mathrm{tr}[S_{mn}S_{mn}]$), and ω is the absolute vorticity at the vortex peak. Merger corresponds to MP near unity and straining out to high MP, with a narrow transition region between them. This is consistent with an earlier finding by Trieling *et al.* (2005) that the occurrence of complete merger of an asymmetric pair (in inviscid flow) was characterized reasonably well by a critical merging distance based on the pair's mean radius ($\bar{a}$), while complete straining out occurred when b_0 was below that associated with an induced relative strain rate sufficient to cause breakup of a single vortex in shear. Dritschel & Waugh (1992) found similar results for highly disparate Rankine vortices. The relative straining, in turn, reflects the deformation (i.e. eccentricity) of each vortex (see Le Dizès & Laporte 2002; Leweke *et al.* 2016), and the onset of detrainment for a given vortex is associated with a consistent critical value $(S/\omega)_{cr} \approx 0.135 \pm 0.003$ (Folz & Nomura 2017). For a symmetric pair, these criteria are equivalent to $(a/b)_{cr}$. This mutuality model (including the detrainment–entrainment processes) constitutes a general model for the interaction of two two-dimensional vortices in isolation.

This paper now examines the influence of linear background shear – which can be considered a first-order approximation of the flow generated by surrounding vortices in a turbulent flow field – on these processes (e.g. Trieling, Dam & van Heijst 2010). The shear is characterized in terms of a shear strength parameter of the form

$$\zeta \equiv \omega_S/\omega_2, \tag{1.2}$$

which compares the constant vorticity of the shear $\omega_S = -\alpha \equiv -\mathrm{d}U/\mathrm{d}y$ to a characteristic vorticity of the pair (which potentially could be time-varying; here the vorticity of the stronger vortex 2 is used). Shear is considered favourable when it has the same rotational sense as the vortices, i.e. when $\zeta > 0$, and adverse when they are opposed, i.e. when $\zeta < 0$. In general, shear deforms a vortex elliptically, with the major axis oriented approximately orthogonal to or aligned with the shear direction in favourable and adverse shear, respectively.

When adverse shear acts on a single isolated vortex, the opposing rotations of the vortex and the shear create a pair of hyperbolic stagnation points in the elliptical streamline pattern about the vortex center, which causes peripheral vorticity of a non-uniform vortex to be advected away, or 'stripped', in the form of filaments (see e.g. Legras & Dritschel 1993; Kimura & Herring 2001; Legras, Dritschel & Caillol 2001; Hurst *et al.* 2016). This is fundamentally the same physical process as detrainment of a vortex in a pair. Increasing the relative strength of adverse shear (i.e. making $\zeta < 0$ more negative) causes detrainment to occur at progressively higher vorticity levels within the non-uniform vortex (Legras & Dritschel 1993), until a generally consistent critical shear strength is reached at which the vortex breaks up and is rapidly elongated into a filament ($\zeta_{bu} = -0.10$ to -0.13; see

also Mariotti, Legras & Dritschel 1994; Paireau, Tabeling & Legras 1997). In viscous flow, the peak vorticity of the vortex, $\omega = \omega(t)$, generally decays in time due to viscous diffusion, causing $|\zeta|$ (of either sense) to increase (as $\sim 1/\omega$, due to conservation of circulation $\Gamma = \pi a^2 \omega = \text{const.}$ as area increases, linearly for the no-shear, i.e. $\zeta_0 = 0$, case, $a^2(t) = a_0^2 + 4\nu t$; see e.g. Meunier *et al.* 2002), ensuring that detrainment and breakup always ultimately occur in adverse shear.

When two co-rotating vortices are present, the shear exerts these same influences directly upon each as they interact with each other. As noted above, all studies of this case to date have considered a symmetric pair (e.g. Carton, Maze & Legras 2002; Perrot & Carton 2010; Marques Rosas Fernandes *et al.* 2016). Additionally, and perhaps most significantly, sufficiently adverse shear, i.e. $\zeta < \zeta_{sep}$, causes separation of the pair, wherein the vortices simply move apart indefinitely rather than merging or orbiting (observed by Kimura & Hasimoto (1985) for point vortices; Maze, Carton & Lapeyre (2004) for finite-area inviscid vortices; and Folz & Nomura (2014) for finite-area vortices with viscosity). If it does not cause separation, the shear causes the vortices to follow elliptical trajectories rather than circular. Note that whether the shear causes $b = b(t)$ to increase or decrease from the initial b_0 depends not only upon the relative sense of shear, as is often stated in the literature, but also upon the initial orientation of the vortices (this is discussed briefly in § 5). In inviscid flow, a stationary case ($\zeta = \zeta_{sep}$) exists between the separation and elliptical motion cases, with two distinct types of cases for $\zeta > \zeta_{sep}$: periodic motion and merger. The occurrence of merger is found to be reasonably well-characterized by the minimum b falling sufficiently low that the aspect ratio surpasses the critical value previously found for symmetric pairs without shear (Trieling *et al.* 2010). In viscous flow, the presence of viscosity effectively ensures that merger always occurs when $\zeta > \zeta_{sep}$, commencing when the combined variation of a and b results in $a/b > (a/b)_{cr}$, where the value of $(a/b)_{cr}$ is similar to that observed in the no-shear case (Folz & Nomura 2014). In these cases, the primary effect of shear is to accelerate or delay the onset of the merging process.

Drawing upon these observations, the convective interaction of two unequal vortices under the influence of linear background shear is now examined. Numerical simulations of an asymmetric pair of two-dimensional viscous vortices in linear background shear are performed. The interaction regimes are identified and supported by analytical and point-vortex results. This study focuses primarily on cases in which the vortices interact to produce a single resulting vortex, i.e. henditions (see § 1.1). For these cases, the influence of shear on vortex motion, deformation and interaction processes is examined both qualitatively and quantitatively. A characterization of the interaction outcomes is developed, in the course of which a quantitative assessment is performed in the manner of Folz & Nomura (2017), and the results are correlated to significant pair parameters. Since the parameter space of this flow is quite large, this study considers primarily the effects of initial shear strength ζ_0 and initial circulation ratio Λ_0, with two sub-categories of the latter. These results elucidate the major effects of shear on a pair of interacting vortices, and show how their interaction outcomes relate to the considered initial flow parameters, forming a basis from which future studies may consider further parameters and flow regimes.

This paper is organized as follows. First, § 2 discusses the motion of a pair of unequal point vortices in linear background shear, and an analytical expression for the critical shear strength for separation is obtained. Next, § 3 describes the flow set-up and simulations. Then § 4 gives general observations for vortex interactions in shear and identifies the main flow regimes: § 4.1 discusses separations, and § 4.2 outlines the vortex-dominated regime.

In § 5 is the heart of the study, which analyses vortex-dominated henditions. The first subsection, § 5.1, describes the method used to perform the quantitative assessment of the hendition outcomes; the second subsection, § 5.2, examines the influence of the shear on the timing and duration of detrainment; and the final subsection, § 5.3, presents the results of the quantitative assessment and discusses the influence of shear. Finally, § 6 summarizes the findings, and discusses some implications and potential areas of further study. Supplementary material is also provided (available online at https://doi.org/10.1017/jfm.2023.525), which includes additional information about the quantities used to evaluate henditions, including their time development in the single-vortex case.

1.1. *A note on nomenclature: hendition*

There is no extant word in the English language that means, simply, 'two things become one thing' without also implying either increase or enhancement (combination, unification, consolidation, fusion, incorporation, etc.). This is certainly the case for 'merger', which is used as a generic term by some researchers (e.g. Melander *et al.* 1987; Tabeling 2002; Jing, Kanso & Newton 2012), while others use it to denote specifically interactions that produce an enhanced resulting vortex (e.g. Dritschel & Waugh 1992; Trieling *et al.* 2005; Brandt & Nomura 2010). Other terms imply only destruction without any increase or enhancement (annihilation, removal, etc.). This muddles the terminology and obscures the distinction between fundamentally different types of interaction (those in which mutual entrainment does, and does not, occur).

As such, the authors introduce the new term 'hendition', from the Greek phrase 'ἓν διὰ δυοῖν' meaning 'one through two'. A hendition is an occurrence in which there are two vortices at the start and only one at the end, regardless of the properties of the resulting vortex (relative to the starting vortices) or the physical process by which this interaction proceeds. Merger and straining out are then specific types of hendition, as is the case of two vortices becoming one through diffusion (not considered here). In a more complicated flow, such as two-dimensional turbulence, the case of a dipole encountering a third vortex, after which the two like-signed vortices interact to produce one, would be considered a hendition. The case of three or more like-signed vortices interacting simultaneously, resulting ultimately in a single vortex, could be referred to by a similar term: henmultion. It is hoped that the use of the term 'hendition' will ensure clarity of this paper, and more generally may be of use in vortex-related discussions going forward.

2. Modified point-vortex model for unequal vortices

The basic behaviour of two well-separated vortices is similar to that of two point vortices (Trieling *et al.* 2010), even in viscous flow (Folz & Nomura 2014). Kimura & Hasimoto (1985) studied the motion of equal point vortices in shear, and Ryzhov, Koshel & Carton (2012) studied the motion of unequal point vortices in an arbitrary deformation flow. Here, the motion of two unequal point vortices in uniform background shear is examined, and the boundary between the major flow regimes is identified.

Two point vortices having circulation ratio $\Lambda \equiv \Gamma_1/\Gamma_2$ are located initially at $x_1 = -b_0/2$ and $x_2 = b_0/2$ and $y_0 = 0$, where b_0 is the initial peak–peak distance, and x and y are the flow and shear directions, respectively. The linear background shear has constant strength $\alpha \equiv \mathrm{d}U/\mathrm{d}y$. The vortices' motion is described by a system of equations (Kimura

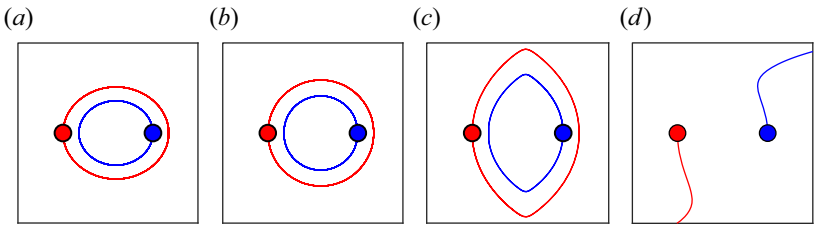

Figure 1. Trajectories of point vortices of pairs (red for vortex 1, blue for vortex 2), having circulation ratio $\Lambda = \Gamma_1/\Gamma_2 = 0.70$, within shear of various strengths $\mu = \alpha b_0^2/\Gamma_2$. For this case, separation shear strength is $\mu_{sep} = 0.0995$. The filled circles indicate the starting positions for the integrated trajectories (2.1)–(2.4), with (*a*) $\mu = -0.0992$, (*b*) $\mu = 0$, (*c*) $\mu = 0.0992$, and (*d*) $\mu = 0.128$.

& Hasimoto 1985)

$$\frac{\mathrm{d}x_1}{\mathrm{d}t} = -\frac{\Gamma_2}{2\pi}\frac{y_1 - y_2}{b^2} + \alpha y_1, \tag{2.1}$$

$$\frac{\mathrm{d}y_1}{\mathrm{d}t} = \frac{\Gamma_2}{2\pi}\frac{x_1 - x_2}{b^2}, \tag{2.2}$$

$$\frac{\mathrm{d}x_2}{\mathrm{d}t} = -\frac{\Gamma_1}{2\pi}\frac{y_2 - y_1}{b^2} + \alpha y_2, \tag{2.3}$$

$$\frac{\mathrm{d}y_2}{\mathrm{d}t} = \frac{\Gamma_1}{2\pi}\frac{x_2 - x_1}{b^2}, \tag{2.4}$$

where (x_i, y_i) are the coordinates of vortex $i = 1, 2$, and the instantaneous peak–peak distance $b = \sqrt{(x_1 - x_2)^2 + (y_1 - y_2)^2}$ may vary in time. The y-coordinate of the centre of rotation of the system is $Y = (\Gamma_1 y_1 + \Gamma_2 y_2)/(\Gamma_1 + \Gamma_2)$, and is always at 0.

These equations can be integrated to find the vortex trajectories. In symmetric flow, these trajectories are either closed or open, with a critical stationary case separating these regimes (Kimura & Hasimoto 1985). Trieling *et al.* (2010) characterized these regimes using a non-dimensional shear strength parameter $\mu_s = \alpha b_0^2/\Gamma$ for symmetric vortices. Closed trajectories occur in favourable ($\mu_s < 0$) to weakly adverse ($\mu_{s,sep} > \mu_s > 0$) shear, where $\mu_{s,sep}$ is the critical shear strength associated with the stationary case. In this regime, from their initial position, the vortices follow overlapping elliptical trajectories where an extremum of b occurs when the vortices are aligned vertically, i.e. along the shear direction. This extremum is minimum b in favourable shear, and maximum b in adverse shear, respectively, with circular trajectories occurring in the no-shear case ($\mu_s = 0$). Open trajectories occur in strongly adverse shear ($\mu_s > \mu_{s,sep} > 0$), and the vortices simply move apart continuously; this behaviour is termed separation.

For the case of unequal vortices, a similar parameter is constructed:

$$\mu = \alpha b_0^2/\Gamma_2 \tag{2.5}$$

based on the stronger vortex, here taken to be 2. Figure 1 shows example trajectories for a pair having $\Lambda = 0.70$ in various μ. Similar regimes are observed, with the vortices following closed concentric elliptical trajectories for favourable ($\mu < 0$) or weakly adverse ($\mu_{sep} > \mu > 0$) shear, and open trajectories for strongly adverse shear ($\mu > \mu_{sep}$), distinguished by a critical separation shear strength μ_{sep}.

In the symmetric case, an analytical expression for the critical shear strength associated with the stationary case, similar to $\mu_{s,sep}$, was derived by Kimura & Hasimoto (1985)

using the Hamiltonian of the system (2.1)–(2.4),

$$H = \frac{-\Gamma_1\Gamma_2}{4\pi}\ln[((x_1-x_2)^2+(y_1-y_2)^2)] + \frac{\alpha}{2}(\Gamma_1 y_1^2+\Gamma_2 y_2^2). \tag{2.6}$$

When the vortices are unequal, many of their simplifying assumptions cannot be made, but an analytical expression for μ_{sep} may nevertheless be found in the following manner.

Rearranging (2.6) gives

$$H - \frac{\alpha}{2}(\Gamma_1 y_1^2+\Gamma_2 y_2^2) = \frac{-\Gamma_1\Gamma_2}{4\pi}\ln[((x_1-x_2)^2+(y_1-y_2)^2)]. \tag{2.7}$$

Then

$$\exp\left(H\frac{-4\pi}{\Gamma_1\Gamma_2} - \frac{-4\pi}{\Gamma_1\Gamma_2}\frac{\alpha}{2}(\Gamma_1 y_1^2+\Gamma_2 y_2^2)\right) = ((x_1-x_2)^2+(y_1-y_2)^2), \tag{2.8}$$

and noting that H is constant,

$$C\exp\left(\frac{4\pi}{\Gamma_1\Gamma_2}\frac{\alpha}{2}(\Gamma_1 y_1^2+\Gamma_2 y_2^2)\right) = ((x_1-x_2)^2+(y_1-y_2)^2) = \xi^2+\eta^2, \tag{2.9}$$

where $\xi \equiv x_1 - x_2$ and $\eta \equiv y_1 - y_2$ (using the nomenclature of Kimura & Hasimoto 1985), and $C = \xi_0^2$ since $\eta = 0$ in the initial condition.

When the vortices are oriented vertically, the coordinates y_1 and y_2 are equal to the distances of the weaker and stronger vortices from the centre of rotation, r_1 and r_2 respectively, since that centre remains fixed in space. Additionally, $\eta = b$ in the vertical orientation. Therefore, at the critical time,

$$y_1 = r_1 \equiv \frac{1}{1+\Lambda}\eta_v, \quad y_2 = r_2 \equiv \frac{\Lambda}{1+\Lambda}\eta_v, \tag{2.10a,b}$$

where η_v is η when the vortices are aligned vertically, and $\Lambda \equiv \Gamma_1/\Gamma_2$. So

$$\xi_0^2\exp\left(\frac{2\pi\alpha}{\Gamma_1\Gamma_2}(\Gamma_1 r_1^2+\Gamma_2 r_2^2)\right) = \eta_v^2, \tag{2.11}$$

$$\xi_0^2\exp\left(\frac{2\pi\alpha}{\Lambda\Gamma_2}\left(\Lambda\frac{\eta_v^2}{(1+\Lambda)^2}+\frac{\Lambda^2\eta_v^2}{(1+\Lambda)^2}\right)\right) = \eta_v^2, \tag{2.12}$$

and ultimately

$$\xi_0^2\exp\left(\frac{2\pi\alpha}{\Gamma_2(1+\Lambda)}\eta_v^2\right) = \eta_v^2. \tag{2.13}$$

Normalizing (2.13) by the initial peak–peak distance $\xi_0 = b_0$,

$$\exp\left(\frac{2\pi\alpha b_0^2}{\Gamma_2(1+\Lambda)}\left(\frac{\eta_v}{b_0}\right)^2\right) = \left(\frac{\eta_v}{b_0}\right)^2. \tag{2.14}$$

For this equation to have a finite solution, it must be true that

$$\frac{2\pi\alpha b_0^2}{\Gamma_2(1+\Lambda)} \leqslant \frac{1}{\mathrm{e}}, \tag{2.15}$$

Λ_0	$a_{1,0}^2/a_{2,0}^2$	$\zeta_{sep,p}$	ζ_{sep}	
			$Re_\Gamma = 5000$	$Re_\Gamma = 1000$
1.0	1.0	−0.0091	-0.0093 ± 0.0001	-0.0093 ± 0.0001
0.9	1.0	−0.0086	-0.0089 ± 0.0002	-0.0089 ± 0.0002
0.8	1.0	−0.0082	-0.0084 ± 0.0002	-0.0084 ± 0.0002
0.7	1.0	−0.0077	-0.0077 ± 0.0002	-0.0079 ± 0.0001
0.6	1.0	−0.0073	-0.0074 ± 0.0001	-0.0074 ± 0.0001
0.5	1.0	−0.0068	-0.0069 ± 0.0001	—
0.9	0.9	−0.0086	-0.0089 ± 0.0002	-0.0089 ± 0.0002
0.8	0.8	−0.0082	-0.0084 ± 0.0002	-0.0084 ± 0.0002
0.7	0.7	−0.0077	-0.0077 ± 0.0002	-0.0080 ± 0.0002
0.6	0.6	−0.0073	-0.0074 ± 0.0001	-0.0074 ± 0.0001
1.0	0.9	−0.0091	-0.0093 ± 0.0002	—
1.0	0.6	−0.0091	-0.0093 ± 0.0003	—
0.9	0.81	−0.0086	-0.0086 ± 0.0002	—
0.9	0.54	−0.0086	-0.0088 ± 0.0002	—

Table 1. Predicted $\zeta_{sep,p}$ from (2.18), with corresponding observed $\zeta_{sep} = -\alpha/\omega_{2,0}$ from numerical simulation of various starting pairs having $a_{2,0}/b_0 = 0.157$ (see § 4.1). The margin of error on the empirical data corresponds to the bracketing values used to determine ζ_{sep}.

so the critical criterion in terms of $\mu = \alpha b_0^2/\Gamma_2$ is

$$\mu_{sep} = \frac{(1+\Lambda)}{2\pi \mathrm{e}}. \tag{2.16}$$

Note that for symmetric vortices, this is identical to the criterion found by Trieling *et al.* (2010).

This criterion can be modified to apply for well-separated finite area vortices. Recalling that each vortex's circulation remains constant in this case, $\Gamma_2 = \Gamma_{2,0} = \pi a_{2,0}^2 \omega_{2,0}$ may be substituted into (2.16), where $a_{2,0}$ and $\omega_{2,0}$ are the stronger vortex's initial characteristic radius and peak vorticity, respectively:

$$\mu_{sep} = (\alpha b_0^2/\pi a_{2,0}^2 \omega_{2,0})_{sep} = \frac{(1+\Lambda)}{2\pi \mathrm{e}}. \tag{2.17}$$

Then

$$\left(\frac{-\alpha}{\omega_{2,0}}\right)_{sep} \equiv \zeta_{sep,p} = \frac{-(1+\Lambda)}{2\mathrm{e}} \left(\frac{a_{2,0}}{b_0}\right)^2, \tag{2.18}$$

where $\zeta_{sep,p}$ is a critical shear strength for the separation of finite-area vortices as predicted by this modified point-vortex model (an equivalent expression can be found by normalizing using vortex 1). It is seen that there is direct dependence between the magnitude of $\zeta_{sep,p}$ and both Λ and $(a_{2,0}/b_0)$: a more disparate pair (i.e. having lower Λ) will separate for weaker adverse shear than a more similar pair, although there is a minimum adverse shear strength required for any separation to occur ($\lim_{\Lambda \to 0} \zeta_{sep,p}(\Lambda) = (a_{2,0}/b_0)^2/(2\mathrm{e}) \neq 0$). Likewise, a given pair (i.e. having a given Λ) will separate for weaker shear the smaller their initial aspect ratio $a_{2,0}/b_0$ is (i.e. the larger their initial normalized peak–peak distance). Values for $\zeta_{sep,p}$ for various pairs are shown in table 1. In § 4.1, these values are compared to empirical results from simulations of finite-area pairs.

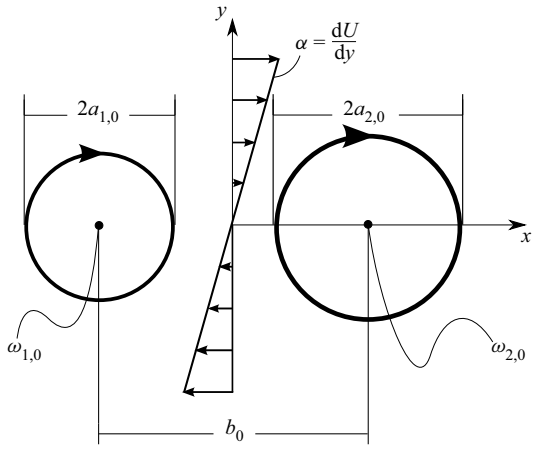

Figure 2. Initial flow configuration: two co-rotating vortices, $i = 1, 2$ (peak vorticity $\omega_{i,0}$, characteristic radius $a_{i,0}$, Gaussian vorticity distribution), whose peak–peak axis is oriented orthogonally to the direction of linear background shear (strength $\alpha = \mathrm{d}U/\mathrm{d}y$). The case shown has $\zeta_0 > 0$.

3. Set-up and numerical simulations

The initial flow configuration is shown in figure 2: for each case, two finite-area, co-rotating vortices are initially oriented along the flow direction of linear background shear, separated by an initial peak–peak distance b_0. Each vortex $i = 1, 2$ is initially circular with a Gaussian vorticity distribution, and has an initial peak vorticity $\omega_{i,0}$ and characteristic radius $a_{i,0}$, giving an initial circulation ratio

$$\Lambda_0 \equiv \frac{\Gamma_{1,0}}{\Gamma_{2,0}} = \frac{\omega_{1,0}a_{1,0}^2}{\omega_{2,0}a_{2,0}^2} \leqslant 1. \tag{3.1}$$

This study focuses primarily on pairs having either $\omega_{1,0}/\omega_{2,0} < 1$, $a_{1,0}^2/a_{2,0}^2 = 1$ (termed 'UPEA' for 'unequal peaks, equal areas'), or $\omega_{1,0}/\omega_{2,0} = 1$, $a_{1,0}^2/a_{2,0}^2 < 1$ (termed 'EPUA' for 'equal peaks, unequal areas'), as well as symmetric pairs (i.e. those having $\omega_{1,0}/\omega_{2,0} = a_{1,0}^2/a_{2,0}^2 = 1$). A handful of pairs having $\omega_{1,0}/\omega_{2,0} \neq 1$, $a_{1,0}^2/a_{2,0}^2 \neq 1$ (termed 'UPUA' for 'unequal peaks, unequal areas') are also included in § 4.1. The overall range of circulation ratios considered is $0.6 \leqslant \Lambda_0 \leqslant 1$ (a few additional UPEA cases with $\Lambda_0 = 0.50$ were also performed to aid in the analysis of separations). The pair's initial aspect ratio $a_{2,0}/b_0 = 0.157$ and the circulation Reynolds number $Re_\Gamma = \Gamma_{2,0}/\nu = 5000$ are maintained at constant values in order to facilitate comparison with the no-shear case ($\zeta_0 = 0$) examined previously in Folz & Nomura (2014, 2017). This also allows each vortex of the initially well-separated pair to adjust to the combined influence of the other vortex and the shear prior to interacting. This methodology helps to ensure that observed differences between the present results and the no-shear case are attributable primarily to the effects of shear.

The numerical simulations are performed using a hybrid finite-difference/pseudo-spectral code with periodic boundary conditions in the flow direction and shear-periodic boundary conditions in the shear direction (see Gerz, Schumann & Elghobashi (1989) for details of the method). The pair is initially positioned at the centre of a square domain of size $L \times L$ with 2048^2 grid points, and $b_0 = 1/24L$. This gives a resolution of approximately 38 points across the larger core. In comparison with a 1024^2 grid for cases

spanning the considered parameter range, differences in computed vortex quantities were found to be small (e.g. core circulation, an integrated quantity, differed by at most 2 %, and the starting relative straining $(S/\omega)_1$, a pointwise quantity, differed by at most 5 %), the quantitative assessments were similar (e.g. the merging efficiency η differed by at most five percentage points, and typically less than two; these quantities are discussed in § 5), and qualitatively all notable phenomena were observed for both resolutions in each case. Domain size independence was also tested using an initial separation distance $b_0 = 1/12L$ in the favourable case and $b_0 = 1/18L$ in the adverse case, with similarly small observed differences (e.g. η differed by at most six percentage points). The higher 2048^2 resolution and smaller $b_0 = 1/24L$ were utilized in all cases in order to minimize spurious variation in core quantities employing the threshold (see § 5), and to maintain maximum fidelity in general (this resolution was also previously found to be sufficient for the no-shear case; see Brandt & Nomura 2007, 2010).

The relative strength of the constant shear, $\alpha \equiv \mathrm{d}U/\mathrm{d}y$, is characterized in terms of its vorticity ω_s relative to that of the stronger vortex in the initial condition $\omega_{2,0}$:

$$\zeta_0 \equiv \frac{\omega_s}{\omega_{2,0}} = \frac{-\alpha}{\omega_{2,0}}. \tag{3.2}$$

In order to allow the vortices to adjust to the shear prior to the start of the main convective interaction, the range of $|\zeta_0|$ considered is limited to $|\zeta_0| < \zeta_{adj}$, where ζ_{adj} is a value chosen such that the viscous increase of $|\zeta|$ ($\sim 1/\omega(t)$; see § 1) would not be sufficient to induce detrainment prior to the end of the adjustment period of the vortices to each other, t^*_{adj}. This value ensures that $|\zeta_1(t^*_{adj})|, |\zeta_2(t^*_{adj})| < |\zeta_{cr,s}|$, where the critical shear strength associated with detrainment, $\zeta_{cr,s} \approx -0.063$, was found through simulations of a single vortex in shear (see the supplementary material). An estimate for t^*_{adj} is made using results from Le Dizès & Verga (2002) for a Gaussian vortex having $Re_\Gamma = 2000$ (the lower Re_Γ result is used to ensure a conservative estimate), which indicate an adjustment period of approximately $t\nu/(\pi a^2_{1,0}) = 0.05$ using their nomenclature. Using analytical results for a single isolated Gaussian vortex (see § 1) gives a requirement that $|\zeta_{i,0}| \leqslant 0.0387$, which in turn gives a value $|\zeta_{2,0}| \leqslant \zeta_{adj} \equiv 0.0387(\omega_{1,0}/\omega_{2,0})$.

In all cases, temporal results are presented on a convective time scale $t^* = t/T_0$, where $T_0 = (4\pi b_0^2)/(\Gamma_{1,0} + \Gamma_{2,0})$ is the period of revolution of a pair of point vortices having the same Λ_0 and $\zeta_0 = 0$.

4. General flow behaviour

First, observations of the general flow behaviour are made, and the major interaction regimes identified, for two unequal vortices interacting in the presence of shear (with finite viscosity). Figures 3 and 4 show vorticity contours of example cases demonstrating the major trends with respect to shear strength ζ_0 and vortex circulation ratio Λ_0. Observations for UPEA and EPUA cases are qualitatively similar, so only UPEA cases are shown. The motion and full flow development of two illustrative cases, $\zeta_0 = 0.0167$, $\Lambda_0 = 0.90$ and $\zeta_0 = -0.0073$, $\Lambda_0 = 0.70$, can be seen in supplementary movies 1 and 2, with useful related information presented in figure 5.

For comparison, a no-shear merger case is included ($\zeta_0 = 0$, $\Lambda_0 = 0.90$, figure 3*d*) and reviewed briefly. As discussed in § 1, when shear is not present, the vortices initially (columns 1–4) revolve along concentric circular trajectories (maintaining constant peak–peak distance b_0; see dashed lines in figures 5*b*,*e*), growing by viscous diffusion and deforming elliptically along the peak–peak axis due to their intensifying mutually induced

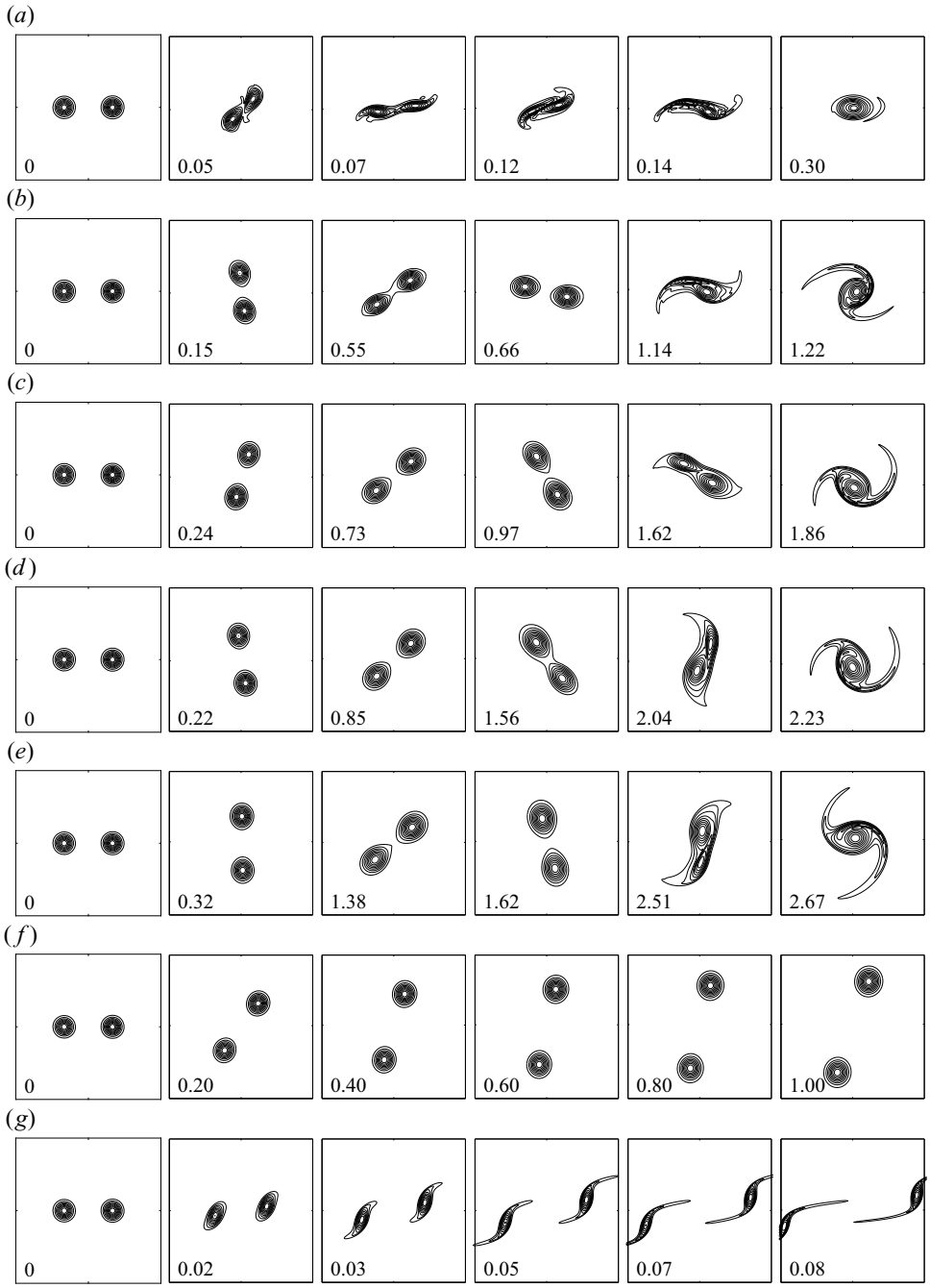

Figure 3. Vorticity contour plots showing time evolution of flows for UPEA pairs having $Re_\Gamma = 5000$ and $\Lambda_0 = 0.90$, with varying shear strength ζ_0: (*a*) $\zeta_0 = 0.1$, (*b*) $\zeta_0 = 0.0167$, (*c*) $\zeta_0 = 0.0045$, (*d*) $\zeta_0 = 0$ (no shear), (*e*) $\zeta_0 = -0.0045$, (*f*) $\zeta_0 = -0.0091$, and (*g*) $\zeta_0 = -0.1$. For $\Lambda_0 = 0.90$, $\zeta_{sep} = -0.0089$ (see table 1) and $\zeta_{adj} = 0.0348$; cases (*b–e*) fall within the vortex-dominated regime, $\zeta_{sep} < \zeta_0 < \zeta_{adj}$. For these cases, each column corresponds to an equivalent stage of flow development (see §§ 4 and 5.2): column 1, initial condition; column 2, first quarter-turn; column 3, oriented approximately 45° above the positive *x*-axis; column 4, start of core detrainment, $t^* = t^*_{start}$; column 5, end of core detrainment and start of mutual entrainment, $t^* = t^*_{det}$; and column 6, end of mutual entrainment, $t^* = t^*_{ent}$. For cases (*a*,*f*,*g*), the column images have been chosen to illustrate the general flow development. The vortices rotate clockwise in favourable shear (counter-clockwise in adverse shear). The contour interval is 10 %, and t^* for each plot is indicated at the lower left. The data in

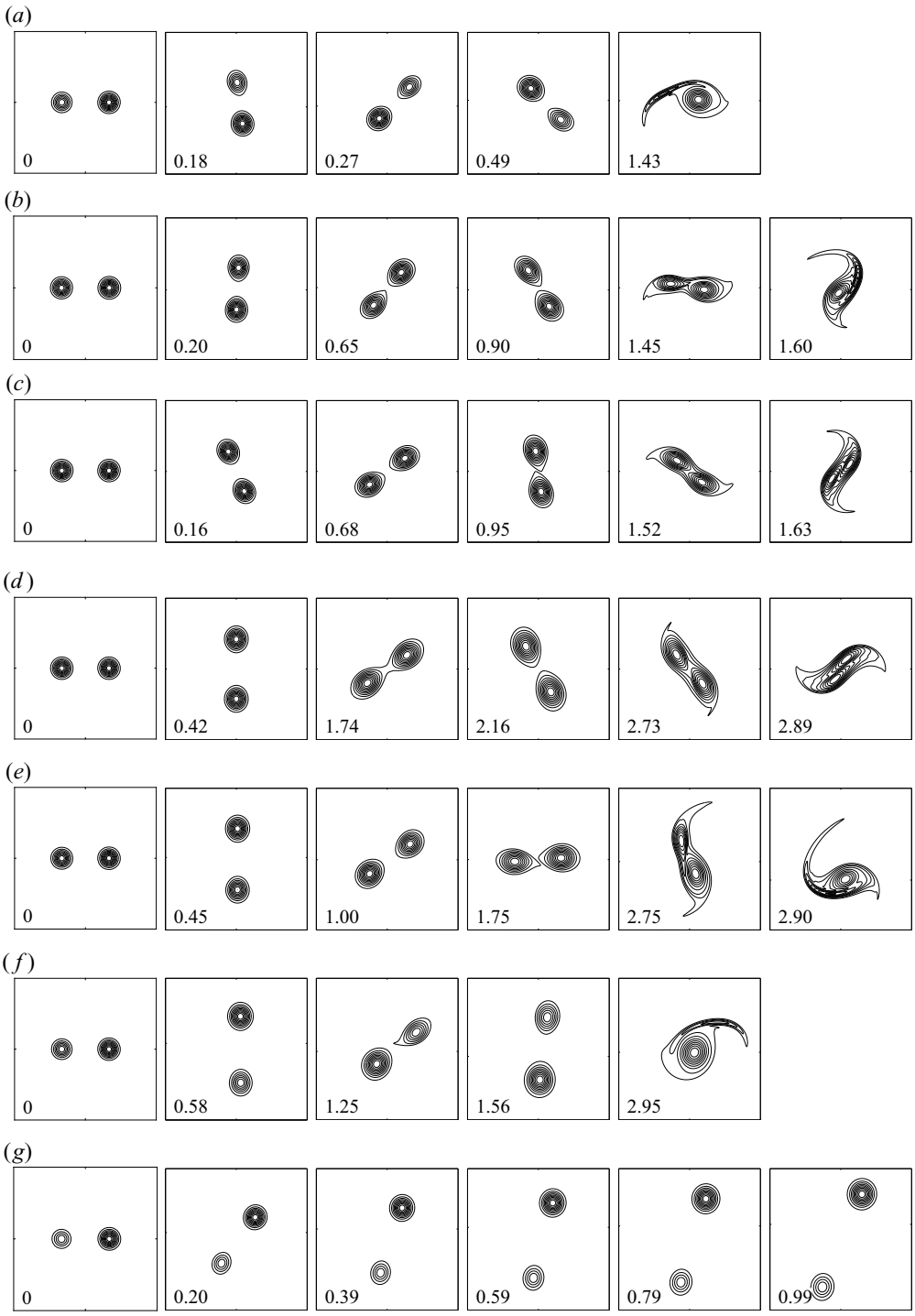

Figure 4. Vorticity contour plots showing time evolution of flows for UPEA pairs having $Re_\Gamma = 5000$ and $|\zeta_0| = 0.0073$, with varying Λ_0: (*a*) $\Lambda_0 = 0.7$, (*b*) $\Lambda_0 = 0.9$, (*c*) $\Lambda_0 = 1.0$ having favourable shear ($\zeta_0 = 0.0073$); and (*d*) $\Lambda_0 = 1.0$, (*e*) $\Lambda_0 = 0.9$, (*f*) $\Lambda_0 = 0.7$, (*g*) $\Lambda_0 = 0.5$ having adverse shear ($\zeta_0 = -0.0073$). The columns have meanings equivalent to those in figure 3, but the sixth column of the straining out cases has been omitted since no entrainment occurs. The vortices rotate clockwise in favourable shear (counter-clockwise in adverse shear). The contour interval is 10 %, and t^* for each plot is indicated at the lower left.

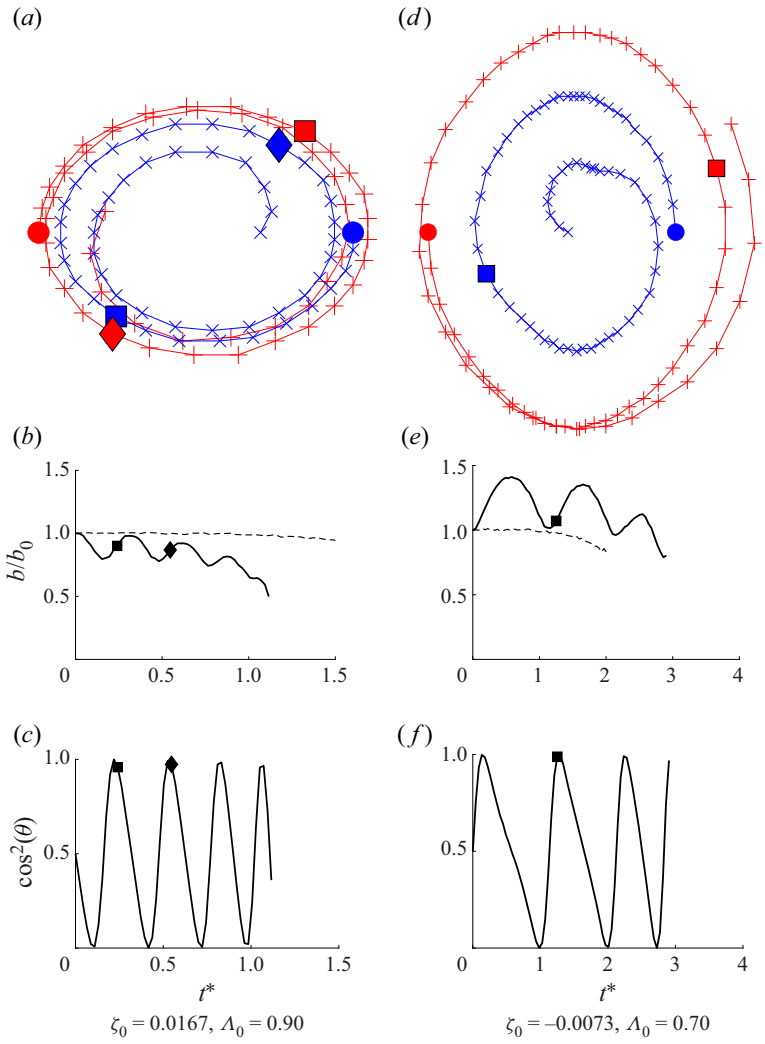

Figure 5. Time development of the vortex pair prior to the end of core detrainment for illustrative cases (solid lines): (*a*,*d*) trajectories of vortex peaks (red × indicates vortex 1, blue + indicates vortex 2); (*b*,*e*) normalized separation distance b/b_0; and (*c*,*f*) $\cos^2(\theta)$ of the angle θ between the peak–peak axis of the pair and the principal extensional strain eigenvector of the shear, $\boldsymbol{e}_\alpha$, which is oriented 45° from the flow direction. The Reynolds number is $Re_\Gamma = 5000$. Filled circles indicate starting positions, a square indicates the time of the first deformation maximum prior to the start of detrainment, and a diamond indicates the second such maximum that occurs in the $\zeta_0 = 0.0167$, $\Lambda_0 = 0.90$ case. These times are taken at the corresponding local maxima in the relative straining of the weaker vortex in each case, $(S/\omega)_1$, as discussed in § 5.1. In (*b*,*e*), the dashed line corresponds to the no-shear case having the same Λ_0.

strain, leading eventually to detrainment of at least one vortex's core fluid in the vicinity of the centre of rotation (column 4). This is the start of the main convective interaction: if both vortex cores detrain (columns 4–5), then a two-way interaction with mutual entrainment (columns 5–6), i.e. merger, occurs (as in figure 3*d*); otherwise, one vortex detrains and breaks up while the other remains relatively unaffected, i.e. straining out occurs. Due to the presence of viscosity, all like-signed pair interactions without shear are henditions, i.e. they result in a single vortex.

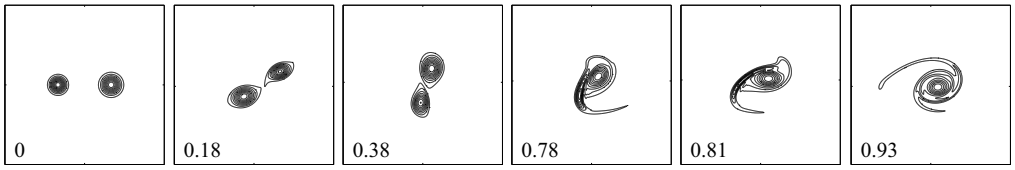

Figure 6. Vorticity contours for $\zeta_0 = 0.033$, $\Lambda_0 = a_1^2/a_2^2 = 0.70$, EPUA case (contour interval is 10 %, and $Re_\Gamma = 5000$). This case is a merger, whereas the equivalent no-shear case is a straining out (discussed further in § 5.1).

When shear is present ($\zeta_0 \neq 0$), it alters the motion and deformation of a pair (having a given Λ_0) in a manner and degree determined by its relative strength (figure 3). When shear is favourable ($\zeta_0 > 0$, figures 3*a–c*) or weakly adverse ($\zeta_{sep} < \zeta_0 < 0$, figure 3*e*), the interaction is a hendition; otherwise, when shear is strongly adverse ($\zeta_0 < \zeta_{sep} < 0$, figures 3*f*,*g*), the vortices undergo separation and move apart continuously. The separation case is discussed in § 4.1.

During shear-influenced henditions (such as those shown in the illustrative cases, i.e. figures 3(*b*) and 4(*f*) and supplementary movies 1 and 2), the vortices follow concentric elliptical trajectories in which the peak–peak distance b reaches a minimum (when $\zeta_0 > 0$) or maximum (when $\zeta_0 < 0$) when the peak–peak axis is aligned with the shear direction, akin to the point-vortex case discussed in § 2 (figures 5*a*,*d*,*b*,*e*). The shear causes periodic amplification of the deformation of the vortices, but, notably, this deformation is greatest when the peak–peak axis is oriented through the first and third quadrants, i.e. approximately along the direction of principal extensional strain of the shear, and not when b is minimal (figures 3*a–c*,*e* and 4*a–f*, columns 1–3, and figure 5). When shear is strongly favourable (figure 3*a*), it reduces b and amplifies deformation so substantially that it is the predominant cause of the hendition. Otherwise, when shear is weakly favourable or adverse, it is the viscous growth of the vortices and concomitant intensification of mutual strain that eventually cause detrainment to initiate and the main interaction to occur, similar to the no-shear case.

For a given shear strength ζ_0, the circulation ratio of the pair, Λ_0, influences whether the interaction is a hendition or a separation, and the type of hendition should one occur (figure 4). For a symmetric pair in weakly favourable or adverse shear (figures 4*c*,*d*), assuming $\zeta_0 > \zeta_{sep}(\Lambda_0 = 1.0)$ (recall from § 2 that $\zeta_{sep} = \zeta_{sep}(\Lambda_0)$), the interaction is a merger, similar to the no-shear case, but with the vortices experiencing equal shear-induced periodic amplification of deformation. For increasing asymmetry of the pairs (figures 4*b–a*,*e–f*), the variation of b increases, the deformation amplification becomes increasingly unequal (greater for the weaker), and during the main convective interaction, the mutual entrainment process becomes increasingly one-sided (e.g. the $\zeta_0 = 0.167$, $\Lambda_0 = 0.90$ illustrative case). When the pair is sufficiently disparate (figures 4*a*,*f*), the interaction is entirely one-sided and the weaker vortex is simply destroyed, leaving the stronger one essentially unaffected, i.e. straining out occurs (e.g. the $\zeta_0 = -0.0073$, $\Lambda_0 = 0.70$ illustrative case). In adverse shear, sufficiently small Λ_0 may result in $\zeta_0 < \zeta_{sep}(\Lambda_0)$ (unless $\zeta_0 > \zeta_{sep}(\Lambda_0 = 0)$), and separation may occur instead, i.e. asymmetry may in a sense 'cause' separation in certain circumstances.

Additionally, merger may occur in certain cases with higher $|\zeta_0|$ that for lower or zero $|\zeta_0|$ are straining out. An example is shown in figure 6, an EPUA case having $\zeta_0 = 0.033$, $\Lambda_0 = 0.70$ (several lower-$|\zeta_0|$ EPUA $\Lambda_0 = 0.70$ cases are straining out, as is the UPEA case with the same ζ_0 and Λ_0; this will be seen in § 5.1). In these cases, the influence of

the shear enables the second vortex to detrain, and thereby allows for mutual entrainment to occur. It can therefore be said that, in general, the outcome of a given interaction is a function of ζ_0, Λ_0, and whether the pair is UPEA or EPUA.

In all cases, the resulting vortex or vortices continue(s) to evolve through viscous diffusion akin to a single vortex under the influence of shear (not shown). In adverse shear, this inevitably leads to filamentation (i.e. detrainment) and, ultimately, breakup. See § 1 and references for general discussion of this case.

4.1. *Separation and determination of ζ_{sep}*

Shear is seen to cause separation when adverse shear strength surpasses a critical value $\zeta_0 < \zeta_{sep}(\Lambda_0)$, consistent with the analysis in § 2. To determine the value of $\zeta_{sep}(\Lambda_0)$ for a given Λ_0, a series of simulations is performed for increasing ζ_0 until separation occurs; ζ_{sep} is taken to be the midpoint of the bracketing ζ_0 values. Empirical results for ζ_{sep} are collected in table 1 for a variety of cases, including UPEA, EPUA and UPUA pairs having several Λ_0 values, and both $Re_\Gamma = 5000$ and 1000 (except UPUA cases). Close agreement is seen, across the entire range of parameters considered, between these empirical ζ_{sep} values and predicted $\zeta_{sep,p}$ values computed using (2.18). Although a full exploration of the separation regime is beyond the scope of this study, these results give a general indication of the behaviour of ζ_{sep} for finite-area unequal vortices, and attest to the accuracy of (2.18) within the parameter range considered: ζ_{sep} decreases with decreasing Λ_0, and is not significantly sensitive to Re_Γ (it is expected that this would remain true as $Re_\Gamma \to \infty$), or whether the pair is UPEA, EPUA or UPUA. These findings are consistent with previous studies of symmetric pairs in inviscid (Trieling *et al.* 2010) and viscous (Folz & Nomura 2014) flow. Note that (2.18) also predicts dependence on $a_{2,0}/b_0$, which is not considered in this study.

Due to ongoing viscous diffusion, the separated vortices eventually detrain and break up (not shown). There is therefore no distinction between 'separation without elongation' and 'separation with elongation' in viscous flow, as there is in the inviscid case (Trieling *et al.* 2010). In the cases considered, separation always occurs before filamentation (i.e. detrainment) and breakup: increasing adverse $|\zeta_0|$ simply causes filamentation to begin earlier, and for more disparate pairs (generally, lower Λ_0, except for the UPUA case) one vortex begins filamentation significantly before the other. It is theoretically possible for a vortex in a UPUA pair to be induced to undergo filamentation and breakup by shear insufficient to cause separation, based on examination of (2.18) in conjunction with known critical values associated with these processes (Moore & Saffman 1971; Mariotti *et al.* 1994; Folz & Nomura 2017; see also this paper's supplementary material), but these cases are difficult to simulate and are beyond the scope of the present study.

4.2. *The vortex-dominated regime*

This study focuses on interactions between the two vortices of a pair, which are influenced by the shear. This excludes cases in which the shear causes the vortices to separate, and cases in which the shear essentially forces them together. Separation is precluded when $\zeta_0 > \zeta_{sep}$, as discussed, whereas the latter set of cases is less clearly delineated. However, a reasonable demarcation can be found in the requirement, discussed in § 3, that the vortices be afforded sufficient time to adjust to each other's presence (i.e. a mutually induced strain field) prior to the onset of detrainment, i.e. that $|\zeta_0| < \zeta_{adj}$. This effectively ensures that the main interaction is initiated primarily through the vortices' influence (i.e. their intensifying mutual strain).

The vortex-dominated regime, therefore, consists of all cases in the range $\zeta_{sep} < \zeta_0 < \zeta_{adj}$ (since $|\zeta_{adj}| > |\zeta_{sep}|$ for the cases considered in this study). Within this range, all interactions occur primarily between the two vortices, with the shear an external influence. Note that both ζ_{sep} and ζ_{adj} are functions of Λ_0, and ζ_{adj} depends on $\omega_{1,0}/\omega_{2,0}$ as well (see § 3; in the full parameter space, both are functions of $a_{2,0}/b_0$ as well). The remainder of this study considers only vortex-dominated interactions, unless noted otherwise.

5. Analysis and characterization of vortex-dominated interactions

When two like-signed vortices interact under the influence of external shear, i.e. when the pair's interaction is vortex-dominated, in viscous flow, hendition always occurs. In these cases, the shear affects primarily the occurrence and timing of core detrainment, which can have a significant effect on the ensuing processes and resulting vortex. As seen in § 4, it can even, in some cases, enable entrainment and merger to occur when, in its absence, they would not. In order to examine the shear's net influence on vortex-dominated henditions, their outcomes must be assessed quantitatively. These results can then be related to basic pair parameters, and, ultimately, a general characterization of vortex-dominated henditions developed.

5.1. *Quantitative assessment of interaction outcomes in shear*

The outcome of any hendition can be assessed quantitatively in terms of an enhancement factor

$$\varepsilon \equiv \frac{\Gamma_{end}}{\Gamma_{2,start}} \tag{5.1}$$

and a corresponding merging efficiency

$$\eta \equiv \frac{\Gamma_{end}}{\Gamma_{tot,start}}, \tag{5.2}$$

based on the ratio of the circulation of the resulting vortex, Γ_{end}, at the end of the main convective interaction, t^*_{end}, to that of the stronger vortex, $\Gamma_{2,start}$, and of the pair combined, $\Gamma_{tot,start}$, respectively, at the start of the main convective interaction, t^*_{start}. (Note that the symbol η has a different meaning here than in § 2.) Mergers correspond to $\varepsilon > 1$, while strainings out correspond to $\varepsilon \approx 1$. Note that η is not a meaningful quantity for strainings out.

In order to identify the appropriate Γ, t^*_{start} and t^*_{end} in the course of the flow development, which proceeds continuously due to the viscosity, a method is used that is similar to that developed for the no-shear case in Folz & Nomura (2017). The vortex cores are identified via a threshold based on the second invariant of the velocity gradient tensor: $II^*_t = II/II_{peak} = 0.10$, where $II = 1/2(\omega^2/2 - S^2)$ is the second invariant at a given location and time, ω is the local vorticity, S is the local strain rate magnitude, and II_{peak} refers to the value of II at the location of the vorticity peak within a contiguous $II > II_t$ region (see Folz & Nomura (2017) for discussion of this choice of II^*_t value).

Aggregate properties of the vortex cores are then computed for the entire flow region meeting the $II > II_t$ criterion, which allows the entire flow development to be monitored

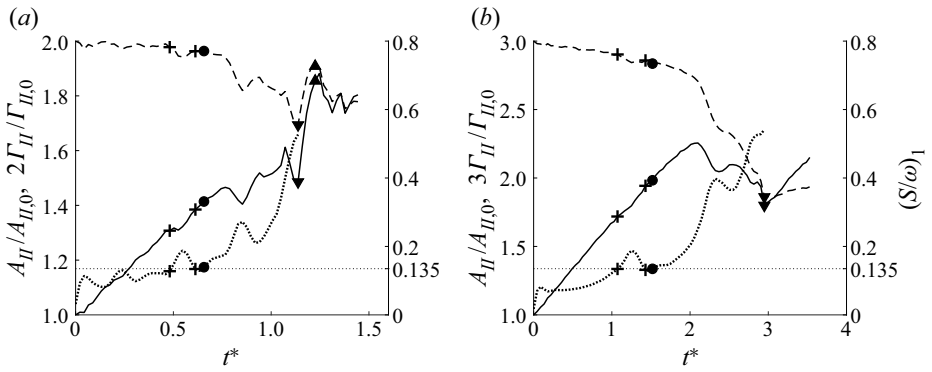

Figure 7. Time development of key quantities for illustrative cases, scaled for better visualization: (*a*) $\zeta_0 = 0.0167$, $\Lambda_0 = 0.90$; (*b*) $\zeta_0 = -0.0073$, $\Lambda_0 = 0.70$. Left-hand axis: normalized core area $A_{II}/A_{II,0}$ (solid line); and normalized core circulation $\Gamma_{II}/\Gamma_{II,0}$ (dashed line), scaled by a factor of 2 in (*a*) and 3 in (*b*). Right-hand axis: relative straining of weaker vortex $(S/\omega)_1$ (through t^*_{det}; thick dotted line), with critical $(S/\omega)_{cr}$ also indicated (thin horizontal dotted line). The + signs indicate the start and end times of a supercritical peak of $(S/\omega)_{cr}$ and corresponding troughs in $A_{II}/A_{II,0}$ and $\Gamma_{II}/\Gamma_{II,0}$. The ● and ▼ symbols indicate the start and end of core detrainment, t^*_{start} and t^*_{det}, respectively. The ▲ symbols indicate the end of mutual entrainment, t^*_{ent} (occurs in (*a*) only). See text for definitions of the times.

continuously, including the transition from two vortices to one:

$$A_{II} = \int_{II>II_t} \mathrm{d}A \tag{5.3}$$

and

$$\Gamma_{II} = \int_{II>II_t} \omega \, \mathrm{d}A, \tag{5.4}$$

where A_{II} is the aggregate core area, Γ_{II} is the aggregate core circulation, and $\mathrm{d}A$ refers to an area element of fluid (similar properties of each individual vortex $i = 1, 2$ are also computed using a separate $II^*_{t,i}$ based on the peak of each, not shown). The time development of the relative straining of each vortex, $(S/\omega)_i$, is also monitored.

The time development of these quantities is presented for the illustrative cases in figure 7; see the supplementary material for the complete flow development of all the cases shown in figures 3 and 4. The salient features (which are observed in every case considered) are similar to those observed in the no-shear case (Folz & Nomura 2017). First, there is a period dominated by growth of A_{II} and simultaneous slight decline of Γ_{II}, corresponding to the initial revolving and viscous growth of the pair. This is followed by diminishing growth (until a local maximum is reached) then decline of A_{II} and simultaneous more rapid decline of Γ_{II}, until each reaches a local minimum, corresponding to core detrainment. In some cases (such as that in figure 7*a*), these local minima are followed by rapid rises to local maxima, i.e. spikes, corresponding to mutual entrainment.

The most significant effect of shear is the introduction of additional local minima in the Γ_{II} development (with corresponding variations in the A_{II} development, e.g. beginning at $t^* = 0.50$ in figure 7(*a*), and at $t^* = 1.1$ in figure 7(*b*)). It is seen that these 'troughs' correspond to local maxima, or 'bumps', in the time development of $(S/\omega)_1$ (which exhibits net growth due to viscous diffusion intensifying $(S/\omega)_1$), which in turn correspond to the periodic amplified deformation, associated with the vortices' orientation, observed in § 4. (The squares and diamonds in figure 5 correspond to the peaks of bumps in $(S/\omega)_1$

in figure 7; corresponding bumps also occur in $(S/\omega)_2$, not shown here.) Notably, $(S/\omega)_i$ of either vortex may temporarily exceed the critical $(S/\omega)_{cr} = 0.135$ (associated with core detrainment) one or more times, with negligible evident detrainment, before $(S/\omega)_1$ (and in some cases, $(S/\omega)_2$) ultimately surpasses it terminally as A_{II} growth diminishes and Γ_{II} decline accelerates.

Due to these nonlinearities, t^*_{start} is taken to be the earlier time at which one vortex achieves – and thereafter maintains – $(S/\omega)_i > (S/\omega)_{cr} = 0.135$ through to the end of detrainment. (In the no-shear case, t^*_{start} had been identified as the time of deviation of A_{II} from linear growth – see Folz & Nomura (2017); t^*_{start} as identified in the present manner produces similar results in those cases, not shown.) This time is indicated for the illustrative cases in figure 7 (in figures 3(*b–e*) and 4(*a–f*), column 4 corresponds to t^*_{start}). Maintaining the critical $(S/\omega)_{cr} = 0.135$ value has been seen to correspond to detrainment both here and in the no-shear case, and is also consistent with the value observed in simulations of a single Gaussian vortex in adverse shear (e.g. Mariotti *et al.* 1994), suggesting that this is a general critical value for Gaussian vortices subject to external strain. In this study, the first detraining vortex is always vortex 1. This identification of t^*_{start} with the maintaining of $(S/\omega)_1 > (S/\omega)_{cr}$ is consistent with the observation in Trieling *et al.* (2010) that symmetric pairs in shear always merge when their peak–peak distance remains within the critical merging criterion for symmetric pairs without shear; it is noted, though, that they do observe merger to occur in cases (typically having favourable shear) in which the vortices only temporarily surpass the critical criterion. The choice of t^*_{start} here therefore likely constitutes a conservative estimate for the start of the main convective interaction.

The end of the interaction, t^*_{end}, is taken to be the time of the first peak (i.e. spike) immediately following the minimum if there is one (i.e. the end of entrainment, t^*_{ent}), or the time of the local minimum otherwise (i.e. the end of detrainment, t^*_{det}). These times are indicated for the illustrative cases in figure 7 (and in figures 3(*b–e*) and 4(*a–f*), column 5 corresponds to t^*_{det}, and column 6 to t^*_{ent}). In all cases considered, t^*_{end} corresponds to the existence of only a single vortical structure meeting the $II > II_t$ criterion. These are identical to the criteria used in the no-shear case (Folz & Nomura 2017).

5.2. *The influence of shear on the timing and duration of detrainment*

The shear has a significant influence on the timing of detrainment, as seen in figures 8(*a*,*b*), which show t^*_{start} and $\Delta_d t^* = t^*_{det} - t^*_{start}$, the duration of the detrainment-dominated portion of the main convective interaction, respectively. The large degree of variation of t^*_{start} with ζ_0 reflects the influence of shear on b, and thereby the overall growth of $(S/\omega)_i$ leading to detrainment: lowering and increasing t^*_{start}, i.e. accelerating or delaying the onset of detrainment, derives from shear reducing or increasing b from b_0, respectively (here associated with favourable and adverse shear; this is discussed further below). The variation of t^*_{start} with Λ_0 (and whether the pair is UPEA or EPUA) is consistent with that observed in the no-shear case: t^*_{start} decreases for increasing pair disparity (lower Λ_0; Folz & Nomura 2017). It is also noted that as ζ_0 increases from 0, the variation of t^*_{start} with Λ_0 is reduced, consistent with the (increasingly strong, favourable) shear playing an increasingly significant role in the initiation of detrainment. The observed variation of $\Delta_d t^*$ likewise reflects the influence of shear on b, with reduction and increase likewise generally shortening and prolonging the duration of detrainment, although the effect here is not strictly monotonic. This is attributed to the complexity of the detrainment process,

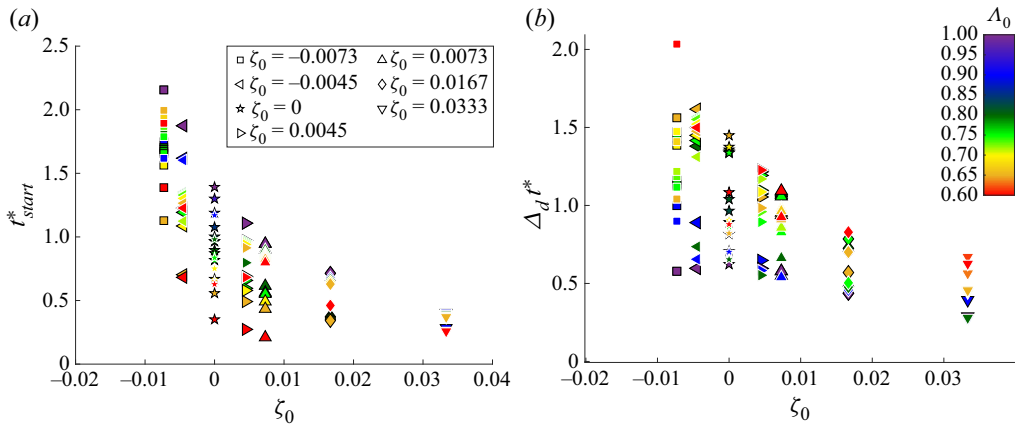

Figure 8. For vortex-dominated henditions: (*a*) time of interaction start, t^*_{start}, and (*b*) the duration of detrainment, $\Delta_d t^* \equiv t^*_{det} - t^*_{start}$, as functions of ζ_0 and Λ_0 (both UPEA and EPUA). The meanings of symbol shapes and colours are indicated in (*a*,*b*), respectively; a black outline indicates UPEA cases (and symmetric), and a white outline indicates EPUA cases ($Re_\Gamma = 5000$).

as well as the method of assigning t^*_{start} and t^*_{end}. It is also seen that $\Delta_d t^*$ increases with decreasing Λ_0 (consistent with Folz & Nomura 2017), and that in some cases this can be quite significant, especially for $\zeta_0 < 0$.

It should be understood that the net influence of the shear on $\Delta_d t^*$ derives not only from the time variation of b, but also from directional effects that inhibit core detrainment. In order to examine this influence, the angle ϕ_i is computed for each vortex $i = 1, 2$, where ϕ_i is the angle between the peak–peak axis and $\boldsymbol{e}_{pk,i}$, the unit vector corresponding to the direction of principal extensional strain evaluated at the vorticity peak. The angle ϕ_i serves as an instantaneous indicator of the vortex's response to the net directional influence of the strain rate fields induced by the shear and the other vortex as their relative prevalence and direction vary in time. The time variations of $\cos^2(\phi_i)$ for each vortex for no-shear cases having $\Lambda_0 = 0.90$ and $\Lambda_0 = 0.70$ are presented in figures 9(*a*,*b*), and it is seen that $\cos^2(\phi_i) \approx 0.5$ is maintained (i.e. $\phi_i \approx 45^\circ$, after the initial adjustment period) until detrainment begins, after which $\cos^2(\phi_i)$ decreases (i.e. ϕ_i increases); this occurs for both vortices in the $\Lambda_0 = 0.90$ case – a merger – and only for the weaker vortex in the $\Lambda_0 = 0.70$ case – a straining out. It can therefore be said that $\cos^2(\phi_i) < 0.5$ is associated with core detrainment. When shear is present (shown for the illustrative cases in figures 9*c*,*d*), its principal extensional strain rate remains fixed in the Eulerian frame (oriented 45° from the background flow direction), which initially causes $\cos^2(\phi_i)$ of both vortices to oscillate about 0.5 as they revolve; this occurs such that the bumps in $(S/\omega)_i$ correspond to maximum $\cos^2(\phi_i)$, i.e. when the directional effects are unfavourable for detrainment. This may explain why little evident detrainment occurs even when $(S/\omega)_i > (S/\omega)_{cr}$ during a bump. After t^*_{start}, one vortex (at least) maintains $(S/\omega)_i > (S/\omega)_{cr}$ and $\cos^2(\phi_i) < 0.5$ simultaneously, thereby undergoing detrainment and causing hendition to occur. These observations suggest that in order for core detrainment to occur, the vortex must maintain both sufficient relative straining ($(S/\omega)_i > (S/\omega)_{cr}$) and conducive directionality ($\cos^2(\phi_i) < 0.5$) of its straining response.

It is critical to note that accelerating/delaying t^*_{start} and shortening/prolonging $\Delta_d t^*$ are not necessarily associated with 'favourable' or 'adverse' shear. If the vortices are initially oriented along the shear direction, then the favourable shear delays/prolongs while adverse

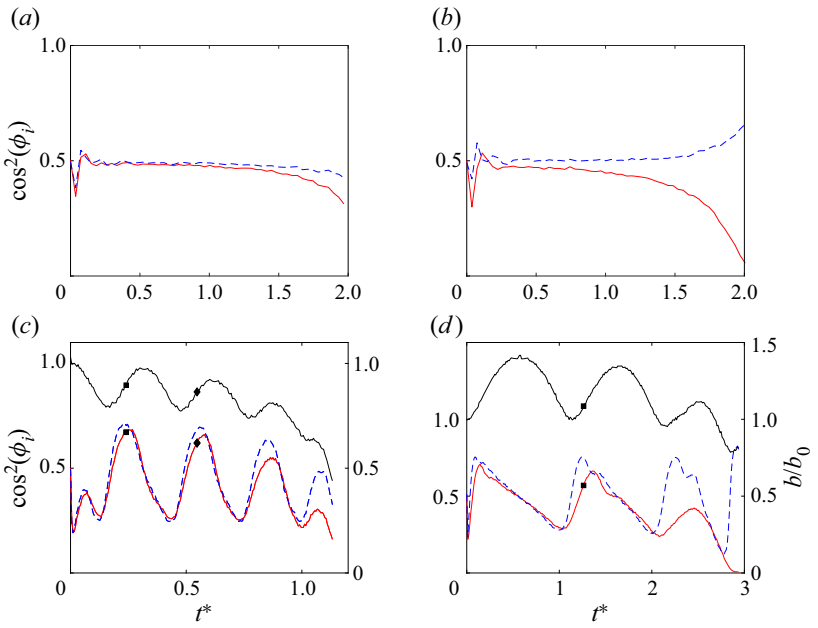

Figure 9. Time development of $\cos^2(\phi_i)$, where ϕ_i is the angle between the peak–peak axis and the principal extensional strain eigenvector at each peak, $\boldsymbol{e}_{pk,i}$ (left-hand axis; solid red line shows vortex 1, dashed blue line shows vortex 2), for no-shear cases having (*a*) $\Lambda_0 = 0.90$ and (*b*) $\Lambda_0 = 0.70$; and the illustrative shear UPEA cases having (*c*) $\zeta_0 = 0.0167$, $\Lambda_0 = 0.90$ and (*d*) $\zeta_0 = -0.0073$, $\Lambda_0 = 0.70$. In all cases, $Re_\Gamma = 5000$. In (*c*,*d*), the time development of b/b_0 is also included for reference (right-hand axis; solid black line), and ■ (and ⧫) indicate times of first (and, in (*c*), second) local S/ω peak (see figures 5 and 7).

shear accelerates/shortens (since, in this orientation, the vortices are initially located at minimum b in the favourable case and maximum b in the adverse). This can be seen in table 2, which shows t^*_{start} and $\Delta_d t^*$ for equivalent cases having each initial orientation (i.e. maintaining all pair parameters described in § 3). A full exploration of the relationship between the initial orientation, the flow development, and outcomes is beyond the scope of this study, but it can be concluded that the observed effects of shear on timing derive primarily from the relative motion of the vortices that it engenders, and not, strictly speaking, the shear's relative sense.

5.3. *Results for ε and η*

It has been seen that shear affects the timing and duration of core detrainment, and it is known that the outcome of an asymmetric pair interaction derives from the relative timing of detrainment and destruction of the vortices (Brandt & Nomura 2010). The influence of the shear on interaction outcomes is therefore most significant when the outcome of the case is particularly sensitive to changes in this timing. To examine this, and the influence of shear on interaction outcomes overall, ε and η are computed for every case using (5.1) and (5.2).

Figure 10 shows each hendition case, with ε indicated via colour, for both UPEA and EPUA cases (similar trends are observed for η). Linear interpolation has also been employed to estimate ε values between the simulated cases, in order to better visualize the overall trends. In the broadest sense, the variation of ε is similar to that of the

ζ_0	Λ_0	Horiz t^*_{start}	Vert t^*_{start}	Horiz $\Delta_d t^*$	Vert $\Delta_d t^*$	Horiz ε	Vert ε
0.0073	1.0	0.95	1.79	0.58	0.58	2.19	1.96
0.0073	0.9	0.90	1.50	0.55	1.10	1.81	1.81
0.0073	0.7	0.49	0.98	0.94	1.43	1.02	1.04
−0.0073	1.0	2.16	1.05	0.58	0.42	2.09	2.09
−0.0073	0.9	1.75	0.75	1.00	0.90	1.81	1.78
−0.0073	0.7	1.56	0.27	1.39	1.07	1.01	1.00
0.0167	1.0	0.71	2.07	0.44	0.55	1.94	2.05
0.0167	0.9	0.66	1.84	0.43	0.79	1.80	1.81
0.0167	0.7	0.35	1.37	0.70	1.33	1.03	1.06

Table 2. Time of start of core detrainment, t^*_{start}, and duration of detrainment, $\Delta_d t^* \equiv t^*_{det} - t^*_{start}$, for equivalent UPEA cases initially oriented horizontally (Horiz) and vertically (Vert) ($Re_\Gamma = 5000$).

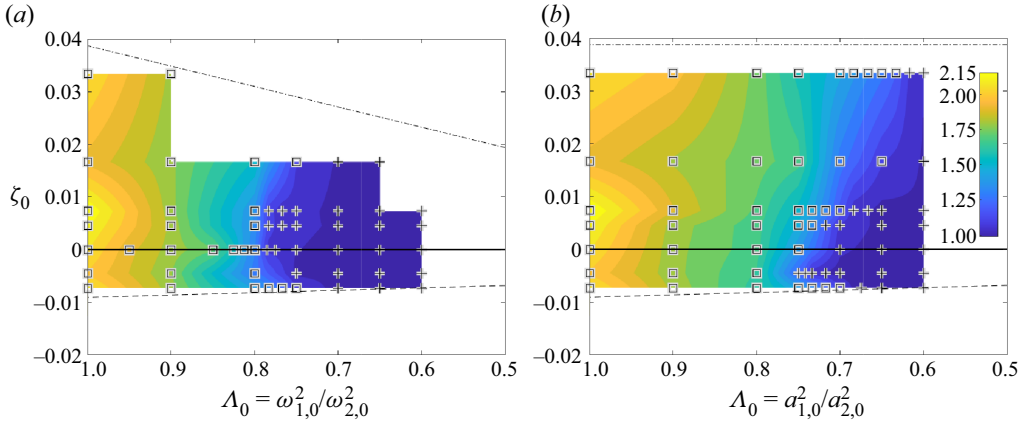

Figure 10. Interaction outcomes for vortex-dominated henditions for (*a*) UPEA and (*b*) EPUA cases. Symbols indicate the outcomes of the cases included in figure 8, categorized: □ indicates merger; + indicates straining out (see § 5.1). Colours indicate enhancement factor ε: values for each denoted case are exact, while those in between are produced by linear interpolation (both plots use same colour map, indicated in (*b*)). The solid black line indicates $\zeta_0 = 0$, the dashed line indicates $\zeta_{sep,p}$ (see § 2), and the dash-dotted line indicates ζ_{adj} (see §§ 3 and 4). The data for the no-shear ($\zeta_0 = 0$) cases were presented previously in Folz & Nomura (2017). Note that ε inherently declines with decreasing Λ_0, since the theoretical maximum is $\varepsilon_{max} = 1 + \Lambda_0$. In all cases, $Re_\Gamma = 5000$.

no-shear case: ε is maximal ($\varepsilon \approx 2$) for symmetric pairs, and minimal ($\varepsilon \approx 1$) for highly disparate ones (approximately $\Lambda_0 < 0.70$ for UPEA, and $\Lambda_0 < 0.60$ for EPUA). The $\Lambda_{0,cr}$ value at which this minimum ε is reached is seen to vary with ζ_0, particularly in the transitional range (approximately $0.80 \geqslant \Lambda_0 \geqslant 0.70$ for UPEA, and $0.80 \geqslant \Lambda_0 \geqslant 0.60$ for EPUA), being generally lower for higher $|\zeta_0|$ (with the notable exception of the $\zeta_0 \leqslant 0$, $0.75 \geqslant \Lambda_0 \geqslant 0.70$ subregion). More generally, the variation of ε with ζ_0 is not always monotonic, for $\Lambda_0 > \Lambda_{0,cr}$.

Also indicated in figure 10, via the symbols, is the occurrence of mutual entrainment (i.e. merger) or not (i.e. straining out) in each case (as ascertained from the presence of one or more spikes post-t^*_{det} in the Γ_{II} time development; see § 5.1). It is seen that the presence of shear can engender entrainment in some cases where it does not occur in the equivalent no-shear case, and that this typically occurs for more disparate pairs when shear is stronger

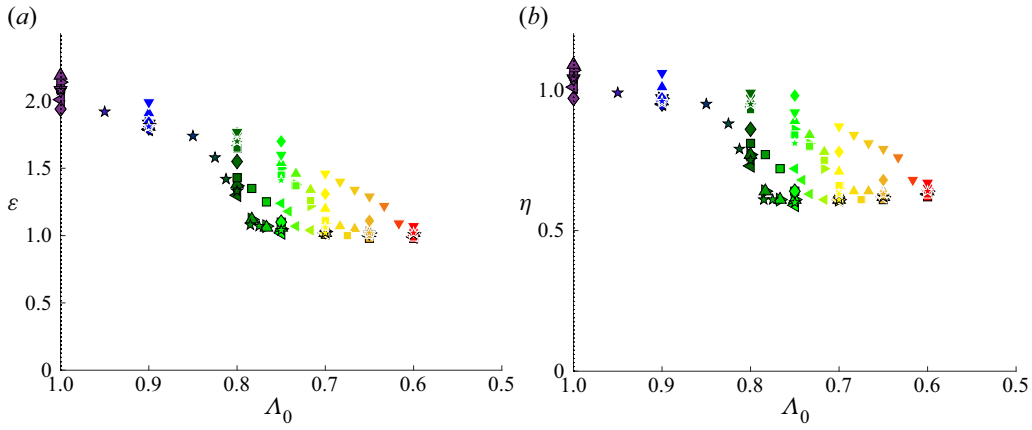

Figure 11. For vortex-dominated henditions: (*a*) ε and (*b*) η, as functions of Λ_0. See figure 8 for meanings of symbol shapes, colours and outlines. In all cases, $Re_\Gamma = 5000$.

(again there are notable exceptions, particularly in the EPUA $\zeta_0 \leqslant 0$, $0.75 \geqslant \Lambda_0 \geqslant 0.70$ subregion). This promotion of merger is attributed to the shear – of either sense – altering the rate of increase of $(S/\omega)_i$ of each vortex, making detrainment of the second vortex more likely prior to the destruction of the first.

The variations of ε and η with ζ_0 and Λ_0 for all hendition cases are presented in figure 11. It is seen that, within the transition region, cases with $\zeta_0 \neq 0$ typically have higher ε and η than the no-shear case with the same Λ_0, and that increasingly favourable shear generally (though not universally) results in greater enhancement and more efficient merger for EPUA cases. (Note that the variation for the symmetric case results largely from the use of II_t in conjunction with its uniquely reciprocal mutual strain.) The handful of cases with lower ε and η than in the no-shear case have $\zeta_0 < 0$: the weaker $\zeta_0 = -0.0045$ cases always produce $\varepsilon < \varepsilon(\zeta_0 = 0)$ for a given Λ_0, while the stronger $\zeta_0 = -0.0073$ begins to produce $\varepsilon > \varepsilon(\zeta_0 = 0)$ for more disparate pairs ($\Lambda_0 \leqslant 0.75$ for EPUA) only until the straining out regime is reached, i.e. stronger adverse shear better enables entrainment to occur. Similar trends are observed in the $\varepsilon - \Lambda$ and $\eta - \Lambda$ variations, where Λ is evaluated at t^*_{start} (not shown). It is noted that the initially vertical cases considered in § 5.2 produce ε and η similar to those for their initially horizontal counterparts (table 2; not otherwise included in the present results or discussion).

An example of shear of either sense promoting merger is presented in figures 12(*a*,*b*,*c*), which show the time development of $(S/\omega)_i$ for EPUA $\Lambda_0 = 0.70$ cases having $\zeta_0 = 0.033$, no shear and $\zeta_0 = -0.0073$, respectively. In these cases, entrainment does not occur for the no-shear case, but it does occur for $\zeta_0 = 0.033$ ($\varepsilon = 1.46$; vorticity contours for this case are shown in figure 6), and to a small degree for $\zeta = -0.0073$ ($\varepsilon = 1.11$; vorticity contours not shown). It is seen that the influence of the shear causes $(S/\omega)_2$ to surpass $(S/\omega)_{cr}$ in both $\zeta_0 \neq 0$ cases, allowing detrainment of the second vortex to occur. For the $\zeta_0 = 0.033$ case, this is done primarily by accelerating the rate of increase of $(S/\omega)_2$ (i.e. reducing t^*_{start}); for the $\zeta = -0.0073$ case, this is done primarily by prolonging the detrainment of vortex 1 (i.e. increasing $\Delta_d t^*$), allowing $(S/\omega)_2$ to increase sufficiently to surpass $(S/\omega)_{cr}$ prior to the end of the interaction.

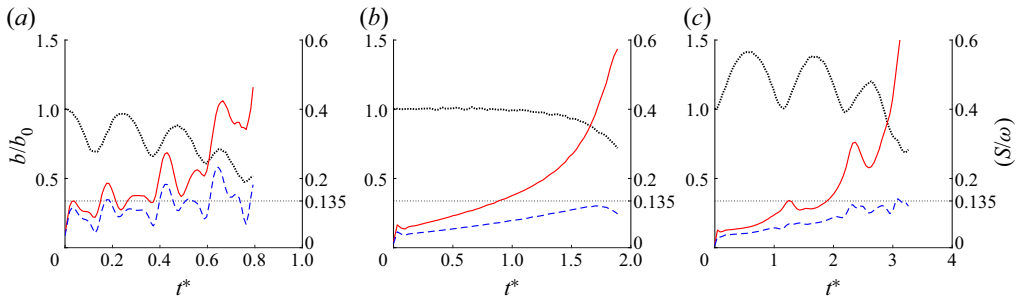

Figure 12. Time development of $(S/\omega)_1$ and $(S/\omega)_2$ (red solid and blue dashed lines, respectively; right-hand axis), along with b/b_0 (thick dotted line; left-hand axis), for EPUA cases having $Re_\Gamma = 5000$ and $\Lambda_0 = 0.70$, with (*a*) $\zeta_0 = 0.0167$, (*b*) $\zeta_0 = 0$ (no shear), and (*c*) $\zeta_0 = -0.0073$. In all plots, the horizontal thin dotted line indicates $(S/\omega)_{cr} = 0.135$. The $\zeta_0 \neq 0$ cases are mergers ($\varepsilon > 1$), whereas the no-shear case is a straining out ($\varepsilon \approx 1$).

5.3.1. *Mutuality and the fundamental characterization of henditions in shear*

Fundamentally, the outcome of the interaction of two like-signed vortices derives from the degree of mutuality of the interaction. In the no-shear case, Folz & Nomura (2017) introduced a mutuality parameter $MP = (S/\omega)_1/(S/\omega)_2$, which compares the relative straining of each vortex at t^*_{start}, and thereby captures the degree of mutuality of the interaction. When the relative straining of both vortices is similar at t^*_{start} (approximately $1 \leqslant MP < 1.8$ for $Re_\Gamma = 5000$), the second vortex can begin to detrain before the first is destroyed, enabling mutual entrainment (i.e. merger occurs); when the disparity is greater (approximately $MP > 1.8$), it cannot, and the first detraining vortex is simply destroyed (i.e. straining out occurs). In the vortex-dominated regime, MP is computed for the shear cases in the same manner.

Figure 13 shows the variations of ε and η with MP. A generally monotonic relationship is observed between ε and MP (likewise η and MP), with $\varepsilon \approx 2$ (and $\eta \approx 1$) near $MP = 1$, then generally declining as MP increases until $MP \approx 2$, at which point $\varepsilon \approx 1$ is reached and thereafter maintained (recall that η ceases to be a meaningful quantity for strainings out). However, significantly more scatter is observed in the shear case (as compared with figure 9 in Folz & Nomura 2017). This is attributed to MP being a pointwise quantity, and therefore sensitive to significant and rapid variations as the vortices revolve.

However, MP is related closely to the vortex enstrophy ratio, an integrated quantity less susceptible to fluctuations:

$$\frac{Z_2}{Z_1} = \frac{\displaystyle\int_{II>II_{t,2}} \omega_2^2 \,\mathrm{d}A_2}{\displaystyle\int_{II>II_{t,1}} \omega_1^2 \,\mathrm{d}A_1}, \tag{5.5}$$

where the integral is evaluated for each vortex at t^*_{start}. This quantity was also seen to effectively characterize the variation of ε and η in the no-shear case (Folz & Nomura 2017).

Figure 14 shows the variations of ε and η with Z_2/Z_1. It is seen that the scatter is greatly reduced (even for high $|\zeta_0|$), such that the variation is essentially monotonic outside of a transition region, reached at 1.65 ± 0.01 and extending to 1.91 ± 0.02 (where the margins of error for each are found from the extremal midpoint between a merger and a straining out case). In this region, cases having similar Z_2/Z_1 but different ζ_0,

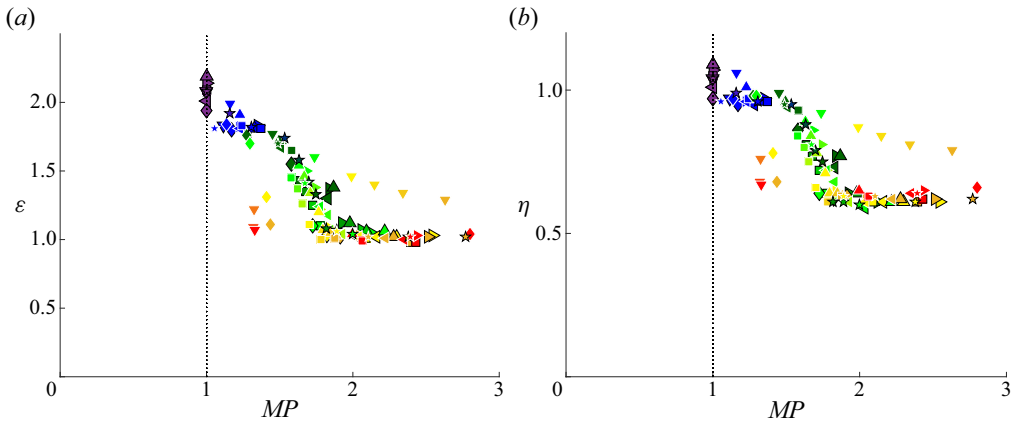

Figure 13. For vortex-dominated henditions: (*a*) ε and (*b*) η as functions of $MP = (S/\omega)_1/(S/\omega)_2$. See figure 8 for meanings of symbol shapes, colours and outlines. The dotted line indicates $MP = 1$. In all cases, $Re_\Gamma = 5000$.

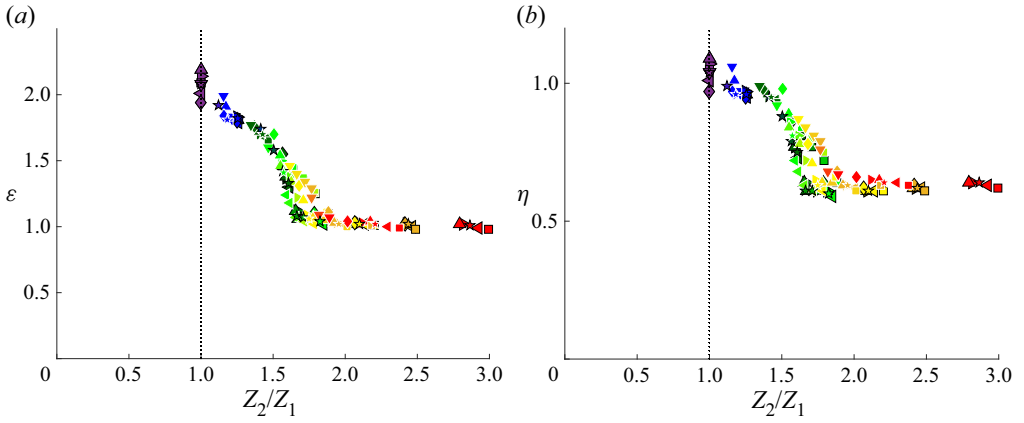

Figure 14. For vortex-dominated henditions: (*a*) ε and (*b*) η as functions of Z_2/Z_1. See figure 8 for meanings of symbol shapes, colours and outlines. The dotted line indicates $Z_2/Z_1 = 1$. In all cases, $Re_\Gamma = 5000$.

Λ_0 and/or UPEA/EPUA status can produce significantly different ε and η, with higher $|\zeta_0|$ generally (though not universally) corresponding to higher ε and η. The consistently lesser enhancement and less efficient merging when weak adverse shear is present ($\zeta_0 = -0.0045$) are attributed to greater dissipation of detrained fluid due to the increase of b, while the greater enhancement and more efficient merging produced by stronger adverse shear ($\zeta_0 = -0.0073$) are attributed to the interaction being sufficiently prolonged to enable entrainment. The lower bound of the transition region is comparable to the critical $(Z_2/Z_1)_{cr} \approx 1.63 \pm 0.03$ for straining out observed in the no-shear case, and merger cases having greater Z_2/Z_1 correspond to higher $|\zeta_0|$.

As such, it can be concluded that favourable and sufficiently strong adverse shear (approximately $\zeta_0 < -0.0045$) promote enhancement and merger for interactions that are moderately disparate (i.e. having approximately $1.65 < Z_2/Z_1 < 1.9$). Efficient merger occurs in interactions with a high degree of mutuality, regardless of shear strength

(typically $\eta > 0.85$ for $Z_2/Z_1 < 1.65$), while more disparate ones always result in straining out of the weaker vortex ($\varepsilon \approx 1$ for $Z_2/Z_1 > 1.9$).

The fact that the variations of ε and η with Z_2/Z_1 are generally monotonic is taken as evidence that the choice of t^*_{start} ($(S/\omega)_1 > (S/\omega)_{cr} = 0.135$ terminally) does effectively characterize the start of convective detrainment (see § 5.2). These trends are also observed when only the relative vorticity is considered (not shown), indicating that they reflect the shear's effect on the physical mechanisms of vortex interaction and not spurious consequences of the use of II_t.

6. Summary and discussion

This study considers the interaction of a pair of unequal vortices in background shear with finite viscosity. In these cases, the flow development is determined by the relative significance of the vortices' mutual influence and that of the shear. Sufficiently adverse shear causes the vortices to separate; the critical adverse shear strength for separation, ζ_{sep}, varies with the pair's circulation ratio Λ_0 (and aspect ratio), and its empirical values are well-predicted by point-vortex analysis. Otherwise, the interaction between the vortices is a hendition (§ 1.1), resulting in a single vortex.

In henditions occurring in background shear, the flow development is essentially governed by three constituent external influences occurring simultaneously, whose relative significance varies in time: the shear causes the peak–peak distance b between the vortices to vary as they revolve; the vortices influence each other through their mutually induced strain, which depends on b; and the strain induced by the constant shear acts directly on each vortex. When the shear is strongly favourable, it causes such significant reduction of b and amplified deformation of the vortices that it is the principal cause of hendition; otherwise, when the shear is weakly favourable or weakly adverse, the flow is vortex-dominated.

In vortex-dominated henditions in shear, viscous diffusion causes the vortices' mutually induced strain to become predominant, which enables sufficient persistence of straining for one vortex to begin detraining core fluid: the relative straining remains sufficiently strong in magnitude ($(S/\omega)_i > (S/\omega)_{cr} = 0.135$ for detraining vortex i), and the directionality of the vortex's response to the external strain field maintains a conducive relative orientation ($\cos^2(\phi_i) < 0.5$) for sustained detrainment despite the continuing influence of shear on b and on each vortex directly. The flow development then proceeds similarly to the no-shear case: if the second vortex is induced to detrain before the first is destroyed, then a two-way interaction leads to a mutual entrainment process that produces an enhanced resulting vortex i.e. merger occurs; otherwise, the interaction is essentially one-way and the detraining vortex is broken up, leaving the other largely unaffected, i.e. straining out occurs.

The post-interaction vortex is assessed quantitatively in terms of an enhancement factor ε and a merging efficiency η, using a method adapted from one utilized in the no-shear case (Folz & Nomura 2017). It is found that all vortex-dominated hendition outcomes across the parameter range considered are effectively characterized by the pair's core enstrophy ratio at the start of detrainment, Z_2/Z_1, which encapsulates the mutuality of the interaction similarly to $MP = (S/\omega)_1/(S/\omega)_2$ (utilized previously in the no-shear case) but is less sensitive to the time variation caused by the shear. For Z_2/Z_1 near unity, merger essentially conserves circulation, while mergers between more disparate vortices become less efficient until straining out occurs. Within the transition region, approximately $1.65 < Z_2/Z_1 < 1.9$, weak adverse shear reduces enhancement; otherwise, the presence of

shear of either sense generally promotes enhancement and merger relative to the no-shear case (in which straining out occurs for $Z_2/Z_1 > (Z_2/Z_1)_{cr} \approx 1.63$ for $Re_\Gamma = 5000$, similar to the value at which it first occurs with shear present). In favourable shear, this results from more rapid increase of $(S/\omega)_2$ due to reduction of b, while in adverse shear, this results from prolonging the interaction due to a combination of increase of b and periodic detrainment-inhibiting orientation effects allowing $(S/\omega)_2$ to reach $(S/\omega)_{cr}$ (with simultaneous $\cos^2(\phi_i) < 0.5$) before the first vortex is destroyed.

Additional study must examine vortex pair parameters beyond those considered here. In particular, it is possible that the boundary values of the Z_2/Z_1 transition region may vary with parameters such as the Reynolds number or initial aspect ratio, either of which would be expected to affect the rate of increase of $(S/\omega)_i$ and therefore promote or inhibit detrainment of the second vortex. It has also been seen that the initial orientation of the vortices relative to the shear is significant: certain effects can be associated with the opposite sense of shear in the orthogonal initial orientation (e.g. when the vortices are initially oriented along the shear direction, favourable shear increases b and prolongs the interaction, while adverse shear reduces and shortens). Moreover, it would be desirable to consider a time-varying background flow, which might better reflect that experienced by a vortex pair in turbulence (the concept of persistence of straining leading to detrainment may be a particularly significant concept in such flows). It is hoped that the current study may provide a step towards a more all-encompassing characterization of vortex interactions in background flow that incorporates these additional parameters, and others (the influence of an opposite-signed vortex would be another priority for consideration). Such studies remain for future work.

Supplementary material. Supplementary material and movies are available at https://doi.org/10.1017/jfm.2023.525.

Funding. This research received no specific grant from any funding agency, commercial or not-for-profit sectors.

Declaration of interests. The authors report no conflict of interest.

Author ORCIDs.
Patrick J.R. Folz https://orcid.org/0000-0001-8441-411X;
Keiko K. Nomura https://orcid.org/0000-0003-3872-2722.

References

Baggaley, A.W. & Barenghi, C.F. 2018 Decay of homogeneous two-dimensional quantum turbulence. *Phys. Rev.* A **97** (3), 033601.

Brandt, L.K. & Nomura, K.K. 2006 The physics of vortex merger: further insight. *Phys. Fluids* **18** (5), 051701.

Brandt, L.K. & Nomura, K.K. 2007 The physics of vortex merger and the effects of ambient stable stratification. *J. Fluid Mech.* **592**, 413–446.

Brandt, L.K. & Nomura, K.K. 2010 Characterization of the interactions of two unequal co-rotating vortices. *J. Fluid Mech.* **646**, 233–253.

Burgess, B.H., Dritschel, D.G. & Scott, R.K. 2017*a* Extended scale invariance in the vortices of freely evolving two-dimensional turbulence. *Phys. Rev. Fluids* **2** (11), 114702.

Burgess, B.H., Dritschel, D.G. & Scott, R.K. 2017*b* Vortex scaling ranges in two-dimensional turbulence. *Phys. Fluids* **29** (11), 111104.

Carton, X., Maze, G. & Legras, B. 2002 A two-dimensional vortex merger in an external strain field. *J. Turbul.* **3**, N45.

Cerretelli, C. & Williamson, C.H.K. 2003 The physical mechanism for vortex merging. *J. Fluid Mech.* **475**, 41–77.

DRITSCHEL, D.G. & WAUGH, D.W. 1992 Quantification of the inelastic interaction of unequal vortices in two-dimensional vortex dynamics. *Phys. Fluids* A **4** (8), 1737–1744.
FOLZ, P.J.R. & NOMURA, K.K. 2014 Interaction of two equal co-rotating viscous vortices in the presence of background shear. *Fluid Dyn. Res.* **46** (3), 031423.
FOLZ, P.J.R. & NOMURA, K.K. 2017 A quantitative assessment of viscous asymmetric vortex pair interactions. *J. Fluid Mech.* **829**, 1–30.
FU, W., LI, H., LUBOW, S., LI, S. & LIANG, E. 2014 Effects of dust feedback on vortices in protoplanetary disks. *Astrophys. J. Lett.* **795** (2), L39.
GERZ, T., SCHUMANN, U. & ELGHOBASHI, S.E. 1989 Direct numerical simulation of stratified homogeneous turbulent shear flows. *J. Fluid Mech.* **200**, 563–594.
HUANG, M.J. 2005 The physical mechanism of symmetric vortex merger: a new viewpoint. *Phys. Fluids* **17** (7), 074105.
HUANG, M.J. 2006 A comparison between asymmetric and symmetric vortex mergers. *WSEAS Trans. Fluid Mech.* **1** (5), 488–496.
HURST, N.C., DANIELSON, J.R., DUBIN, D.H.E. & SURKO, C.M. 2016 Evolution of a vortex in a strain flow. *Phys. Rev. Lett.* **117** (23), 235001.
JING, F., KANSO, E. & NEWTON, P.K. 2012 Insights into symmetric and asymmetric vortex mergers using the core growth model. *Phys. Fluids* **24** (7), 073101.
KIMURA, Y. & HASIMOTO, H. 1985 Motion of two identical point vortices in a simple shear flow. *J. Phys. Soc. Japan* **54** (11), 4069–4072.
KIMURA, Y. & HERRING, J.R. 2001 Gradient enhancement and filament ejection for a non-uniform elliptic vortex in two-dimensional turbulence. *J. Fluid Mech.* **439**, 43–56.
LE DIZÈS, S. & LAPORTE, F. 2002 Theoretical predictions for the elliptical instability in a two-vortex flow. *J. Fluid Mech.* **471**, 169–201.
LE DIZÈS, S. & VERGA, A. 2002 Viscous interactions of two co-rotating vortices before merging. *J. Fluid Mech.* **467**, 389–410.
LEGRAS, B. & DRITSCHEL, D.G. 1993 Vortex stripping and the generation of high vorticity gradients in two-dimensional flows. In *Advances in Turbulence IV* (ed. F.T.M. Nieuwstadt), pp. 445–455. Springer.
LEGRAS, B., DRITSCHEL, D.G. & CAILLOL, P. 2001 The erosion of a distributed two-dimensional vortex in a background straining flow. *J. Fluid Mech.* **441**, 369–398.
LEWEKE, T., LE DIZÈS, S. & WILLIAMSON, C.H.K. 2016 Dynamics and instabilities of vortex pairs. *Annu. Rev. Fluid Mech.* **48**, 507–541.
MARIOTTI, A., LEGRAS, B. & DRITSCHEL, D.G. 1994 Vortex stripping and the erosion of coherent structures in two-dimensional flows. *Phys. Fluids* **6** (12), 3954–3962.
MARQUES ROSAS FERNANDES, V.H., KAMP, L.P.J., VAN HEIJST, G.J.F. & CLERCX, H.J.H. 2016 Interaction of monopoles, dipoles, and turbulence with a shear flow. *Phys. Fluids* **28** (9), 093603.
MAZE, G., CARTON, X. & LAPEYRE, G. 2004 Dynamics of a 2D vortex doublet under external deformation. *Regular Chaotic Dyn.* **9** (4), 477–497.
MELANDER, M.V., ZABUSKY, N.J. & MCWILLIAMS, J.C. 1987 Asymmetric vortex merger in two dimensions: which vortex is 'victorious'? *Phys. Fluids* **30** (9), 2610–2612.
MELANDER, M.V., ZABUSKY, N.J. & MCWILLIAMS, J.C. 1988 Symmetric vortex merger in two dimensions: causes and conditions. *J. Fluid Mech.* **195**, 303–340.
MEUNIER, P., EHRENSTEIN, U., LEWEKE, T. & ROSSI, M. 2002 A merging criterion for two-dimensional co-rotating vortices. *Phys. Fluids* **14** (8), 2757–2766.
MEUNIER, P., LE DIZÈS, S. & LEWEKE, T. 2005 Physics of vortex merging. *C. R. Phys.* **6** (4–5), 431–450.
MOORE, D.W. & SAFFMAN, P.G. 1971 Structure of a line vortex in an imposed strain. In *Aircraft Wake Turbulence and its Detection* (ed. J.H. Olsen, A. Goldburg & M. Rogers), pp. 339–354. Springer.
PAIREAU, O., TABELING, P. & LEGRAS, B. 1997 A vortex subjected to a shear: an experimental study. *J. Fluid Mech.* **351**, 1–16.
PERROT, X. & CARTON, X. 2010 2D vortex interaction in a non-uniform flow. *Theor. Comput. Fluid Dyn.* **24** (1–4), 95–100.
RYZHOV, E.A., KOSHEL, K.V. & CARTON, X. 2012 Passive scalar advection in the vicinity of two point vortices in a deformation flow. *Eur. J. Mech. (*B*/Fluids)* **34**, 121–130.
SUTYRIN, G.G. 2019 On vortex intensification due to stretching out of weak satellites. *Phys. Fluids* **31** (7), 075103.
TABELING, P. 2002 Two-dimensional turbulence: a physicist approach. *Phys. Rep.* **362** (1), 1–62.
TRIELING, R.R., DAM, C.E.C. & VAN HEIJST, G.J.F. 2010 Dynamics of two identical vortices in linear shear. *Phys. Fluids* **22** (11), 117104.

TRIELING, R.R., VELASCO FUENTES, O.U. & VAN HEIJST, G.J.F. 2005 Interaction of two unequal corotating vortices. *Phys. Fluids)* **17** (8), 087103.

VELASCO FUENTES, O.U. 2005 Vortex filamentation: its onset and its role on axisymmetrization and merger. *Dyn. Atmos. Oceans* **40** (1–2), 23–42.

XIAO, Z., WAN, M., CHEN, S. & EYINK, G.L. 2009 Physical mechanism of the inverse energy cascade of two-dimensional turbulence: a numerical investigation. *J. Fluid Mech.* **619**, 1–44.

YASUDA, I. & FLIERL, G.R. 1997 Two-dimensional asymmetric vortex merger: merger dynamics and critical merger distance. *Dyn. Atmos. Oceans* **26** (3), 159–181.

The contents of this chapter have been published in the Journal of Fluid Mechanics, Folz, Patrick J. R.; Nomura, Keiko K., “On asymmetric vortex pair interactions in shear”, Cambridge University Press, 2023. The dissertation author was the primary researcher and the research supervisor was the co-author of the paper.

Chapter 6

Conclusions and future work

The goal of this dissertation was to help bridge the gap between the understanding of the interaction of a single co-rotating two-dimensional vortex pair and the overall behavior of flows that include many such interacting vortices, such as two-dimensional turbulence. This work consists of three basic components, which were published in peer-reviewed journals:

- a first study was done to confirm the consistency of key concepts for a symmetric pair interaction in shear flow when viscosity is present, namely the critical merging distance and the critical shear strength for separation (Folz & Nomura 2014, Chapter 3);
- a second study to develop tools to understand and quantitatively assess the outcome of an interaction between unequal co-rotating vortices that could be used in the presence of viscosity and/or background flow (Folz & Nomura 2017, Chapter 4);
- the ultimate (third) study, which builds upon the synthesis of the first two in order to examine the influence of shear on a pair of unequal co-rotating vortices (Folz & Nomura 2023, Chapter 5).

This ultimate study examines the influence of background flow on the possible interaction regimes for the pair, demonstrates that the background flow primarily influences the timing of the inter-vortex interaction processes such that enhancement of the resulting vortex typically (but not necessarily) occurs, and, perhaps most significantly, demonstrates that this influence is

largely encompassed within the pair's enstrophy ratio – i.e., the outcomes of vortex interactions are well-characterized almost entirely by a single parameter, the core enstrophy ratio. This constitutes a meaningful step towards bridging vortex-pair studies and the overall behavior of two-dimensional turbulence, as recently- and independently-developed scaling laws also derive from measures of vortex enstrophy (Burgess & Scott, 2017).

More generally, this work provides a useful qualitative model for understanding the influence of background flow on an interacting vortex pair: the vortices' mutually induced strain acts on each vortex directly; the strain rate imposed by the background flow also acts on each vortex directly; and the background flow varies the distance between the vortices in time, which indirectly affects their mutually induced strain. These alter the occurrence and relative timing of detrainment and destruction of the vortices, the key mechanisms of their interaction (as established by Brandt & Nomura 2010). In the parameter range considered, the influence of the shear has the ultimate effect of promoting detrainment of the second vortex, and thereby entrainment and merger. This may not necessarily be true in stronger shear and other parameter ranges, which must be explored in future work. Nevertheless, this constitutes a first step upon which future hypotheses may be developed.

This work also provides tools and insights that may be of use to future vortex interaction research generally. These include:

- the onset of core detrainment is associated with a critical value of the *relative straining*, $(S/\omega)_{cr} \approx 0.135$, that appears to be a consistent value for Gaussian vortices regardless of the source of external strain;

- core detrainment is associated not only with a critical value of the relative straining, but also the *directionality* of the vortex's response, i.e., the orientation of the deformed vortex with respect to the underlying flow field – in other words, that detrainment requires *both* sufficient magnitude and conducive directionality of the imposed strain;

- relatedly, and more generally, the relative straining – essentially the vortex's *eccentricity* –

is an important quantity for monitoring the development of a given vortex in time;

- further, the key concept governing hendition outcomes is *mutuality* – the degree to which each vortex "participates" in the main convective interaction – which is well-characterized by the mutuality parameter, MP, which is remarkably accurate at characterizing henditions between even highly disparate vortices;

- mutuality and MP may also be well-characterized by the *core enstrophy ratio*, an easily accessible integrated quantity that may be particularly useful in time-varying flows;

- the utility of *aggregate core properties*, which allow for the monitoring of the time development of a vortex pair continuously through the interaction process without presupposing start or end times for the main interaction, especially useful for viscous flows;

- the derivation of an accurate expression for the boundary of the separation regime in shear flows;

- the observation that "favorable" and "adverse" shear can have opposite effects on the distance between the vortices depending on their initial relative orientation;

- the term *hendition* to denote any interaction between two vortices that produces a single final vortex (and its companion term *henmultion* for the like interaction of three or more vortices simultaneously), which solves the problem of researchers sometimes using "merger" as a general term and sometimes to mean specifically an enhancement-producing interaction.

There are many avenues for this work to be continued and further developed. Most significantly, the concept of directionality of the vortex's straining response must be fleshed out with, at the very least, more data and ideally a better metric than the ϕ_i of Chapter 5 (and Appendix B), which is unfortunately based upon the vortices' peak-peak axis rather than anything intrinsic to the vortex itself. The present study (including the material in Appendix B) suggests a

simple basic underlying concept for vortex behavior in general: when the flow field engenders a hyperbolic stagnation point within the vortex core, core detrainment occurs, and what happens thereafter depends on the particulars of the flow field (e.g., a like-signed vortex in proximity leads to hendition if the hyperbolic point is sustained within the core through destruction of the original vortex, or a "partial" interaction occurs if it is not, which may or may not result in the detrained fluid enhancing the other depending on its ability to entrain the ejected fluid, which is in turn predicated on the presence of a hyperbolic point within that vortex's core, and so on). This in turn suggests the potential to *control* vortex detrainment by controlling the degree and orientation of its deformation with respect to the flow field (i.e. hyperbolic point) would allow for useful practical applications, including the mitigation of airplane trailing vortices near runways, active flow control on lifting bodies, and a method for chemical mixing. The incorporation of more complex and time-varying background flows than simple shear would be an important next step in these matters.

Those interested in vortex pairs in shear can consider additional and larger parameter ranges as limitations (computational and/or experimental) permit. The author anticipates that the enhancement-promoting effect of shear here observed may be lesser or even reversed for larger initial aspect ratios (i.e., greater initial vortex separation); this may be the simplest parameter to explore further. This is likely related to Reynolds number effects as well, which should also be studied, although the range in which such effects are significant may be surprisingly limited; additional work by Scott Carlson in the Nomura Group suggests that vortex interaction outcomes are largely insensitive to Reynolds number difference above roughly $Re_\Gamma = 5000$, while interactions below roughly $Re_\Gamma = 1000$ are largely viscosity-driven and thus involve completely different physical processes than those here. Future research should also consider more UPUA cases, and in particular explore the "weak winner" regime when shear is present, which may particularly give important insights into the development and scaling behavior of complicated flows. A thorough study of vortex interactions in shear should also consider various initial orientations, which were considered only briefly in Chapter 5; the present results suggest little

difference in interaction outcomes, although the sample of cases is quite limited, and the design of a proper experiment to test these effects is subtle and somewhat difficult, since e.g., orienting the vortices initially orthogonal to or along the shear direction is also orienting along the major or minor axis of their elliptical trajectory, such that matching initial shear strength is not matching initial separation distance (potentially causing resolution difficulties when attempting to match aspect ratio), and moreover one must consider whether to match the initial peak-peak distance or *starting* peak-peak distance, which may be more relevant but difficult to control.

It goes without saying that future work should also explore the strong favorable shear regime further. For one thing, the delineation between that and the vortex-dominated regime developed here is arbitrary and based in part on computational considerations that may not be relevant in the near future; a more robust delineating heuristic should be developed. More generally, since it was observed that reduction of the peak-peak distance by the shear promotes enhancement and merger, it might be expected that even stronger favorable shear might cause significantly greater enhancement in some cases and engender merger of more disparate pairs (or those at smaller initial aspect ratios). It is noted, though, that studies of vortex merger in shear in inviscid flow (symmetric pair studies only, all of them) essentially do consider this regime, since inviscid merger only occurs if the vortices are arbitrarily placed sufficiently close together – as though brought together by strong shear. For example, the merger shown in figure 7f of (Trieling *et al.* 2010, see also their figure 4f, showing similarly for Rankine vortices) qualitatively resembles the shear-dominated merger shown in figure 3a in Chapter 5, with highly deformed (elliptical) cores early in the development, sharply curled outer filaments, and ejection of additional filaments near the center as the cores approach.

In fact, if the author may editorialize a bit further, a common question (criticism) of this research has been the choice to use viscous flow – but this illustrates exactly why this was necessary. The vortex-dominated regime of the interaction of a pair in shear *cannot* be explored with inviscid methods, because inviscid vortices will not interact unless forced together by some external influence, be it the shear or the hands of the omnipotent researcher creating the initial

condition. However, this does mean that most inviscid studies of vortices "in isolation" are in fact similar to studies of the shear-dominated regime, since they are always initially "forced" to be within the critical distance for symmetric merging, or the equivalent criteria for asymmetric pairs – which means that their results give insight into this regime (it is acknowledged that the deformation of the vortices differs from what would occur with strong background flow, including attempts to obviate the need for circular vortices to mutually adjust by imposing an initially deformed geometry such as is typically done by Dritschel's group, although it is suggested that this is all the more reason to be very careful in setting up and interpreting the results of inviscid pair studies). It is notable, then, that the results of Trieling *et al.* (2005) show increasing merging efficiency with decreasing initial separation distance for asymmetric henditions in inviscid flow – consistent with the present finding that efficiency generally increases the more shear reduces the peak-peak distance (occuring in favorable shear here). It would be desirable to simulate the strong favorable case "properly," with the shear modeled explicitly, but the existing body of vortex research (including the present study) collectively gives fairly strong indications of the expected behaviors.

More important, in the author's estimation, is to start directly considering the interaction of vortices in relative motion along the peak-peak axis – equivalent to two co-rotating vortices being brought into proximity by a translating opposite-sign dipole. This has been argued to be the most common type of vortex interaction in two-dimensional tubulence (Sire *et al.*, 2011), yet very little research to date has considered this case directly. This is certainly a more common case in most flows than that of two co-rotating vortices being forced together by strong like-signed background flow, which has received more consideration (considerably more widely than is perhaps consciously realized, as noted above), and basic questions remain: What are the major interaction regimes? Under what circumstances does the interaction between the co-rotating vortices become predominant? How does the continuous inward motion affect enhancement and merging efficiency? And how do these results vary with offset distance and angle of incidence of their translation axes? The results and analytical tools developed in the present study provide a

basis to begin to tackle these questions, and the others that will inevitably arise.

Appendix A

Supplement to On asymmetric vortex pair interactions in shear

Supplementary material to: On asymmetric vortex pair interactions in shear

Patrick J. R. Folz[1]†, Keiko K. Nomura[1]

[1]Department of Mechanical and Aerospace Engineering, University of California, San Diego, 9500 Gilman Drive, La Jolla, CA, 92093-0411, USA

In this supplementary material, the time evolution of the key quantities utilized in the flow analysis — namely, core area, A_{II}, core circulation, Γ_{II}, and relative straining, $(S/\omega)_i$ — are presented for example cases of a single vortex in shear (§S1) and vortex pairs in shear (§S2), accompanied by brief description highlighting salient features. This reference is intended to benefit readers desiring a fuller understanding the flow development and the quantities utilized to compute the outcome quantities ε and η.

As indicated in the main text, the core area and circulation correspond to the aggregate flow region meeting the threshold, $II > II_t$, where $II = 1/2(\omega^2/2 - S^2)$ is the second invariant at a given location and time, and the threshold $II_t^* = II/II_{peak} = 0.10$:

$$A_{II} = \int_{II>II_t} dA$$

and

$$\Gamma_{II} = \int_{II>II_t} \omega dA,$$

where dA refers to an area element of fluid. See main text and Folz & Nomura (2017) for details.

These simulations are all performed using the computational methods described in §3 of the main text. Note that these simulations were terminated after the main convective interaction has been completed and the final vortex has begun to axisymmetrize, in order to conserve computational resources; the end times of each curve therefore have no significant physical meaning.

S1. Single vortex in shear

This section briefly reviews the flow development of a single vortex in favorable and adverse shear, a useful reference when considering the pair case. In the adverse case, the start of core detrainment is identified and found to correspond to a critical $(S/\omega)_{cr}$ value similar to that found for pairs in Folz & Nomura (2017).

A single vortex in shear deforms elliptically along a direction roughly orthogonal to or aligned with the shear direction in favourable or adverse shear, respectively, and in the adverse case, the intensifying deformation and relative straining eventually leads to filamentation — i.e. detrainment — and breakup, as discussed in §1 and references therein. These processes are reflected in the time evolution of A_{II}, Γ_{II}, and (S/ω), which are presented in figure S1 along with the instantaneous shear strength $|\zeta|$, for a single vortex in favourable and adverse shear, respectively, having $|\zeta_0 = 0.01|$ and $Re_\Gamma = 1000$ (in order to accelerate the flow development

† Email address for correspondence: pjfolz@ucsd.edu

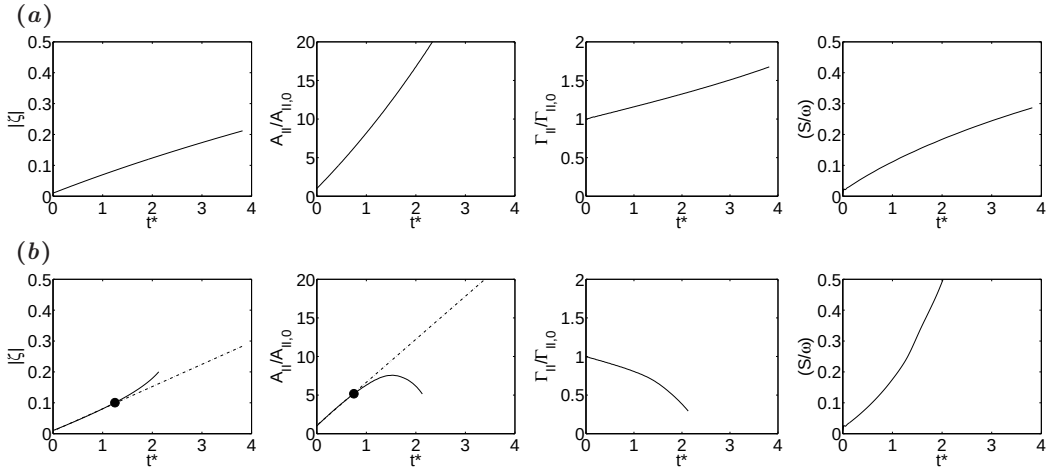

Figure S1: Time development of shear strength parameter magnitude $|\zeta|$, and key quantities: normalized core area $A_{II}/A_{II,0}$, normalized core circulation $\Gamma_{II}/\Gamma_{II,0}$, and relative straining S/ω, for a single vortex: (a) favourable shear ($\zeta_0 = 0.01$), and (b) adverse shear ($\zeta_0 = -0.01$). In (b), the dash-dot line indicates the linear fit to the early portion used to ascertain the time of departure from linear behavior ($\bullet$ at $t^* = 1.25$ in ζ plot, and $t^* = 0.75$ in $A_{II}/A_{II,0}$ plot). This departure is found by computing the correlation coefficient (R^2) for a linear fit to progressively larger portions of the time development (beginning with the first $N = 20$ output times) until R^2 falls below a pre-selected threshold value ($R^2_{thresh} = 0.999$).

for better visualization of the major processes). In all cases, $|\zeta(t)| = \alpha/\omega(t)$ increases continuously due to viscous diffusion reducing ω. For reference, in the case of a single vortex diffusing without shear ($\zeta_0 = 0$), A_{II} grows linearly and Γ_{II} remains constant (shown in Folz & Nomura 2017), while the relative straining of this vortex remains $(S/\omega) = 0$ (consistent with no deformation).

It is seen that, in favourable shear ($\zeta_0 > 0$), ζ, A_{II}, Γ_{II}, and S/ω all increase monotonically throughout the flow development, which consists of viscous spreading, elliptical deformation, and little else (the increase of Γ_{II} here, where it was constant in the no-shear case, results from the use of II_t as the vortex diffuses and deforms). The increasing deformation results from the intensifying shear strength ζ and is reflected in the increasing of S/ω. Although there is a slight growth acceleration of A_{II} and Γ_{II}, and deceleration of S/ω and ζ over the entire flow development, the growth of each of these quantities could reasonably be approximated as linear in this case (a linear fit with $R^2 = 0.99$ can be made to each, not shown). These processes continue until the ultimate dissipation of the vortex.

Conversely, in adverse shear ($\zeta_0 < 0$), a significant qualitative change in the behavior of key quantities is observed, reflecting detrainment of the core and subsequent breakup. The shear strength magnitude $|\zeta|$ again increases monotonically, but this growth is seen to accelerate significantly in the latter portion of the flow development (at $t^* \approx 1.25$, see figure S1 caption). The growth of A_{II}, after an initial approximately linear increase, begins to decelerate (earlier than $|\zeta|$'s acceleration), reaching a local maximum and then decreasing; Γ_{II} declines approximately linearly at first, then more rapidly beginning at approximately the same time as A_{II}'s deviation from linear (at $t^* \approx 0.75$). The growth of S/ω

is likewise monotonic and accelerates slightly throughout, but most significantly when $|\zeta|$ does as well. The deviation of A_{II} growth from linear coincides with the start of *core* detrainment (note that filamentation of low-level, i.e. non-core, peripheral vorticity occurs before this time); this detrainment is reflected in the accelerating decline of Γ_{II}. In other words, the deviation of A_{II} from linear growth in this case reflects the transition from viscosity-dominated to convection-dominated flow development, as it did in the case of no-shear pairs (see e.g. Brandt & Nomura 2007; recall also that adverse shear approximates the influence of a co-rotating vortex pair partner, see §1). The later deviation of $|\zeta|$'s growth from linear (as well as the concomitant significant acceleration of S/ω's) reflects the final, rapid *breakup* of the vortex, during which the $II > II_t$ core is swiftly eroded away and the vortex is ultimately dissipated (see e.g. Mariotti *et al.* 1994).

Significantly, the deviation of A_{II} from linear growth — the start of core detrainment — and the transition from viscosity-dominated to convection-dominated flow development occurs when $S/\omega \approx 0.128$, very close to the critical value of $(S/\omega)_{cr} \approx 0.135 \pm 0.03$ associated with detrainment in no-shear pairs (Folz & Nomura 2017; the estimate made here derives in part from additional simulations having $\zeta_0 = -0.005$ and $\zeta_0 = -0.02$, not shown). This suggests that this critical value associated with core detrainment is generally consistent for a Gaussian vortex in viscous flow. The value of ζ associated with vortex *breakup*, $\zeta_{bu} \approx -0.10$, is comparable to the values $\zeta_{bu} = -0.10$ to -0.13 found by Mariotti *et al.* (1994) and Paireau *et al.* (1997).

These observations and critical values inform the discussion and analysis of vortex pairs in shear.

S2. Vortex pairs in shear

This section briefly reviews the flow development of vortex pairs, which may be unequal, in both favorable and adverse shear, utilizing the core quantities A_{II} and Γ_{II}, as well as the relative straining of both the weaker and stronger vortices, $(S/\omega)_1$ and $(S/\omega)_2$, respectively.

First, the time development of these quantities in no-shear flow, observed in Folz & Nomura (2017), is here briefly reviewed: A_{II} grows approximately linearly during the viscosity-dominated portion of the interaction, then declines and, in some cases, thereafter spikes during the convection-dominated portion, corresponding to detrainment and entrainment, respectively; Γ_{II} declines slightly but steadily during the viscosity-dominated portion (due to the vortices' intensifying mutual strain), followed by a more rapid drop during detrainment, and then a spike in cases in which entrainment occurs; and $(S/\omega)_i$ grows continuously throughout both the viscosity-dominated and convection-dominated portions, through the end of detrainment (at which point either the vortex is destroyed, or, if it is the "winner" of the interaction, $(S/\omega)_i$ then declines during reaxisymmetrization). Significantly, the initiation of detrainment of a vortex is seen to be associated with the critical value, $(S/\omega)_i \approx (S/\omega)_{cr} = 0.135$.

For vortex pairs in background shear ($\zeta_0 \neq 0$), these properties are presented in figures S2 and S3 (A_{II} and Γ_{II} are normalized by their initial values); these figures correspond to the vortex-dominated cases shown in figures 3 and 4 in the main text. Figure S2c shows an example of no-shear merger, in which one can observe the behaviors just discussed. In the $\zeta_0 \neq 0$ cases, as discussed in the main text (§5.1), the time evolution of these quantities follows a similar pattern

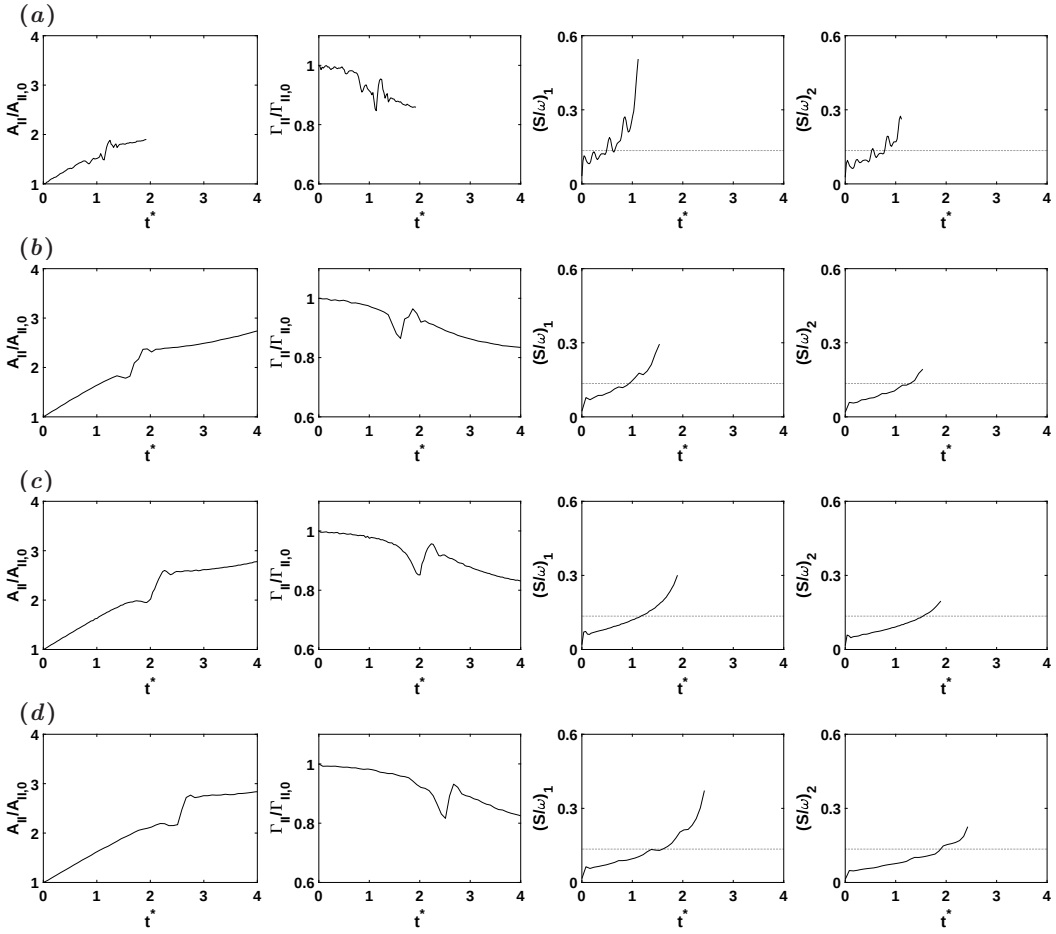

Figure S2: Time development of key quantities (aggregate normalized core area $A_{II}/A_{II,0}$ and circulation $\Gamma_{II}/\Gamma_{II,0}$, and relative straining of each vortex $(S/\omega)_i$, $i = 1, 2$) for the vortex-dominated cases shown in figure 3 of the main text, UPEA pairs having $Re_\Gamma = 5000$ and $\Lambda_0 = 0.90$, with varying shear strength ζ_0: (a) $\zeta_0 = 0.0167$, (b) $\zeta_0 = 0.0045$, (c) $\zeta_0 = 0$ (no shear), and (d) $\zeta_0 = -0.0045$. Dashed line in $(S/\omega)_i$ plots indicates critical relative straining $(S/\omega)_{cr} = 0.135$. The data in case (c) was previously presented in Folz & Nomura 2017.

to the no-shear case, with the primary exception of nonlinear troughs in the development of A_{II} and Γ_{II}, which correspond to times of amplified deformation of the vorticies due to the shear and concomitant local maxima, i.e. bumps, in the time development of $(S/\omega)_i$.

For a given Λ_0 (figure S2), as $|\zeta_0|$ increases, $(S/\omega)_i$ generally grows more rapidly and the bumps become larger. Also, smaller "secondary" bumps become apparent at high ζ_0, between those already discussed, i.e. at an orientation of the peak-peak axis approximately orthogonal to theirs (e.g. in figure 7a of the main text at $t^* \approx 0.4$). For a given ζ_0 (figure S3), when the pair is asymmetric the increase of $(S/\omega)_1$ is more rapid, and the bumps larger, than for $(S/\omega)_2$, with this disparity increasing with decreasing Λ_0 (indicating more disparate deformation amplification, seen in figures 3-4 of the main text). For highly disparate pairs

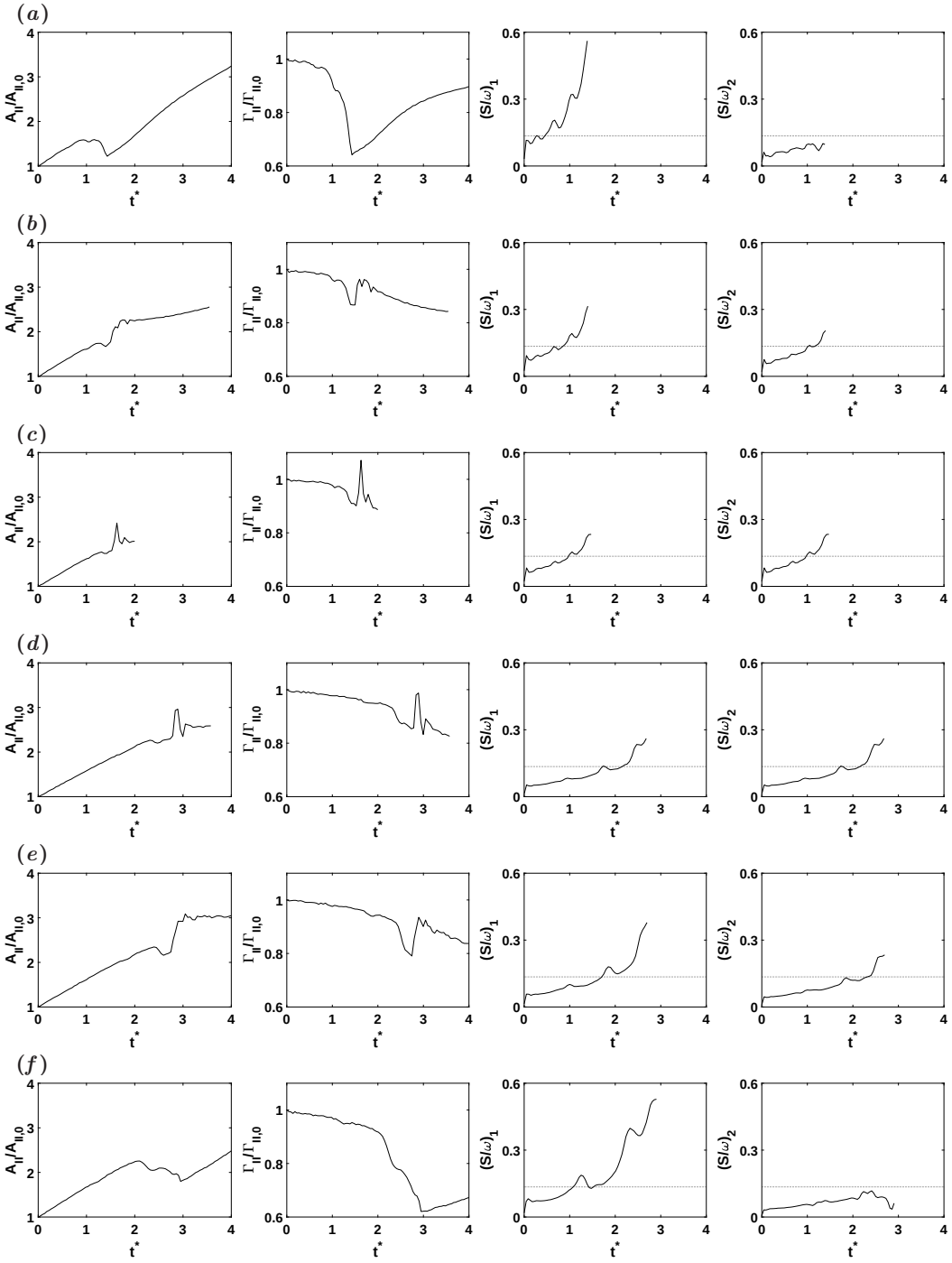

Figure S3: Time development of key quantities (aggregate normalized core area $A_{II}/A_{II,0}$ and circulation $\Gamma_{II}/\Gamma_{II,0}$, and relative straining of each vortex $(S/\omega)_i$, $i = 1, 2$) for the vortex-dominated cases shown in figure 4 of the main text, UPEA pairs having $Re_\Gamma = 5000$ and $|\zeta_0 = 0.0073|$, with varying Λ_0: (a) $\Lambda_0 = 0.7$, (b) $\Lambda_0 = 0.90$, (c) $\Lambda_0 = 1.0$ having favourable shear ($\zeta_0 = 0.0073$); (d) $\Lambda_0 = 1.0$, (e) $\Lambda_0 = 0.90$, and (f) $\Lambda_0 = 0.70$ having adverse shear ($\zeta_0 = -0.0073$). Dashed line in $(S/\omega)_i$ plots indicates critical relative straining $(S/\omega)_{cr} = 0.135$.

(typically $\Lambda_0 < 0.80$), the "bumps" in $(S/\omega)_2$ are low-amplitude and often multi-peaked, indicating minimal deformation amplification.

In all cases, the start of the significant slowing of A_{II} growth and acceleration of Γ_{II} decline — behaviors associated with the start of core detrainment in no-shear pairs — coincides with $(S/\omega)_1$ surpassing *and maintaining* $(S/\omega)_{cr} = 0.135$, the value associated with the onset of core detrainment of a vortex in a no-shear pair or in adverse background shear. It is also seen that, in the cases identified as mergers in figures 3 and 4 in the main text, $(S/\omega)_2$ also surpasses (S/ω_{cr}) at or after the time that $(S/\omega)_1$ does. Because of this, and the correspondence to qualitative observations of the vorticity contours, and the fact that these flows are vortex-dominated, these behaviors are taken to correspond to detrainment (and the spikes, entrainment) in these $\zeta_0 \neq 0$ pairs. The outcomes of these interactions and their quantitative assessment are discussed in §5.

The contents of this chapter have been published in the Journal of Fluid Mechanics, Folz, Patrick J. R.; Nomura, Keiko K., “On asymmetric vortex pair interactions in shear”, 2023. The dissertation author was the primary researcher and the research supervisor was the co-author of the paper.

Appendix B

The influence of shear on vortex deformation and detrainment

The following material was developed as part of the article included in Chapter 5, and included in the initial submission, but was removed in revision for scope and length considerations. It builds directly on many of the concepts discussed in that Chapter, and references terms and variables therein; therefore, see Chapter 5 for definitions.

It has been seen in Chapter 5 that the presence of shear alters the manner and rate at which each vortex deforms (as indicated by $(S/\omega)_i$). This affects the occurrence and timing of detrainment of each vortex, which in turn can affect the outcome of a given interaction. Here, the influence of the shear on the flow development leading to detrainment is examined in further detail.

When two vortices interact in background shear, vortex deformation and development of $(S/\omega)_i$ are essentially governed by *three* constituent external influences occurring simultaneously, whose relative significance varies in time: the shear causes the peak-peak distance b between the vortices to vary as they revolve; the vortices influence each other through their mutually induced strain, which depends on b (the strain rate magnitude induced on vortex 2 by vortex 1 varies as $S_2 \sim \Gamma_1/(2\pi b^2)$, and vice versa); and the strain field induced by the shear acts directly on each vortex. The latter two intensify in time due to viscous diffusion of ω_i increasing $(S/\omega)_i$. These influences combine in a complex manner due to their time variation and directionality.

Most significantly, the periodic reduction (or increase) of b from its initial value, b_0, ensures that $b \leq b_0$ (or $b \geq b_0$; figure 5b. Since the strain induced by one vortex on the other is therefore generally increased (or reduced), $(S/\omega)_i$ accordingly increases at a greater (or lesser) overall rate than in the corresponding no-shear case, thereby accelerating (or delaying) the onset of detrainment. The periodic b variation would also be expected to cause local peaks in the time development of $(S/\omega)_i$, but as has been noted, the observed peaks do *not* correspond to b minima (e.g. compare figures 5 and 7). The bumps must therefore arise at least in part due to the *directionality* of the strain rate fields induced by the other vortex and by the shear.

In order to examine the influence of this directionality on vortex development, ϕ_i, the angle between the peak-peak axis and $\mathbf{e}_{pk,i}$, the unit vector corresponding to the direction of principal extensional strain evaluated at the vorticity peak, is computed for each vortex $i = 1,2$. The angle ϕ_i serves as an instantaneous indicator of the vortex's *response* to the net directional influence of the strain rate fields induced as their relative prevalence and direction vary in time. For a no-shear pair, ϕ_i remains approximately 45° as the vortices revolve ($cos^2(\phi_i) = 0.5$), and then begins to increase once that vortex begins to detrain ($cos^2(\phi_i) < 0.5$), as seen in figures B.1a-b (and $cos^2(\phi_i)$ does *not* decrease for a vortex that does not detrain, as in the straining out case shown in figure B.1b). When shear is present ($\zeta_0 \neq 0$), its principal extensional strain rate is directed 45° from the flow direction, which remains fixed. These directions are aligned at b_{max} and orthogonal at b_{min}, for both favourable and adverse shear. Recall that for a no-shear pair, the vortices tend to deform each other elliptically with the major axis oriented along the peak-peak axis (e.g. Chapter 4, while shear tends to deform a single vortex with the major axis oriented along a fixed direction that depends on its relative sense (along the flow direction for favourable shear and along the shear direction for adverse); these deformation-directions are also aligned at b_{max} and opposed at b_{min}. The appearance of the bumps (and associated amplification of deformation) is attributed to the alternating mitigating tendencies associated with directionality and varying b: at b_{max}, the deformation induced by the other vortex is mitigated by higher b, and at b_{min}, it is mitigated by the orthogonal deformation-direction of the shear; the bumps

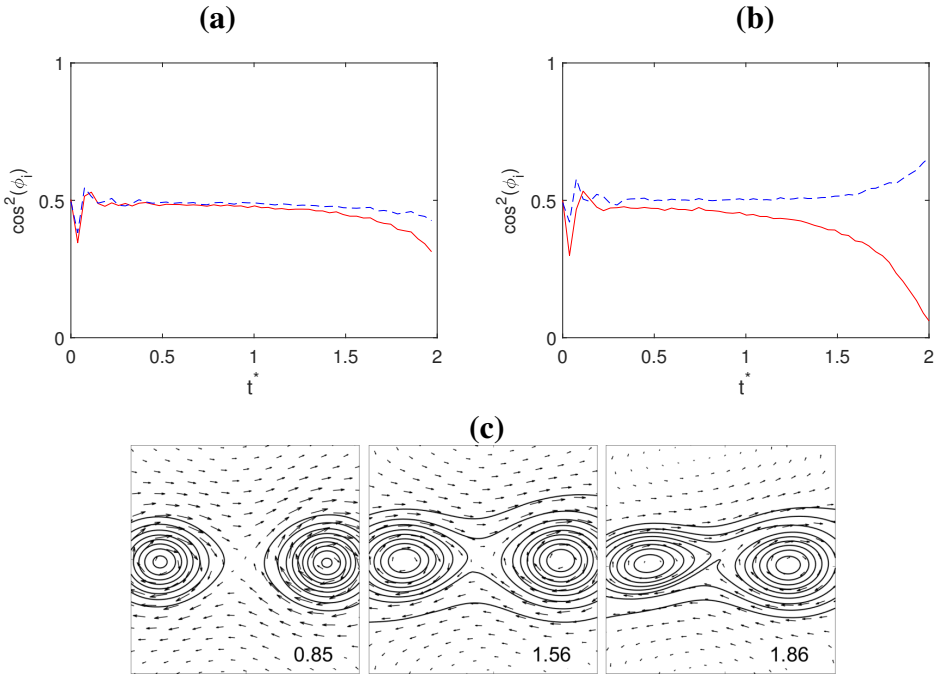

Figure B.1. For the no-shear case ($\zeta_0 = 0$): time development of $cos^2(\phi_i)$ (where ϕ_i is the angle between the peak-peak axis and the principal extensional strain eigenvector at each peak, $\mathbf{e}_{pk,i}$), for (a) $\Lambda_0 = 0.90$ and (b) $\Lambda_0 = 0.70$ (UPEA); and (c) vorticity contours (10% contour interval) as viewed in a frame co-rotating with the vortices, with instantaneous velocity vectors showing the development of the tilt, for the case shown in (a). The solid red line in (a) and (b) corresponds to the weaker vortex (which detrains in both cases), and the dashed blue line corresponds to the stronger vortex (which detrains in case (a)). The early nonlinear behavior is due to vortex adjustment to the initial condition.

occur in-between, where the net mitigation is minimal (the larger amplification of $(S/\omega)_i$ and deformation for a primary bump is attributed to b increasing as it occurs).

However, the directionality of these influences can also inhibit detrainment, even when they cause $(S/\omega)_i > (S/\omega)_{cr}$ during a bump. This can be seen in figures B.2 and B.3. Figures B.2a and B.3a show vorticity contours for the illustrative cases at $1/8$ turn intervals for a half-turn of each case while the vortices are well-separated (times I-V), with arrows indicating the directions of $\mathbf{e}_{pk,i}$ and $\mathbf{e}_\alpha$, the unit vector indicating the direction of principal extensional strain of the shear (it is noted that time V for the $\zeta_0 = -0.0073$, $\Lambda_0 = 0.70$ case occurs shortly after the start of core detrainment, $t^*_{start} = 1.56$). The time development of $cos^2(\phi_i)$ is shown in figures

B.2b and B.3b, with times I-V indicated. As the vortices revolve, $cos^2(\phi_i)$ oscillates between $cos^2(\phi_i) < 0.5$ and $cos^2(\phi_i) > 0.5$ (prior to the onset of detrainment). At time I, corresponding to b_{max}, $cos^2(\phi_i) > 0.5$. As the vortices revolve through time II to time III, corresponding to b_{min}, $cos^2(\phi_i)$ first diminishes (attributed to the reduction of b increasing the influence of the other vortex) but then rises (attributed to the deformation-directions of the other vortex and the shear approaching orthogonality); this corresponds to a secondary bump. From time III (b_{min}), the vortices revolve through time IV to time V, corresponding to b_{max} again, and $cos^2(\phi_i)$ continues rising at first but then diminishes again (attributed to the increase of b reducing the influence of the other vortex, despite the deformation-directions becoming aligned again); this corresponds to a primary bump. It is seen that although $(S/\omega)_1$ surpasses $(S/\omega)_{cr}$ during the bump (figure 7a); the net influence of the shear ensures that $cos^2(\phi_i) > 0.5$ throughout its duration, i.e., this amplified deformation is *not* conducive to detrainment. This process repeats every half-turn until the onset of core detrainment.

Once $(S/\omega)_1$ surpasses *and remains* above $(S/\omega)_{cr} \approx 0.135$ (at $t^* > 0.66$ for the $\zeta_0 = 0.0167$, $\Lambda_0 = 0.90$ case and $t^* > 1.56$ for the $\zeta_0 = -0.0073$, $\Lambda_0 = 0.70$ case), core detrainment proceeds, and $cos^2(\phi_1) < 0.5$ is maintained (although local maxima and minima are still observed, since the aforementioned mitigating phenomena persist, albeit too weakly to stop core detrainment entirely). Likewise, $cos^2(\phi_2) < 0.5$ is maintained if and when $(S/\omega)_2 > (S/\omega)_{cr}$ is also maintained, i.e., if the hendition is a merger (as in figure B.2).

The significance of ϕ_i, therefore, is that it gives an indication of the relative orientation of the deformed vortex (strictly speaking, in the vicinity of the vorticity peak) with respect to the underlying velocity field. For the no-shear case, $cos^2(\phi_i) = 0.5$ reflects elliptical deformation along the peak-peak axis, with diminishing $cos^2(\phi_i)$ then reflecting the developing "tilt" of the vorticity contours with respect to the peak-peak axis that leads to detrainment (an example is presented in figure B.1c; it should be noted that this tilt, and the similar phenomena observed in the $\zeta \neq 0$ cases, result from spatial variation of the vortices' mutually-induced strain field across the finite-area vortex). This tilt is discussed in Brandt & Nomura (2006) and can be seen

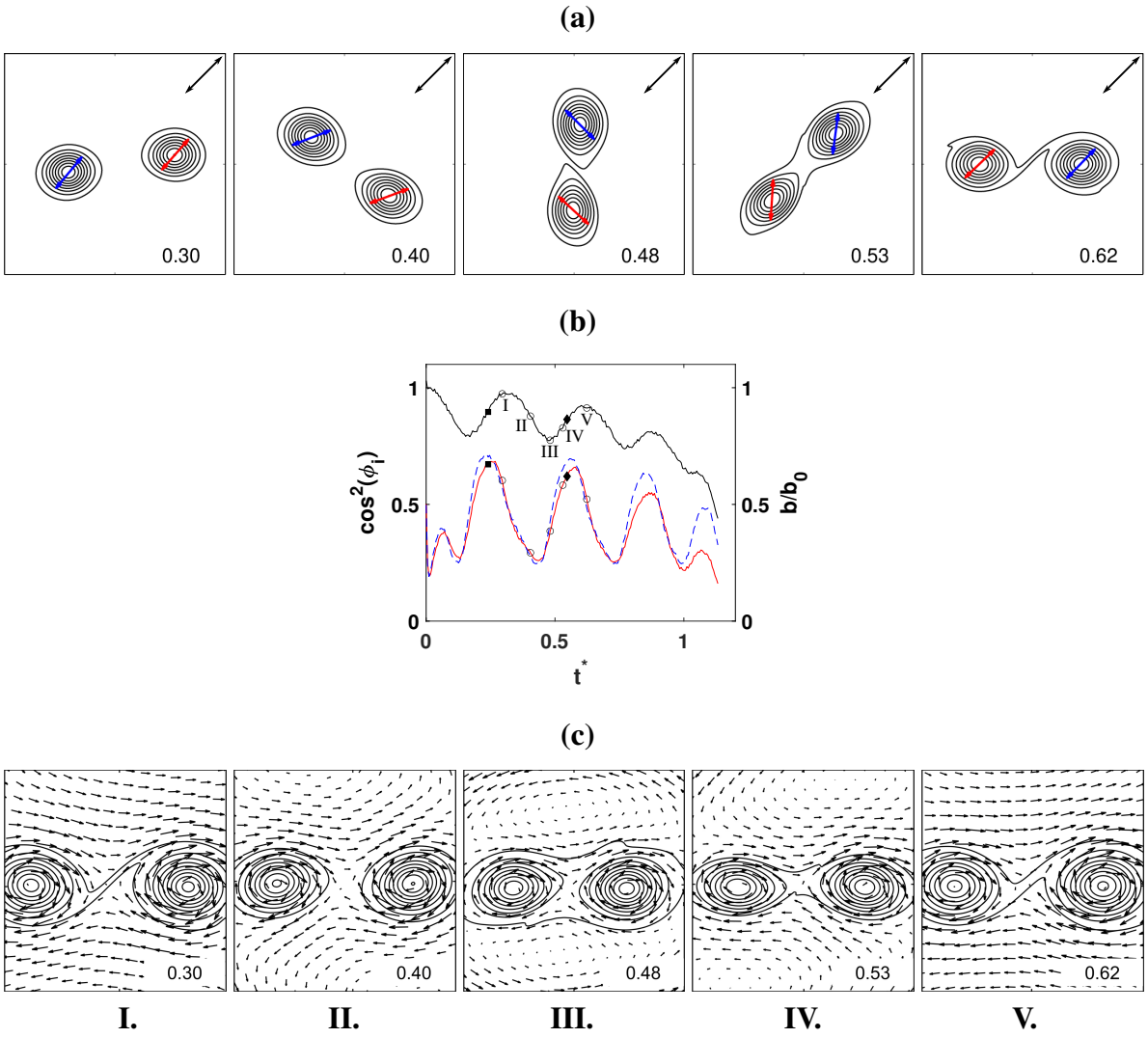

Figure B.2. For the $\zeta_0 = 0.0167$, $\Lambda_0 = 0.90$ UPEA illustrative case: (a) Vorticity contours of the at $1/8$ turn intervals corresponding to the indicated t^* times, with the principal extensional strain unit eigenvectors indicated at each peak, $\mathbf{e}_{pk,i}$ (blue: stronger, red: weaker), and that of the shear, $\mathbf{e}_\alpha$, in the corner (black); (b) time development of $cos^2(\phi_i)$ (left axis; dashed line: stronger, solid line: weaker), along with the time development of b/b_0 (right axis; solid black line); (c) vorticity contours with instantaneous velocity vectors as viewed in a frame co-rotating with the vortices (the weaker vortex is on the left). In (a) and (c), the subfigures correspond to times I-V (labels under figure), and the contour interval is 10%. In (b), ○ indicate times I-V, and ■ and ♦ indicate times of local S/ω peaks (see figure 5a of Chapter 4).

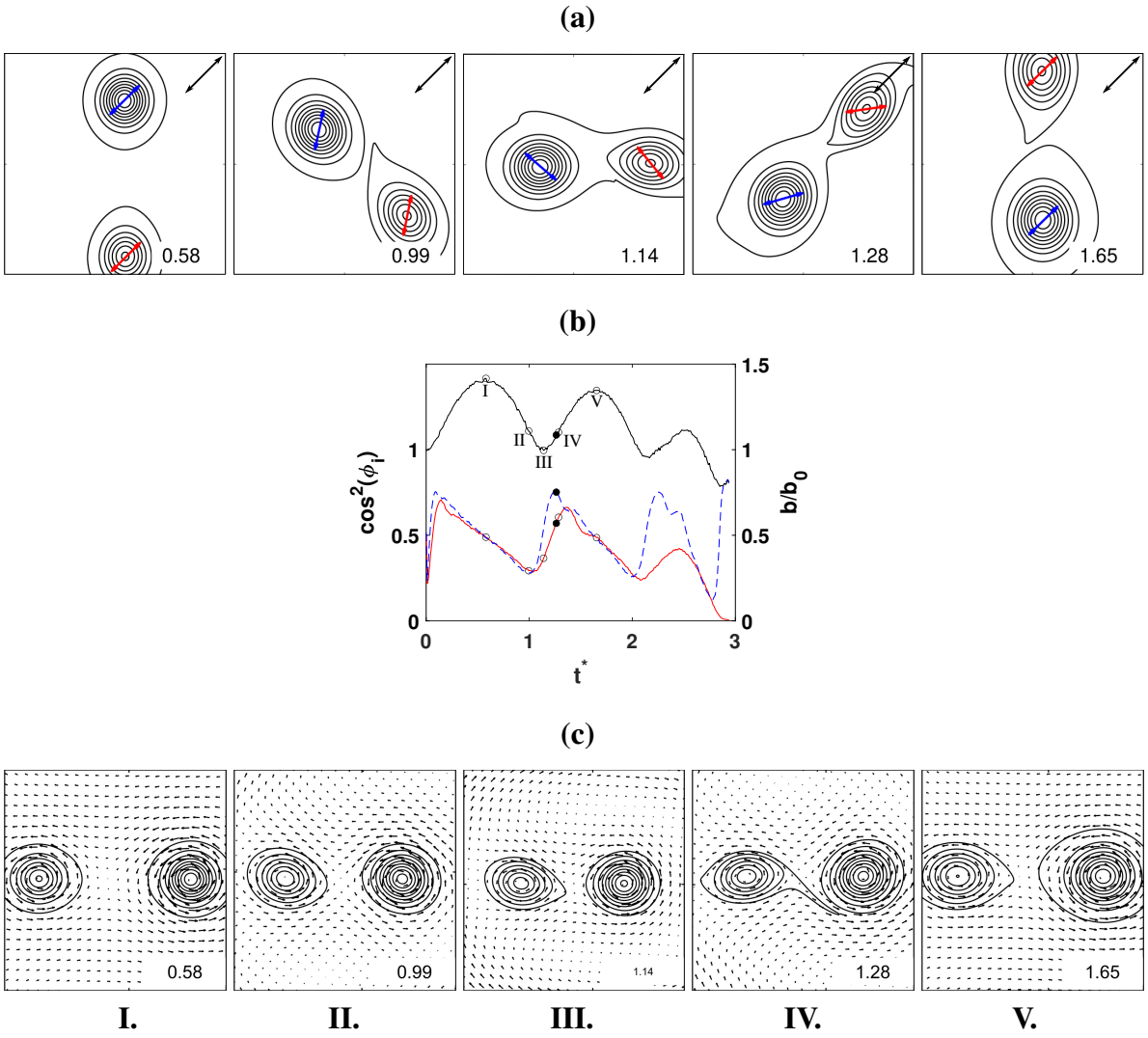

Figure B.3. For the $\zeta_0 = -0.0073$, $\Lambda_0 = 0.70$ UPEA illustrative case: (a) Vorticity contours of the vortices at $1/8$ turn intervals corresponding to the indicated t^* times, with the principal extensional strain unit eigenvectors indicated at each peak, $\mathbf{e}_{pk,i}$ (blue: stronger, red: weaker), and that of the shear, $\mathbf{e}_\alpha$, in the corner (black); (b) time development of $cos^2(\phi_i)$ (left axis), along with the time development of b/b_0 (right axis; solid black line); (c) vorticity contours with instantaneous velocity vectors as viewed in a frame co-rotating with the vortices (the weaker vortex is on the left). In (a) and (c), the subfigures correspond to times I-V (labels under figure), and the contour interval is 10%. In (b), ∘ indicate times I-V, and ■ indicates time of local S/ω peak (see figure 5b of Chapter 4). Note that time V is shortly after the start of core detrainment, $t^*_{start} = 1.56$.

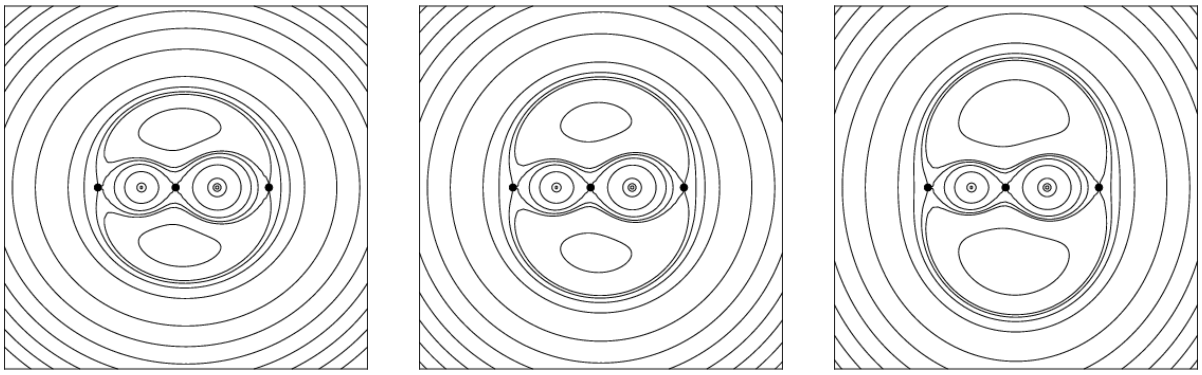

(a) $\zeta_0 = 0.0073$ **(b)** $\zeta_0 = 0$, **(c)** $\zeta_0 = -0.0073$

Figure B.4. Streamline pattern produced by a pair of point vortices having $\Lambda_0 = 0.70$ (as viewed in the co-rotating frame), for: (a) favourable shear ($\zeta_0 = 0.0073$); (b) no shear ($\zeta_0 = 0$); and (c) adverse shear ($\zeta_0 = -0.0073$). The • indicate locations of the hyperbolic stationary points in the streamline pattern; their occurrence and relative position is similar throughout the vortex-dominated regime.

most clearly in their figures 3 and 5, but in brief: the tilt corresponds to a misalignment between the vorticity contours and instantaneous streamlines in the vicinity of the central hyperbolic point in the streamline pattern, an example of which is shown in figure B.4b. This misalignment causes vorticity initially within the separatrix streamline surrounding a vortex core to cross into the "exchange band" region, i.e., between the separatrices about each core and the larger separatrix that encompasses both (see also Le Dizès & Verga 2002; for further discussion of the flow regions within the streamline pattern, see also Brandt & Nomura 2007, 2010). This detrainment-causing misalignment is associated with $cos^2(\phi_i) < 0.5$ (as seen in figure B.1). Note in figures B.4a and c that the presence and position of the central hyperbolic point is essentially unchanged by the presence of shear.

Vorticity contours and the associated instantaneous velocity field, as observed in a frame co-rotating with the pair, are presented at times I-V for the illustrative cases in figures B.2c and B.3c. It is seen that from times I-III (i.e., during a secondary bump) the detrainment-favouring tilt develops (the tilt and deformation may diminish slightly from times II-III, corresponding to the "bump"). But from times III-V, the "tips" of the deformed vorticity contours then "sweep" past each other, from one side of the peak-peak axis to the other, reversing the tilt. This is

associated with $cos^2(\phi_i) > 0.5$, By time V, the contours have become re-aligned such that core fluid does not cross streamlines, preventing it from being advected away and thereby inhibiting core detrainment. This is consistent with the lack of evident Γ_{II} loss after the troughs associated with (S/ω) bumps in figure 7.

Regardless of the varying directional influences and tilt-sweep processes, the vortices' continuous growth by viscous diffusion ensures that ultimately the vortices' mutual strain becomes predominant, and that one vortex (at least) eventually maintains the tilt (i.e., $cos^2(\phi_i) < 0.5$, and $(S/\omega)_i > (S/\omega)_{cr}$), thereby undergoing detrainment and causing hendition to occur. However, the directional effects continue to cause oscillations in the tilt (i.e., $cos^2(\phi_i)$) and b until the end of detrainment. This means that even once detrainment of the first vortex is initated, the influence of shear (on both b and the vortices' deformation) affects the occurrence and timing of any potential detrainment of the second vortex, and thereby the outcome of the interaction. This contributes significantly to the timing of vortex detrainment and destruction, and thus the interaction outcomes, as discussed in Chapter 5.

The contents of this chapter were submitted for publication in the Journal of Fluid Mechanics, Folz, Patrick J. R.; Nomura, Keiko K., "On asymmetric vortex pair interactions in shear", although they were not included in the published article. This material is instead being prepared for potential submission as a separate article in the future. The dissertation author was the primary researcher of this paper.

Bibliography

AUSTEN, J. orig 1813 *Pride and Prejudice*. Project Gutenberg, accessed: 2023-07-29.

BAGGALEY, A. W. & BARENGHI, C. F. 2018 Decay of homogeneous two-dimensional quantum turbulence. *Physical Review A* **97** (3), 033601.

BENAVIDES, S. J. & ALEXAKIS, A. 2017 Critical transitions in thin layer turbulence. *Journal of Fluid Mechanics* **822**, 364–385.

BENZI, R., PATARNELLO, S. & SANTANGELO, P. 1987 On the statistical properties of two-dimensional decaying turbulence. *EPL (Europhysics Letters)* **3** (7), 811.

BRANDT, L. K. & NOMURA, K. K. 2006 The physics of vortex merger: further insight. *Physics of Fluids (1994-present)* **18** (5), 051701.

BRANDT, L. K. & NOMURA, K. K. 2007 The physics of vortex merger and the effects of ambient stable stratification. *Journal of Fluid Mechanics* **592**, 413–446.

BRANDT, L. K. & NOMURA, K. K. 2010 Characterization of the interactions of two unequal co-rotating vortices. *Journal of Fluid Mechanics* **646**, 233–253.

BURGESS, B. H., DRITSCHEL, D. G. & SCOTT, R. K. 2017*a* Extended scale invariance in the vortices of freely evolving two-dimensional turbulence. *Physical Review Fluids* **2** (11), 114702.

BURGESS, B. H., DRITSCHEL, D. G. & SCOTT, R. K. 2017*b* Vortex scaling ranges in two-dimensional turbulence. *Physics of Fluids* **29** (11), 111104.

BURGESS, B HELEN & SCOTT, RICHARD K 2017 Scaling theory for vortices in the two-dimensional inverse energy cascade. *Journal of Fluid Mechanics* **811**, 742–756.

BURGESS, BELLE HELEN & SCOTT, RICHARD KIRKNESS 2018 Robustness of vortex populations in the two-dimensional inverse energy cascade. *Journal of Fluid Mechanics* **850**, 844–874.

BYRNE, D. & ZHANG, J. A. 2013 Height-dependent transition from 3-d to 2-d turbulence in the hurricane boundary layer. *Geophysical Research Letters* **40** (7), 1439–1442.

CARLSON, SCOTT, FOLZ, PATRICK & NOMURA, KEIKO 2018 Vortex interactions in two-dimensional turbulence. 71st Annual Meeting of the APS Division of Fluid Dynamics.

CARNEVALE, G. F., MCWILLIAMS, J. C., POMEAU, Y., WEISS, J. B. & YOUNG, W. R. 1991 Evolution of vortex statistics in two-dimensional turbulence. *Physical review letters* **66** (21), 2735.

CARNEVALE, G. F., MCWILLIAMS, J. C., POMEAU, Y., WEISS, J. B. & YOUNG, W. R. 1992 Rates, pathways, and end states of nonlinear evolution in decaying two-dimensional turbulence: Scaling theory versus selective decay. *Physics of Fluids A: Fluid Dynamics (1989-1993)* **4** (6), 1314–1316.

CARTON, X., MAZE, G. & LEGRAS, B. 2002 A two-dimensional vortex merger in an external strain field*. *Journal of Turbulence* **3**, 37–37.

CERRETELLI, C. & WILLIAMSON, C. H. K. 2003 The physical mechanism for vortex merging. *Journal of Fluid Mechanics* **475**, 41–77.

DRITSCHEL, D. G. 1990 The stability of elliptical vortices in an external straining flow. *Journal of Fluid Mechanics* **210**, 223–261.

DRITSCHEL, DAVID G 1995 A general theory for two-dimensional vortex interactions. *Journal of Fluid Mechanics* **293**, 269–303.

DRITSCHEL, D. G., SCOTT, R. K., MACASKILL, C., GOTTWALD, G. A. & TRAN, C. V. 2008 Unifying scaling theory for vortex dynamics in two-dimensional turbulence. *Physical review letters* **101** (9), 094501.

DRITSCHEL, D. G. & WAUGH, D. W. 1992 Quantification of the inelastic interaction of unequal vortices in two-dimensional vortex dynamics. *Physics of Fluids A: Fluid Dynamics (1989-1993)* **4** (8), 1737–1744.

ECKE, R. E. 2017 From 2d to 3d in fluid turbulence: unexpected critical transitions. *Journal of Fluid Mechanics* **828**, 1–4.

FANG, L. & OUELLETTE, N. T. 2016 Advection and the efficiency of spectral energy transfer in two-dimensional turbulence. *Physical review letters* **117** (10), 104501.

FOLZ, P. J. R. & NOMURA, K. K. 2014 Interaction of two equal co-rotating viscous vortices in the presence of background shear. *Fluid Dynamics Research* **46** (3), 031423.

FOLZ, P. J. R. & NOMURA, K. K. 2017 A quantitative assessment of viscous asymmetric vortex pair interactions. *Journal of Fluid Mechanics* **829**, 1–30.

FOLZ, P. J. R. & NOMURA, K. K. 2023 On asymmetric vortex pair interactions in shear. *Journal of Fluid Mechanics* To appear.

FU, W., LI, H., LUBOW, S., LI, S. & LIANG, E. 2014 Effects of dust feedback on vortices in protoplanetary disks. *The Astrophysical Journal Letters* **795** (2), L39.

GARTEN, J. F., ARENDT, S., FRITTS, D. C. & WERNE, J. 1998 Dynamics of counter-rotating vortex pairs in stratified and sheared environments. *Journal of Fluid Mechanics* **361**, 189–236.

GERZ, T., SCHUMANN, U. & ELGHOBASHI, S. E. 1989 Direct numerical simulation of stratified homogeneous turbulent shear flows. *Journal of Fluid Mechanics* **200**, 563–594.

GODON, P. & LIVIO, M. 1999 Vortices in protoplanetary disks. *The Astrophysical Journal* **523** (1), 350.

HUANG, M. J. 2005 The physical mechanism of symmetric vortex merger: A new viewpoint. *Physics of Fluids (1994-present)* **17** (7), 074105.

HUANG, M. J. 2006 A comparison between asymmetric and symmetric vortex mergers. *WSEAS Transactions on Fluid Mechanics 1* (5), 488–496.

HUNT, J. C. R., WRAY, A. A. & MOIN, P. 1988 Eddies, streams, and convergence zones in turbulent flows. *Center for Turbulence Research Report CTR-S88* .

HURST, N. C., DANIELSON, J. R., DUBIN, D. H. E. & SURKO, C. M. 2016 Evolution of a vortex in a strain flow. *Physical review letters* **117** (23), 235001.

JING, F., KANSO, E. & NEWTON, P. K. 2012 Insights into symmetric and asymmetric vortex mergers using the core growth model. *Physics of Fluids (1994-present)* **24** (7), 073101.

KIDA, SHIGEO 1981 Motion of an elliptic vortex in a uniform shear flow. *Journal of the Physical Society of Japan* **50** (10), 3517–3520.

KIMURA, YOSHIFUMI & HASIMOTO, HIDENORI 1985 Motion of two identical point vortices in a simple shear flow. *Journal of the Physical Society of Japan* **54** (11), 4069–4072.

KIMURA, Y. & HERRING, J. R. 2001 Gradient enhancement and filament ejection for a non-uniform elliptic vortex in two-dimensional turbulence. *Journal of Fluid Mechanics* **439**, 43–56.

KUNNEN, R., TRIELING, R. R. & VAN HEIJST, G. J. 2010 Vortices in time-periodic shear flow. *Theoretical and Computational Fluid Dynamics* **24** (1-4), 315–322.

LE DIZÈS, S. & LAPORTE, F. 2002 Theoretical predictions for the elliptical instability in a two-vortex flow. *Journal of Fluid Mechanics* **471**, 169–201.

LE DIZÈS, S. & VERGA, A. 2002 Viscous interactions of two co-rotating vortices before merging. *Journal of Fluid Mechanics* **467**, 389–410.

LEGRAS, B. & DRITSCHEL, D. G. 1993 Vortex stripping and the generation of high vorticity gradients in two-dimensional flows. In *Advances in Turbulence IV*, pp. 445–455. Springer.

LEGRAS, B., DRITSCHEL, D. G. & CAILLOL, P. 2001 The erosion of a distributed two-dimensional vortex in a background straining flow. *Journal of Fluid Mechanics* **441**, 369–398.

LEWEKE, T., LE DIZÈS, S. & WILLIAMSON, C. H. K. 2016 Dynamics and instabilities of vortex pairs. *Annual Review of Fluid Mechanics* **48**, 507–541.

MARIOTTI, A., LEGRAS, B. & DRITSCHEL, D. G. 1994 Vortex stripping and the erosion of coherent structures in two-dimensional flows. *Physics of Fluids (1994-present)* **6** (12), 3954–3962.

MARQUES ROSAS FERNANDES, V. H., KAMP, L. P. J., VAN HEIJST, G. J. F. & CLERCX, H. J. H. 2016 Interaction of monopoles, dipoles, and turbulence with a shear flow. *Physics of Fluids* **28** (9), 093603.

MAZE, G., CARTON, X. & LAPEYRE, G. 2004 Dynamics of a 2d vortex doublet under external deformation. *Regular and Chaotic Dynamics* **9** (4), 477–497.

MCWILLIAMS, J. C. 1990 The vortices of two-dimensional turbulence. *Journal of Fluid Mechanics* **219**, 361–385.

MELANDER, M. V., MCWILLIAMS, J. C. & ZABUSKY, N. J. 1987*a* Axisymmetrization and vorticity-gradient intensification of an isolated two-dimensional vortex through filamentation. *Journal of Fluid Mechanics* **178**, 137–159.

MELANDER, M. V., ZABUSKY, N. J. & MCWILLIAMS, J. C. 1987*b* Asymmetric vortex merger in two dimensions: Which vortex is victorious? *Physics of Fluids (1958-1988)* **30** (9), 2610–2612.

MELANDER, M. V., ZABUSKY, N. J. & MCWILLIAMS, J. C. 1988 Symmetric vortex merger in two dimensions: causes and conditions. *Journal of Fluid Mechanics* **195**, 303–340.

MEUNIER, P. 2001 Etude expérimentale de deux tourbillons corotatifs. PhD thesis, Université de Provence-Aix-Marseille I.

MEUNIER, P., EHRENSTEIN, U., LEWEKE, T. & ROSSI, M. 2002 A merging criterion for

two-dimensional co-rotating vortices. *Physics of Fluids (1994-present)* **14** (8), 2757–2766.

MEUNIER, P., LE DIZÈS, S. & LEWEKE, T. 2005 Physics of vortex merging. *Comptes Rendus Physique* **6** (4-5), 431–450.

MININNI, P. D. & POUQUET, A. 2013 Inverse cascade behavior in freely decaying two-dimensional fluid turbulence. *Physical Review E* **87** (3), 033002.

MOORE, D. W. & SAFFMAN, P. G. 1971 Structure of a line vortex in an imposed strain. In *Aircraft wake turbulence and its detection*, pp. 339–354. Springer.

NIELSEN, A. H., HE, X., RASMUSSEN, J. JUUL & BOHR, T. 1996 Vortex merging and spectral cascade in two-dimensional flows. *Physics of Fluids* **8** (9), 2263–2265.

ORLANDI, P. 2000 *Fluid Flow Phenomena: A Numerical Toolkit*. *Fluid Flow Phenomena: A Numerical Toolkit* v. 1. Springer.

OVERMAN II, E. A. & ZABUSKY, N. J. 1982 Evolution and merger of isolated vortex structures. *Physics of Fluids (1958-1988)* **25** (8), 1297–1305.

PAIREAU, O., TABELING, P. & LEGRAS, B. 1997 A vortex subjected to a shear: an experimental study. *Journal of Fluid Mechanics* **351**, 1–16.

PERROT, X. & CARTON, X. 2010 2d vortex interaction in a non-uniform flow. *Theoretical and Computational Fluid Dynamics* **24** (1-4), 95–100.

RICCARDI, G., PIVA, R. & BENZI, R. 1995 A physical model for merging in two-dimensional decaying turbulence. *Physics of Fluids (1994-present)* **7** (12), 3091–3104.

RYZHOV, E. A., KOSHEL, K. V. & CARTON, X. 2012 Passive scalar advection in the vicinity of two point vortices in a deformation flow. *European Journal of Mechanics-B/Fluids* **34**, 121–130.

SAFFMAN, P. G. 2001 *Vortex dynamics*. Cambridge university press.

SAFFMAN, P. G. & SZETO, R. 1980 Equilibrium shapes of a pair of equal uniform vortices. *Physics of Fluids (1958-1988)* **23** (12), 2339–2342.

SIRE, C., CHAVANIS, P. H. & SOPIK, J. 2011 Effective merging dynamics of two and three fluid vortices: Application to two-dimensional decaying turbulence. *Physical Review E* **84** (5), 056317.

SUTYRIN, G. G. 2019 On vortex intensification due to stretching out of weak satellites. *Physics of Fluids* **31** (7), 075103.

TABELING, P. 2002 Two-dimensional turbulence: a physicist approach. *Physics Reports* **362** (1), 1–62.

TRIELING, R. R., DAM, C. E. C. & VAN HEIJST, G. J. F. 2010 Dynamics of two identical vortices in linear shear. *Physics of Fluids (1994-present)* **22** (11), 117104.

TRIELING, R. R., VELASCO FUENTES, O. U. & VAN HEIJST, G. J. F. 2005 Interaction of two unequal corotating vortices. *Physics of Fluids (1994-present)* **17** (8), 087103.

TSATSOS, M. C., TAVARES, PEDRO E. S., CIDRIM, A., FRITSCH, A. R., CARACANHAS, M. A., DOS SANTOS, F. E. A., BARENGHI, C. F. & BAGNATO, V. S. 2016 Quantum turbulence in trapped atomic bose–einstein condensates. *Physics Reports* **622**, 1–52.

VELASCO FUENTES, O. U. 2005 Vortex filamentation: its onset and its role on axisymmetrization and merger. *Dynamics of atmospheres and oceans* **40** (1-2), 23–42.

WAUGH, D. W. 1992 The efficiency of symmetric vortex merger. *Physics of Fluids A: Fluid Dynamics (1989-1993)* **4** (8), 1745–1758.

XIAO, Z, WAN, M, CHEN, S & EYINK, GL 2009 Physical mechanism of the inverse energy cascade of two-dimensional turbulence: a numerical investigation. *Journal of Fluid Mechanics* **619**, 1–44.

YASUDA, I. & FLIERL, G. R. 1997 Two-dimensional asymmetric vortex merger: merger dynamics and critical merger distance. *Dynamics of atmospheres and oceans* **26** (3), 159–181.